MASTER THESIS

INVESTIGATION OF TAYLOR BUBBLE PROPERTIES AND THEIR REACTION ON THE CO-CURRENT UPWARD SLUG FLOW FROM EXPERIMENTAL DATABASE OF ULTRAFAST X-RAY TOMOGRAPHY

In Partial Fulfillment
of the Requirements for Degree
Master of Engineering in Mechanical Engineering

Submitted by:

AKMAL IRFAN MAJID
12/375444/PTK/10083

MASTER PROGRAM OF MECHANICAL ENGINEERING
DEPARTMENT OF MECHANICAL AND INDUSTRIAL ENGINEERING
FACULTY OF ENGINEERING UNIVERSITAS GADJAH MADA
YOGYAKARTA
2015

TESIS

Investigasi Mengenai Sifat-Sifat *Taylor Bubble* dan Reaksinya terhadap Aliran *Slug* Searah ke Atas dengan Memanfaatkan Data Eksperimen Menggunakan *Ultrafast X-Ray Tomography*

Investigation of Taylor Bubble Properties and Their Reaction on the Co-Current Upward Slug Flow from Experimental Database of Ultrafast X-Ray Tomography

Dipersiapkan dan disusun oleh:
Akmal Irfan Majid
12/375444/PTK/10083

Telah dipertahankan di depan Dewan Penguji
pada tanggal 20 Januari 2015

Pembimbing Utama

Dr. Eng. Deendarlianto, S.T., M.Eng.
NIP. 197208032008121001

Anggota Dewan Penguji Lain

Prof. Dr. Ir. Indarto, DEA.
NIP. 195306241981011001

Anggota Dewan Penguji Lain

Dr. Eng. Adhika Widyaparaga, S.T., M.Biomed.
NIP. 198007162005011001

Anggota Dewan Penguji Lain

Dr. Eng. Khasani, S.T., M.Eng.
NIP. 196806171994121001

Tesis ini telah diterima sebagai salah satu persyaratan untuk memperoleh gelar Magister

Tanggal, 20 Januari 2015
Pengelola Program Studi: Teknik Mesin

Fauzun, S.T., M.T., Ph.D.
NIP. 197111261998031002

Mengetahui,
Wakil Penanggung Jawab Program Studi Teknik Mesin

Prof. Ir. Jamasri, Ph.D.
NIP. 196107041988031002

DECLARATION

I hereby declare that this master thesis is originally made by myself under the supervision of the Advisors. All information in this thesis has been obtained in accordance with academic rules and submitted to comply the requirements of Master of Engineering degree at the Department of Mechanical and Industrial Engineering, Faculty of Engineering, Universitas Gadjah Mada. As far as I know, there are no similar works, reports, or theses, except as I cited and mentioned in the references.

Yogyakarta, 30th November 2014

Akmal Irfan Majid
09/284701/TK/35449

DEDICATION

In the spirit of Holy Qur'aan:

إِنَّ فِي خَلْقِ السَّمَاوَاتِ وَالْأَرْضِ وَاخْتِلَافِ اللَّيْلِ وَالنَّهَارِ لَآيَاتٍ لِأُولِي الْأَلْبَابِ

Indeed, in the creation of the heavens and the earth and the alternation of the night and the day are signs for those of understanding. (Qur'aan - 'Āli `Imrān:190)

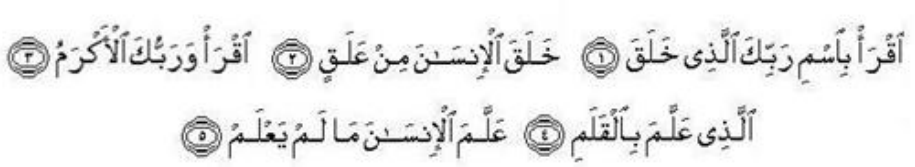

1) Read! In the Name of your Lord, Who has created (all that exists); 2) (Allah) has reated man from a clot (a piece of thick coagulated blood); 3) Read! And your Lord is the Most Generous; 4) Who has taught (the writing) by the pen; 5) Has taught man that which he knew not. (Qur'aan - 'Āl-`Alaaq:1-5)

This Master Thesis is dedicated to:

- **ALLAH SWT,** *The Almighty, Greatest, Merciful, and only one God.*
- **Rasulullah, Prophet Muhammad SAW**

  The Uswatun Khasanah, ideal role model who guided from the dark ages into the truth.
- **My beloved Father and Mother**

  For all lessons of life, patience, affections, guidance, nurtures… thanks for all, Bapak & Ibu !
- **Eyang Nurman and Almh. Eyang Putri (all of my mother's family)**

  For all tremendous supports… though they could not directly see my struggling steps.
- **Simbah KH. Muh. Sjahri and Mbah Putri (all of my father's family)**

  For all religious values, unstopped prays for me, and modesties which you have taught to me.
- **My Future Wife**

  Someone who will be sent by Allah for coloring my life in the frame of happiness and faith.

also dedicated for:

The development of multiphase flow at Indonesia
… and the world

ACKNOWLEDGEMENT

Bismillahirrahmaanirrahim,

All compliments, gratitude, and glories are only belong to The Almighty God Allah *subhaanahu wa ta'ala* who gives me the valuable occasions, encouragements, and guidance throughout the completion of this work. Blessing and peace of Allah SWT are praised to the last and great prophet Rasulullah Muhammad SAW.

I would like to deserve my deepest gratitude to my Supervisor, Dr. Deendarlianto. You are more than a good advisor for me by showing an ideal role model as lecturer and researcher. Thank you for introducing me great scholars in this field and providing me a space to be further developed in the fascinating world of modern multiphase flow. I wish him the best career stage for the future and I hope can working together again in the near future.

My deep appreciation to Dr. Dirk Lucas from the Institute of Fluid Dynamics, Helmholtz-Zentrum Dresden-Rossendorf for this valuable opportunity to conduct this research at there and also for showing me many insights of multiphase flows. Special thanks to my Advisor, Dipl.-Ing. Manuel Banowski for his support, help, and supervise along the way. I will miss working with them very much.

Special reverence to Prof. Dr. Indarto, Dr. Khasani, and Dr. Adhika Widyaparaga for accepting to be the examiner boards of this thesis. I thank for advices and suggestions to improve the thesis quality.

The financial and accommodation supports from Institute of Fluid Dynamics, Helmholtz-Zentrum Dresden-Rossendorf are gratefully acknowledged during the research. I also sincere my gratefulness to Ministry of Education and Culture of Republic of Indonesia, for giving me a Fast-Track Scholarship for my Master Program. I would especially thanks to Prof. Dr. Bambang Hari Wibisono (former Vice Dean of Academic Affair, Faculty of Engineering UGM) who wisely supported me to get this scholarship.

The enormous thanks and prays are always delivered to Drs. Agus Budiman, M.Pd., M.T. (father) and Dra. Nurul Indriani (mother) who tirelessly support and give their infinite prayers for me. The great acknowledgement should be extended for their nurtures, immeasurable affections, understanding, guidance, and discussion along my maturity as their son. I also express my thanks to my big family for your support during this work. Hopefully, Allah always blessing your kindness.

Many thanks to the Academic Boards of Gadjah Mada University: Dr. Fauzun as Head of Mechanical Engineering Postgraduate Program, Prof. Dr. Jamasri as Head of Mechanical and Industrial Engineering Dept., and Prof. Dr. Panut Mulyono as Dean of Faculty of Engineering. The deep respects for the great lecturers, among them are Prof. Dr.-Ing. Harwin Saptoadi, Prof. Dr. Samsul Kamal, Prof. Dr. M. Noer Ilman, Dr. Suyitno, Dr. Jayan Sentanuhady, Dr. Tri Agung Rohmat, Dr. Budi Hartono, for your kind hospitality, discussion, and a freedom way of thinking as a student. Moreover, I would like to sincere all of my lectures in Dept. of Mechanical and Industrial Engineering UGM, all administration staffs of postgraduate program administration, securities, and all staffs of this department.

Experimental Thermal and Fluid Dynamics Department at the HZDR is an excellent place for me to complete my Master Thesis. Many thanks to Prof. Uwe Hampel (Head of Department), Mathias Beyer, (Head of TOPFLOW Facility), Mathias Ignaczak, Thomas Geißler, Tobias Seidel, Lutz Szalinski, Peter Schütz, Heiko Pietruske, Chi Beichang, Debasish Sarker, Michael Piechotta, Christian Bock, and Sebastian Unger for your help and good friendship. Thanks to Dr. Thomas Barth, Dr. Sebastian Reinecke, Dr. Thomas Höhne, Dr. Andre Bieberle, Gustavo Montoya, and Tian Ma for your hospitality. I surely enjoyed not only a conducive research climate but also the insightful discussions. For all HZDR crews and administration staffs, I thanks for your help and hospitality during my internship, *Dankeschön!*

I also appreciate a great friendship with Hadiyan Yusuf Kuntoro who encouraging each other during the research experience at Dresden. I enjoy to discuss, laugh, joke, and even sometimes compete with you. I will miss spending the enjoyable moment together.

Members of Fluid Dynamics Research Group, such as Pak Okto, Pak Windy, Pak Apip, Pak Andri, Pak Sudarja, Pak Zidni (doctoral), Aqli, Ade, Wira (master), Fikri Makhluf, Sugi, Wilson, Ian, Afrian (bachelor). Thank you for making the research life at Fluid Mechanics Laboratory UGM more colorful. I also have enjoyed some occasions to contribute for Center for Energy Studies UGM.

My friendship appreciation is extended to my friends of Postgraduate Program of Mechanical Engineering batch 2012. Special thanks to my friends in the class of Energy Conversion, especially Pak Bambang Akmil, Pak Bagiyo Condro, Pak Joni Kasmara, Pak Adryan Warokka, Mas Dodi, and Mas Achileus Hermawan. To all "Fast Track Batch 2012" guys: Gustav, Wendy, Fransisko, Erick, Gery, Widhi, Jundan, Aji Saka, Afwan, and Fredrick Neo, I deliver my warm brotherhood spirit.

I respect and thank to Anindityo Patmonoaji and Shakti Nuryadin. Both of you are great example and more than an ideal student. Your advice and support were very useful during the research internship. My thanks are also conveyed to Pak Ryan Anugrah Putra, a Ph.D. student in HZDR from Mechanical Engineering Gadjah Mada University. I learnt and discussed many lesson from him as a good senior.

Living in Dresden gave me an experience for social learning. I felt a family spirit by contributing in FORMID *(Forum Masyarakat Indonesia Dresden)*. Special thanks to Bu Ida who always help and cheers my journey. I also thanks to Bu Tri, Gilang, Hakim, Om Beny and family, Bang Maradona, Kelvin, Bang Haposan, Alfi, Ismail, Pak Adhi Nugraha and family, and some other great friends in Dresden, Berlin, and Munich who have kindly helped me. Keep in contact and *silaturahim* guys!

Thank you for a nice friendship with all former housemates in Siedlung Rossendorf 28, especially Soma Istvàn Kovàc (Hungarian), Nigar Özey (Turkish), Anirrudh Das (Indian), Xing Ming Fan, Wang Chao (Chinese), Dr. Tomàs David (Czech), and Marco Zennaro (Italian).

My warm thanks and appreciation to Binda Anissa and her family for their big support and understanding during the intensive stages of this work. My special thanks to her for coloring the days with smile and laugh.

Finally, I would like to acknowledge all people who have contributed in my academic journey during this work. I might not able to write all names who contributed in this process. However, I am really sure, that their roles and contributions never be forgotten.

As the manifestation of the continuous development on this field, the author will open for any discussion or suggestion regarding this work. Hopefully, this thesis gives valuable contributions for the headway of Multiphase Flow in worldwide and also especially Indonesia.

Alhamdulillaahirrabbil 'aalamiin.

A master thesis – joint work between UGM (Indonesia) and HZDR (Germany)
August-November 2014

Akmal Irfan Majid
12/375444/PTK/10083

TABLE OF CONTENTS

LIST OF FIGURES

LIST OF TABLES

NOMENCLATURES

Latin symbols	Denomination	Unit
A	Cross-sectional area	m^2
C_0	The distribution parameter of drift-flux	-
d	Bubble diameter	m
D	Pipe diameter	m
F	Force	N
f	Bubble frequency	bubble/s
fr	Frame rate	frame/s
g	Gravity acceleration factor	N/kg
g'	Modified gravity acceleration factor	N/kg
I	Time identity	s
i	Identity for temporal (time) axis	s
J	Superficial velocity	m/s
j	Identity for x-direction	m
k	Identity for y-direction	m
L	Length	m
$\dot{m}$	Mass flow rate	kg/s
n	Number of image frame	-
p	Pressure	Pa
r	Radial coordinate	m
R	Radius	m
t	Time	s
T	Temperature	K
U	Velocity	m/s
v	Bubble volume	m^3
w	Velocity	m/s
x	x-direction in Cartesian coordinate	m
y	y-direction in Cartesian coordinate	m
z	Pipe height	m

Greek letters	Denomination	Unit
$\alpha°$	Polar angle	°
α	Void fraction	-
β	Azimuthal angle	°
δ	Film thickness	m
ε	Void fraction	-
ϕ	Probability	-
γ	Surface tension	N/m
μ	Dynamic viscosity	Ns/m^2
ν	Kinematic viscosity	m^2/s
π	Phi	-

θ	Pipe inclination	°
ρ	Density	kg/m^3
σ	Sigma – probability range (in Gaussian function)	-
τ	Wall-shear stress	N/mm
Δ	Delta	-
∞	Infinite	-

Index	**Denomination**
avg	Averaged
axial	Axial direction
azm	Azimuthal direction
back	Bubble rear position
B	Bubble
b	Bubble
Buo	Buoyancy
BP	Bubble-pair
crit	Critical
D	Drag
drift	Drift
equiv	Equivalent
exp	Expected
FF	Falling film
front	Bubble front position
G	Gas
GLS	Gas in liquid slug
H	Horizontal
hor	Horizontal
L	Liquid
LLS	Liquid in liquid slug
LS	Liquid slug
m	Bubble center of mass
mix	Mixture (air and water mixture)
nicklin	Nicklin et al. (1962) proposed velocity correlation
O	Upper measurement plane *("Obere" – German Language)*
pos	Position
rad	Radial direction
range	Range
rel	Relative
TB	Taylor bubble
TD	Turbulent dispersion
U	Upper measurement plane *("Unter" – German Language)*
VM	Virtual mass
vel	Velocity
vol	Volume
W	Wall

wake	Wake region
xymax	Maximum in cross-sectional direction

Abbreviation	**Denomination**
CFD	*Computational Fluid Dynamics*
CIWH	*Condensation-Induced Water Hammer*
CT	*Computer-Tomography*
CZT	*Cadmium Zinc Telluride*
DCC	*Direct Contact Condensation*
ECC	*Emergency Core Cooling*
FFT	*Fast-Fourier Transformation*
fps	*Frame per second*
ID	*Inner Diameter*
LOCA	*Loss Of Coolant Accident*
HZDR	*Helmholtz-Zentrum Dresden-Rossendorf*
NRS	*Nuclear Reactor Safety*
PDA	*Photochromic Dye Activation*
PDF	*Probability Distribution Function*
PIV	*Particle Image Velocimetry*
PTS	*Pressure Thermal Shock*
PWR	*Pressurized Water Reactor*
ROFEX	*Rossendorf Fast Electron Beam X-Ray Tomography*
RPV	*Reactor Pressure Vessel*
TOPLOW	*Transient Two-Phase Flow – Test Facility*
3-D	*Three-dimensions*

Dimensionless number		
Ar	Archimedes number	$Ar = \frac{\rho_L(\rho_L - \rho_G)gD^3}{{\mu_L}^2}$
Eo	Eötvös number	$Eo = \frac{(\rho_L - \rho_G)gD^2}{\gamma}$
Fr	Froude number	$Fr = \frac{U_\infty}{\sqrt{gD}}$
Mo	Morton number	$Mo = \frac{g\mu^4(\rho_L - \rho_G)}{{\rho_L}^2\,\gamma^3}$
Nf	Inverse viscosity number	$Nf = \frac{\rho\sqrt{gD}}{\mu}$
Re	Reynolds number	$Re = \frac{(\rho_L - \rho_G)UD}{\mu}$

ABSTRACT

Investigation of Taylor Bubble Properties and Their Reaction on the Co-Current Upward Slug Flow from Experimental Database of Ultrafast X-Ray Tomography

Akmal Irfan Majid

Supervised by:
Deendarlianto [1)], Manuel Banowski [2)], Dirk Lucas [2)]

[1)] Department of Mechanical and Industrial Engineering, Faculty of Engineering, Gadjah Mada University – INDONESIA
[2)] Institute of Fluid Dynamics, Helmholtz-Zentrum Dresden-Rossendorf - GERMANY

Slug flow is a complex two-phase flow pattern that characterized by the presence of Taylor bubbles and liquid slugs with small bubbles inside. Due to the intermittent and irregular natures, the pattern might causes high mechanical impact to the pipeline, corrosion and high pressure fluctuation. Therefore, it is common avoided in engineering applications. On the other hand, the rapid developments of new Computational Fluid Dynamics (CFD) models need to be supported by high quality experimental database to validate and improve the simulation models. Investigations about detail properties of Taylor bubbles are necessary to obtain physical mechanisms of slugging phenomena.

At the Helmholtz-Zentrum Dresden-Rossendorf, experiments on co-current upward air-water flow in 54.8 mm diameter vertical pipe with various gas-liquid superficial velocities were performed. As measurement technique, an ultrafast dual-layers X-ray tomography was developed to fulfil the requirement of an accurate measurement with high spatial and temporal resolutions. Results of tomography scanning were reconstructed and segmented to carry out each gas bubble size and parameters. A bubble pair algorithm is to estimate the instantaneous movement of each bubble. This method is able to assign the correct paired bubbles from both measurement layers by considering the highest probability of position, volume, and velocity. Therefore, each gas-bubble individual characteristics can be revealed. A statistical analysis was also used to support the data analysis.

General characteristics of slug flow were explained in the form of qualitative observation and quantitative explanation of void fraction characteristics. Taylor bubble properties such as the velocity, frequency, and length were observed and reasons of velocity distribution were carried out. The presence of Taylor bubble generates different flow behaviors for small bubbles around it such as bubbles in falling film region and behind area of the Taylor bubble. Reasons of the Taylor bubble velocity distributions were explained. Relationship between Taylor bubble properties and as well liquid slug to the velocities are also revealed. The increase of axial station along the pipe influences flow pattern, void fraction, and properties of Taylor bubble and liquid slug as well. Bubble pair method was able to reveal the Taylor bubble properties and slug flow characteristics. A relevant agreement between the previous studies was carried-out.

Keywords: Bubble, Slug flow, Taylor bubble, Bubble pair algorithm, Ultrafast X-ray tomography

CHAPTER I
INTRODUCTION

1.1. Research Background

The simultaneous flow of gas and liquid inside a co-current vertical pipe requires more intricate analysis than the analysis of single-phase flow. Since the distinctive properties of each phase, various flow patterns are generated. Consequently, every flow configuration contains particular flow characteristics due to the complex interfacial behaviors. When gas-liquid two-phase flows exist in fluid transportation process, more attentions are needed especially to develop effective and efficient engineering processes. Examples of multiphase flow phenomena are encountered in various events of nuclear reactor accident scenarios. Additionally, the gas-liquid two-phase flow phenomena also occurs inside boiler tubes, along the pipelines and wells of hydrocarbon production plants, within bubble column reactors, and inside geothermal power plant wells.

Specifically, the basic understanding on multiphase flow system are needed relating on the Nuclear Reactor Safety (NRS) analyses in Pressurized Water Reactor (PWR). In general, the aforementioned cases are related to the mixing process, main cooling system, or Emergency Core Cooling (ECC) system. During the Loss of Coolant Accident (LOCA) scenario, a counter-current flow of condensate and steam, known as “reflux condensation mode”, flows in the opposite direction of normal operation and may enter the reactor pressure vessel, inhibiting the emergency cooling process (Deendarlianto et al., 2011). When Direct Contact Condensation (DCC) process occur, the saturated steam condenses on a sub-cooled water interface. Hence, the cold water temperature increases and leads steam bubbles be entrapped by cold water slugs. The bubbles rapid condensation can be followed by a water hammer, known as the Condensation-Induced Water Hammer (CIWH) phenomenon (Strubelj et al., 2010). The boiling phenomena inside the Reactor Pressure Vessel (RPV) also shows an example of vertical two-phase flow system. Examples of multiphase flow system are illustrated in Figure 1.1. (a) and (b).

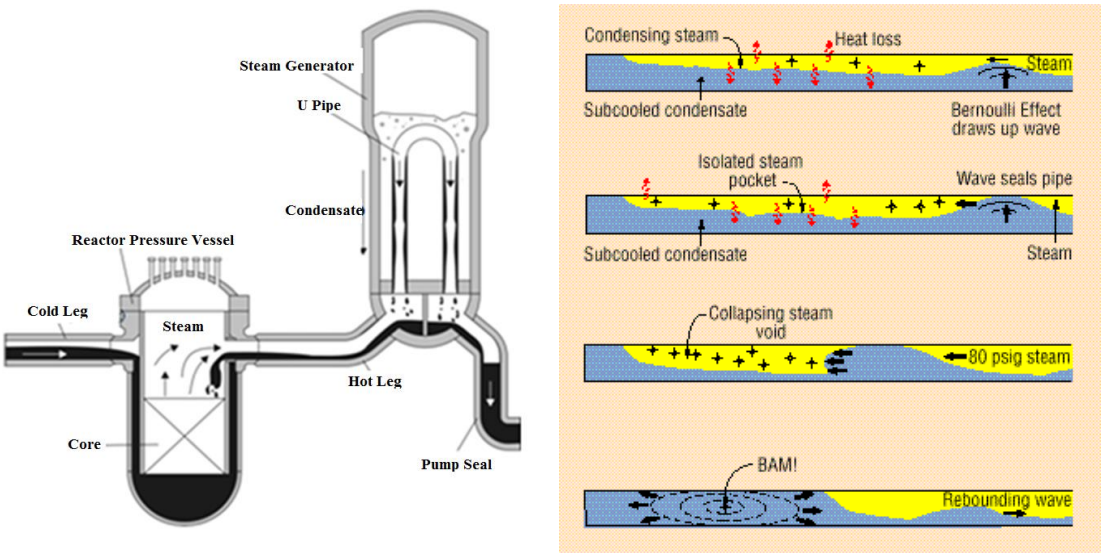

(a) (b)

Figure 1.1. (a) Schematic diagram of German Konvoi Nuclear Reactor (Seidel et al., 2010); (b) Schematic diagram of slug formation in Condensation Induced Water Hammer (Kirsner, 1998 - *accessed on July 2014*)

In order to describe the complexity of the two-phase flow behaviors, the fundamental equations of fluid dynamics, namely: continuity, momentum, and energy conservation are manifested in various investigations by physical experiments, computational simulations, and analytical approaches. As the increase of the computer capability, the new simulation models as well as the Computational Fluid Dynamics (CFD) is increasingly being used in safety-related industries due to the cost-effectiveness and minimum risks. Consequently, the rapid development of new CFD models needs to be supported by high spatial and temporal experimental data to construct and validate fundamental mechanisms of two-phase flow cases. Improvements of the models are strongly depended on the powerful measuring technique that able to reveal physical information of the flow.

Air-water two-phase flow inside a vertical pipe is the simplest case for investigating the basic phenomena of multiphase flow. Moreover, it represents an ideal place for observing flow evolution along the pipe with a well-defined boundary condition. One critical issues on the co-current vertical flow is the slugging phenomenon. It is characterized by the existence of the long-bullet shaped bubble - recognized as the Taylor bubble, followed by the liquid-slugs that

aerated by the small dispersed bubbles (Davies and Taylor, 1950; Fernandes et al., 1983; Fabre and Line, 2002). The intermittent and irregular appereances of this pattern influence the flow structures and stability. Moreover, slug flow has the high attributes of pressure fluctuation and local pressure difference inside the pipe. To ensure the safety operations, including prevention of high pipe oscillation, corrosion, and high structural vibration, those extreme conditions should be well controlled. In practical conditions, slug flow enhances the possibilities of mechanial impact and structural damages such as multiphase flow induced internal corrosion, which is governed by some of the crucial parameters include the mass transfer coefficient and wall shear stress (Liu,1997; Maley and Jepson, 2000; Wang and Nesic, 2003, Yan and Che, 2011). Due to those reason, the study of Taylor bubble properties and their reaction to the surroundings becomes substantially important.

Currently, the dynamics of the Taylor bubbles are still producing some challenges regarding their unique behaviors. The presence of Taylor bubble, which has different properties than the small gas-bubbles, gives reactions in two-phase flow system. In addition, the dynamics of small bubbles inside liquid slugs are still rarely observed due to lack temporal and spatial resolution devices which has the capability to describe clearly the interfacial boundaries of high dense bubbly flows. Meanwhile, the advanced visualization methods are really needed to solve the difficulties to reveal the interfacial problems. Therefore, the flow characteristics and the important flow properties can be carried out through the visual data.

A unique ultrafast X-ray tomography named **Ro**ssendorf **F**ast **E**lectron Beam **X**-ray Tomography (ROFEX) was developed at the Institute of Fluid Dynamics of Helmholtz-Zentrum Dresden-Rossendorf (HZDR). It provides an advanced non-intrusive measurement system with high spatial and temporal resolution. By sequence of data processing, the device was able to reveal three-dimensional movements and individual properties of each gas-phase inside the flow. Therefore, a good agreement between experimental and simulation works is expected.

The present work has a relation with the previous study of Patmonoaji (2014). Previously, an algorithm namely "bubble pair algorithm" was applied to determine the individual bubble velocities. It works by finding the appropriate "paired" bubbles which detected in lower and upper measurement planes. General implementation of this algorithm showed a suitable result for bubbly and slug flows. However, an additional information of Taylor bubble properties and general flow characteristics should be revealed to find the properties relation during the co-current upward air-water slug flow. Bubble pair algorithm is expected to contribute for carrying out the Taylor bubble properties. A good agreement between the previous studies is expected.

1.2. Problems formulation

In many practical applications, the slugging phenomena are often undesired due to the mechanical impact and high pressure fluctuation, characrterized by the presence of Taylor bubbles and liquid slugs. An investigation on the slug flow behaviors is needed to provide better understanding of this flow pattern. On the other hand, measurement by an ultrafast X-ray tomography gives important contribution to produce high quality data in time and space function. The scanning results were then processed by the sequential processes including a bubble pair algorithm (Patmonoaji, 2014) on the velocities determination in bubbly and slug flow regimes. However, the previous study was only focused on the algorithm development. The implementation of this method to study more deeply about the Taylor bubble properties and hydrodynamics of slug flow region are required. Moreover, reason and interpretation of the previous results are also need to be investigated to ascertain slug flow characteristics.

In the previous results, Taylor bubble average axial velocity confirmed the correlation of Nicklin et al. (1962). Nevertheless, the velocity distributions occur, either a distribution of each Taylor bubble inside a particular flow condition or the discrepancy with theoretical predictions (Nicklin et al., 1962 and Fernandes et al., 1983). Therefore, reasons for the velocity distributions need to be investigated. In addition, the presence of dispersed bubbles in liquid slug attracts a study to reveal

detail characteristics and their properties. In more detail, the research problems lead into these research questions, as mentioned:

1. How to explain the general slug flow characteristics from experimental database of ultrafast two-layer electron beam X-ray tomography?
2. How to determine the Taylor bubble properties from experimental database of ultrafast two-layer electron beam X-ray tomography?
3. How do the Taylor bubble properties and its dynamics affect the surroundings?

1.3. Research objectives

The research was designated to process the experimental database of ultrafast X-ray tomography in order to determine the Taylor bubble properties. The properties relations to the surroundings of co-current upward slug flow were also investigated. Moreover, the detail of research objectives can be specified as follows:

1. To obtain general characteristics of co-current slug flow.
2. To obtain the Taylor bubble physical properties and to investigate the properties reaction to the surroundings.
3. To investigate the gas-bubble characteristics in other slug flow regions, such as bubbles in falling film, wake region, and developed bubble region.

1.4. Benefit of the research

The present work was included as the fundamental research to study physical phenomena of a particular flow regime of air-water two-phase flow. This research was expected to bring on some usefulness:

1. Validation and improvement of the two-phase flow simulation codes and the other measurement techniques.
2. Contribution to enrich the database of gas-liquid two-phase flow inside the vertical pipes.
3. Contribution to both of industrial and academic sites by providing the accurate and comprehensive data of vertical two-phase flow.

1.5. Problem assumptions

In order to simplify the analysis of the research problems, the present work involves several assumptions due to the limitations of the measurement condition and process. Those are given as follows:

1. This work was carried-out in adiabatic condition (no heat influence). Therefore, no phase transformation among liquid to gas and vice versa.
2. The internal surface inside the vertical pipe was assumed as smooth surfaces (friction factor is neglected).
3. The working fluids were tap water (as liquid-phase) and air (as gas-phase) which co-currently flow in a upward direction inside 54.8 mm titanium pipe. The available measurement length of pipe is 3.3 m.
4. Due to the small gaps between dual measurement planes, the occurrence of bubble coalescence and breakup were assumed in very small numbers.
5. The present study was only focused on the co-current upward vertical slug flow regime from the available processed experimental data of ultrafast X-ray tomography.

CHAPTER II
LITERATURE STUDY

2.1. Co-current gas-liquid flow pattern in vertical pipes

Due to the different physical properties among gas and liquid, various flow configurations are performed for the vertical two-phase flow. The specific behaviors of each gas-liquid mixture are strongly depended on the flow pattern characteristics. Ghiaasiaan (2008) defined some factors which are able to contribute in flow morphological variations, including:

a) Difference of each phase density

   Each phase has a different respond to forces acting on the mixture flow, such as gravity and centrifugal force.

b) Deformability of the gas–liquid interphase

   This often occurs as the results of incessant coalescence and breakup processes.

c) Surface tension forces.

   The existence of surface tension force keeps to maintain each single phase from the phase dispersal.

Additionally, flow regime and its transitions are strongly affected by the tube geometric attributes. The important attributes involve tube orientation - affiliated to size and shape of the channel, gravitational vector, aspect ratio (comparison of the tube length to its diameter), and any features that may cause flow disturbances. Otherwise, liquid properties also contribute to the formation and the transitions of flow regime, including surface tension, liquid viscosity, and liquid-gas density ratio (Ghiaasiaan, 2008).

There are four possibilities of flow pattern for gas-liquid two-phase flow inside a vertical pipe. Based on the interfacial direction of two-phase, gas and liquid flow along vertical pipe are divided into two configurations: co-current and counter-current flow. It is important to be noted that the gas downward and liquid upward of counter-current flow case is impossible to be occurred. This present study is only focussing on the co-current upward flow pattern. The co-current gas-liquid in a

vertical pipe are divided into two-cases base on the flow direction. When the mixture of gas and liquid co-currently moves toward the top of a vertical pipe, the upward flow is obtained. Otherwise, the downward flow occurs when gas and liquid move down along a vertical pipe. Typical of gas-liquid flow pattern in vertical pipe is well summarized in Figure 2.1.

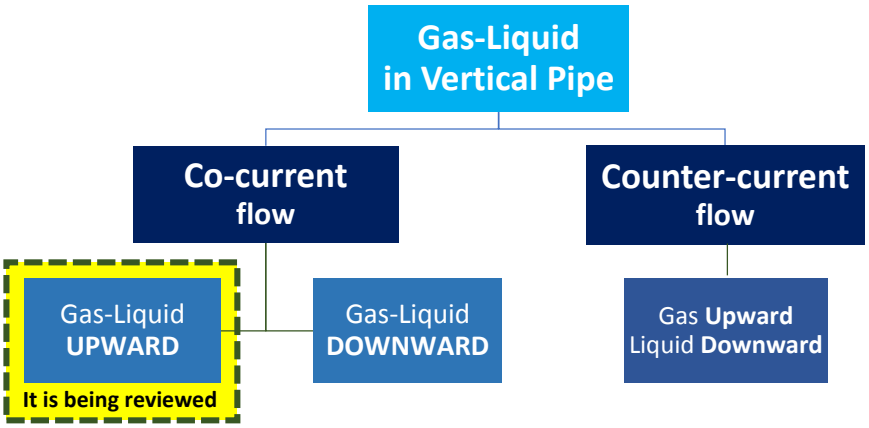

Figure 2.1. Possibilities of flow pattern for gas-liquid vertical flow

Classification of flow pattern for co-current upward flow have been proposed by some investigators, for instance Hewitt and Roberts (1969), Hewitt and Hall-Taylor (1970), and Taitel et al. (1980). The previous studies explained each flow configuration and produced flow pattern maps for each case. In general, four types of flow pattern are classified, as well stated by Hewitt and Hall-Taylor (1970) and Taitel et al. (1980), namely bubbly flow, slug flow, churn flow, and annular flow. Based on Taitel et al. (1980), there are four flow pattern basics of co-current upward flow. Visualization of the flow configurations for co-current upward gas-liquid flow are shown in Figure 2.2. A brief description of each flow pattern are described as follow:

1) Bubbly flow

When the gas-phase is uniformly distributed as the discrete bubbles in a continuous liquid phase.

2) Slug flow

The pattern is characterized when most of the gas-phase form a large bullet shaped bubble with diameter of an almost equal to the pipe diameter. They move

uniformly upward and are sometimes designated as "Taylor bubbles". There are continuous separations, called as "liquid slug" between each Taylor bubble which contain small gas. When the Taylor bubble moves upward, a thin liquid film, located between Taylor bubble and pipe wall, flows downward in the form of a thin falling film.

3) Churn flow:

This regime has an almost similar characteristics with slug flow, but it is much more chaotic, frothy and disordered. Shape of the Taylor bubble becomes narrow and distorted. A high local gas concentration in the slug repeatedly destroys the continuity of the liquid in the slug among the Taylor bubbles. Liquid slugs are fallen and accumulated, forms a bridge and is again lifted by the gas, and has oscillatory motion in alternating direction. Some observers refer to a froth flow pattern for higher liquid and gas rates where the system appears more finely dispersed.

4) Annular flow:

Annular flow is characterized by the continuity of the gas phase along the pipe in the core. The liquid phase moves upwards partly as wavy liquid film and partially in the form of drops entrained in the gas core. When the entrained phase is in the form of large lumps or "wisps", an annular flow has been described as a wispy-annular pattern. Terms of "froth", "mist" or "semi-annular" flow patterns have also been used to describe the churn and annular patterns.

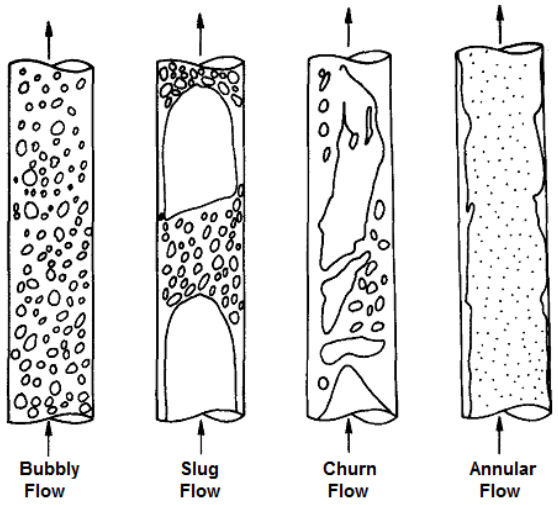

Figure 2.2. Flow patterns visualization for co-current upward (Taitel et al., 1980)

The flow pattern maps show the flow pattern classification depend on the fluid properties and gas-liquid superficial velocities as well. There are various flow pattern maps for co-current upward flow. Among them, Hewitt and Roberts (1969) map use the mass-flux to classify each flow pattern. The maps is presented in Figure 2.3 (a). Moreover, gas and liquid superficial velocities were used by Taitel et al. (1980) to form a flow pattern map for air-water co-current upward flow inside about 50 mm pipe diameter, presented in Figure 2.3. (b).

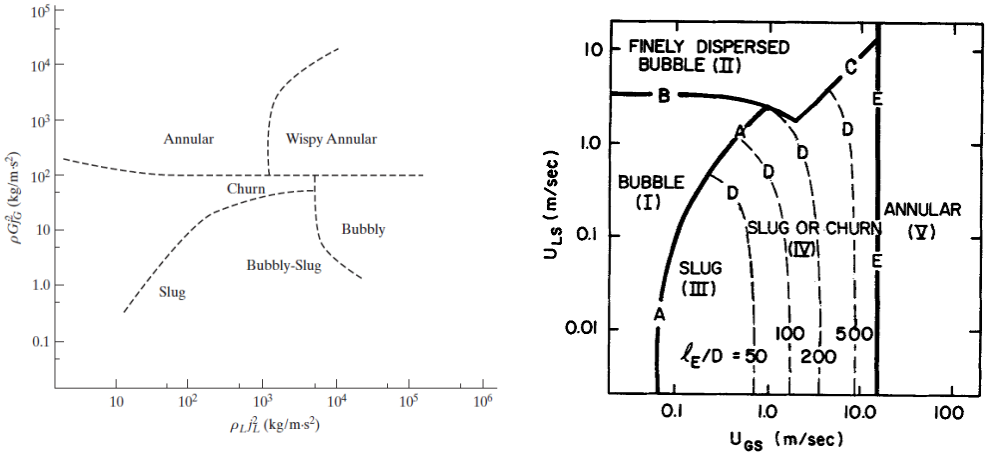

(a) (b)

Figure 2.3. (a) Flow pattern map for upward flow (Hewitt and Roberts, 1969); (b) Taitel et al. (1980) flow pattern map

2.2. Slug flow transition

Transition from the condition of dispersed bubbles to slug flow requires a process of agglomeration or coalescence (Taitel et al., 1980; Lucas and Krepper, 2007; Krepper et al., 2008). In detail, Taitel et al. (1980) attributed that an increase of gas flow rates in low liquid flow rates contributes to increase the bubble density, the closer bubble spacing, and the bubble coalescence rate. At higher number of dispersed bubble collisons, the rate of agglomeration increases rapidly. Thus, the transition of dispersed bubble to slug flow is obtained. Otherwise, at higher liquid flow rates, the turbulent fluctuations are able to cause breakup of the agglomerated bubbles.

Essentially, the dispersed bubble regime can be maintained if the breakup, influenced by the turbulent fluctuations, sufficiently intense to prevent re-

coalescence of the bubbles (Taitel et al., 1980). The movement of a bubble is influenced by the forces acting on it. A complex interaction between the bubble forces leads the flow evolution along the pipe, inducing a lateral bubble migration, bubble coalescence, and bubble breakup (Krepper et al., 2008). Hence, the interaction affects the bubbly to slug flow transition. A transition model from bubbly flow to slug flow is shown in figure 2.4.

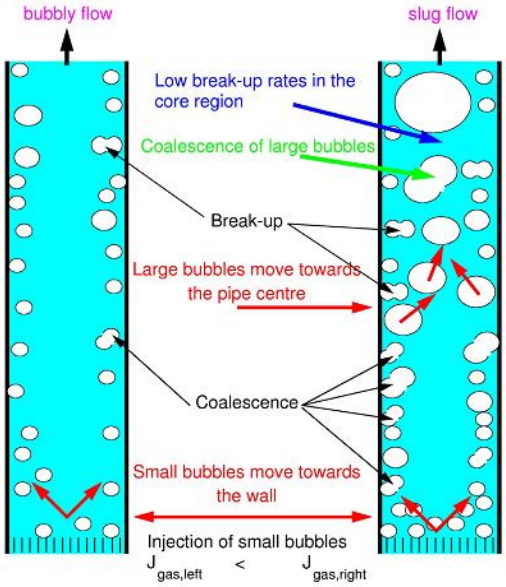

Fig 2.4. Stable bubbly flow and transition to slug flow
(Lucas and Krepper, 2007; Krepper et al., 2008)

As shown in Fig. 2.4, A number of small bubbles (with diameter less than 5.8 mm) are injected at different gas superficial velocity. In the low gas superficial velocity (left side), a stable bubbly flow is ensued, producing the equilibrium of bubble coalescence and breakup. The local gas fraction in the wall region is larger than the average gas fraction, but it is still low. In case gas superficial velocity is increased (right side), the balance of bubble coalescence and breakup is switched over into larger bubble diameter (Krepper et al., 2008). The tendency of coalescence is also strengthened by Prince and Blanch (1990) who also revealed that breakup rate is only proportional to the bubble density while coalescence rate increase with the square of the bubble density. Due to the larger rate of coalescence, the larger bubbles thus migrate into the pipe center region which is also affected by lift and wall-lubricated forces. Lucas and Krepper (2007) and Krepper et al. (2008) stated

that if there are sufficient large bubbles generated by coalescence in the wall region, some of them can reach the core region without further breakup. Due to the characteristics of core region: lower dissipation rate of turbulent energy and lower shear rate, the bubbles are able to grow into larger and elongated size (Taylor bubble) by the series of coalescence with lower breakup rates.

On the other hand, the presence of spherical cap bubbles also can be attributed as an initial trait of bubbly to slug flow transition. Radovcich and Moissis (1962) conducted that bubble to slug flow transition is identified by the collisions among the small bubbles and coalescence afterwards, then shift to be a spherical cap bubbles, hence producing a long bubbles that have a similar length in at least one-diameter to the pipe diameter, known as Taylor bubbles.

Taitel et al. (1980) also stated that bubbles begin to deform and have a zig-zag motion with major randomness (collide and coalesce), establishing the larger individual bubbles with a spherical cap. By much more agglomeration and collision, slug flow is formed. In addition, this point is obtained for bubbles which move inside a tube with diameter above 15 mm (for air-water at low-pressure). A spherical cap bubble is the larger individual bubble which has a similar shape with Taylor bubble but with diameters smaller than the pipe.

The critical void fraction (α_c) is corresponded to describe the collision and thus the coalescence frequencies of the bubble-slug transition. Griffith and Synder (1964) proposed the α_c from the experimental work which ranging from 25 to 30%. Taitel et al. (1980) suggested the criterion of bubble-slug flow transition was that gas void fraction reaches 25%. Nevertheless, Omebere-Iyari et al. (2007) also stated that the critical void fraction was depended on the ratio of bubble to tube diameter. The larger ε_c comes from the smaller ratio.

In addition, the several models of slug to churn flow transition in vertical upward pipe has been proposed by several investigators. Jayanti and Hewitt (1992) explained the four major models by summarized them as follows:

(a) Entrance effect mechanism (Dukler and Taitel, 1986; Taitel et al., 1980).

Churn flow comes as an oscillatory movement of the rising and collapsing

liquid slugs in the region between the entrance and the point where stable slugs are formed.

(b) Flooding mechanism (McQuillan and Whalley, 1985; Nicklin and Davidson, 1962; Wallis, 1969; Govan et al., 1991). Slug to churn flow is associated by a flooding of the liquid film around the Taylor bubble. Due to the formation of large interfacial waves, the liquid film in countercurrent flow of gas and liquid breaks down

(c) Wake effect of Taylor bubble (Mishima and Ishii, 1984). The transition is attributed by a strong wake effects due to the very short liquid slug and very close gap of Taylor bubbles within each other, potentially destabilize and destroy the liquid slug. Churn flow occurs when the mean void fraction in the pipe ($\overline{\alpha}_{avg}$) has a greater value than the average void fraction over the Taylor bubble region ($\overline{\alpha}_{TB}$).

(d) Slug collapse by bubble coalescence mechanism (Brauner and Barnea, 1986). Formation of highly aerated liquid slugs causes the gas entrainment inside the liquid slugs and the bubbles is still kept dispersed inside due to the turbulence of the slug flow. A transition occurs if the void fraction inside the liquid slug is greater than a value of 0.52. In this circumstance, it is very difficult to avoid bubble collison and coalescence between the adjacent bubbles.

Through their study, Jayanti and Hewitt (1992) suggested that the flooding model is applicable at low liquid flow rates, while the bubble entrainment model give good results at high liquid flow rates. They also proposed an improvement of flooding model of McQuillan and Whalley (1995) by substituting an empirical correlation and consiedering the effect of falling film length on flooding velocity.

2.3. Brief explanation of bubbly flow

In this present section, general explanation of bubbly flow is presented as the basic understanding of gas-bubble dynamics. Therefore, only a brief explanation Moreover, a deeper explanation of bubble formation and bubble rise velocity has been written in the form of review by Kulkarni and Joshi (2005). Moreover, bubble

coalescence and breakup mechanism Liao and Lucas (2010, 2011), respectively. These reviews give a models and development of coalescence and breakup mechanism.

2.3.1. Basic terminology

In the bubbly flow, gas-phase dispersedly flow into small size bubbles inside liquid phase. According to Clift et al. (1978), shape of the bubbles in are generally classified into these categories. These are spherical, ellipsoidal, and elongated bubbles, as well described as follow:

a) Spherical bubbles

The spherical shape is obtained when interfacial tension and-or viscous forces are more important than inertia forces.

b) Ellipsoidal bubbles

Bubbles which have oblate with a convex interface around the entire surface are classified. It is common for this bubble type for having a periodic dilations or random wobbling motions. Preview of the bubble shape is depicted in Figure 2.5.

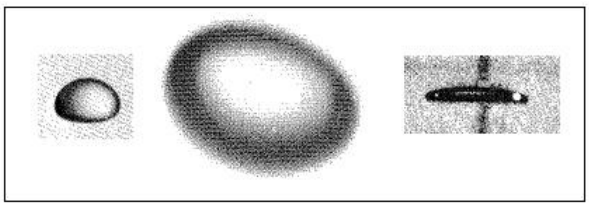

Figure 2.5. Examples of ellipsoidal bubbles (Clift et al., 1978).

c) Spherical-cap or ellipsoidal cap

These term are suitable for large bubbles tend to adopt flat or intended bases and to lack any semblance of fore and aft symmetry. This shape is looked like a segment cut from sphere or oblate spheroid of low eccentricity. Large spherical or ellipsoidal caps may trail thin envelopes of dispersed fluid, referred as “skirt”. These kind of shapes are previewed in Figure 2.6.

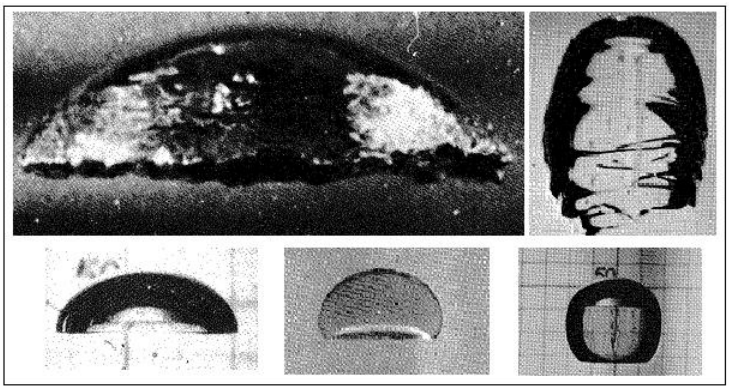

Figure 2.6. Examples of spherical or ellipsoidal cap bubbles (Clift et al., 1978).

d) Taylor bubble or slug flow regime

When a bubble sufficiently large, it is able to fill most of the pipe cross-sectional section. The large bullet shaped or elongated bubble is often defined as "Taylor bubble" after the findings of Dumitrescu (1943) and Davies and Taylor (1950). The presence of Taylor bubble can be treated as the existence of slug flow regime. Visual image of this bubble type is presented in Figure 2.7.

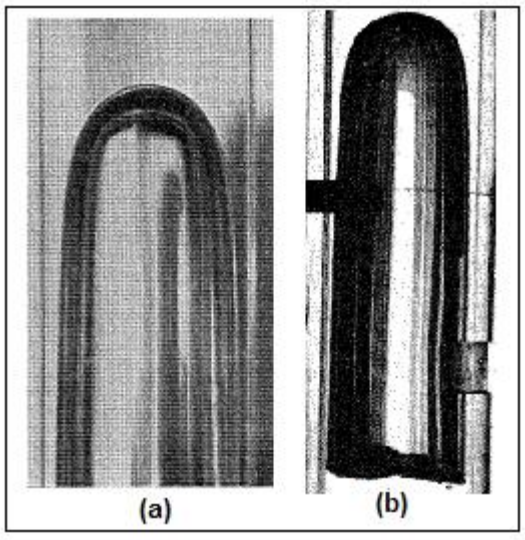

Figure 2.7. Examples of Taylor bubbles or slug flow regime.
(Taken from: (a) Davies and Taylor, 1950; (b) Clift et al., 1978).

The characteristics of gas bubble, such as their shape and size depend on the physical properties of gas and liquid, represented in non-dimensional number of Morton, Eötvös, and Reynolds numbers, summarized in Table 2.1.

Table 2.1. Dimensionless group definition (Mayor, 2007; Araújo et al, 2013)

Number	Symbol	Definition	Representation
Eötvös number	Eo	$\frac{(\rho_L - \rho_G) g D^2}{\gamma}$	Bouyancy vs. interfacial forces
Morton number	Mo	$\frac{g\mu^4(\rho_L - \rho_G)}{{\rho_L}^2 \gamma^3}$	Viscosity vs. surface tension
Reynolds number	Re	$\frac{(\rho_L - \rho_G) U D}{\mu}$	Inertia vs. viscosity

Clift et al. (1978) also proposed a correlation for determining the bubbles aspect ratio in liquid. It is shown in Figure 2.8. According to this figure, the aspect ratio, which represents bubble shape, depends on both Eötvös and Morton numbers. Hence, various shapes such as ellipsoidal and spherical cap regions are classified.

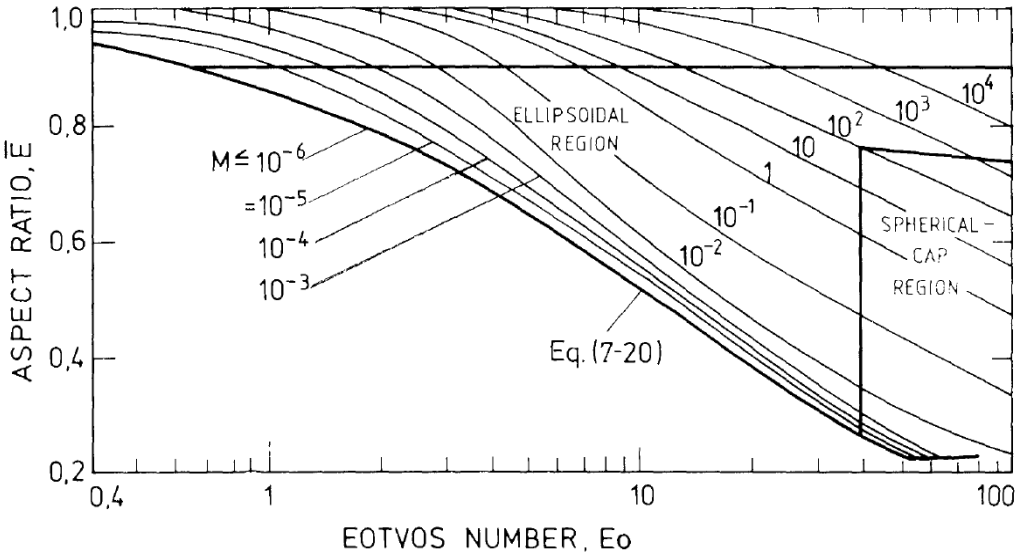

Figure 2.8. Correlation for bubble aspect ratio in liquid phase (Clift et al., 1978)

In case of low Morton number, for instance air-water, it is common to use Wellek et al. (1966) correlation which stated in Equation 2.1. The equation is relevant for Eo < 40 and M ≤ 10^{-6}.

$$\bar{E} = \frac{1}{(1 + 0.163\, Eo^{0.757})} \tag{2.1}$$

Distribution of dispersed bubbles shows a specific pattern. Commonly, bubbles are distributed and dispersed homogeneously inside the pipe, as well stated by Taitel et al. (1980) for high liquid flow rates. The turbulent fluctuation in high liquid velocity prevents the bubble possibility to be agglomerated into larger size. It also causes the bubbles dispersedly scattered inside liquid flow. As the result, bubbles dispersed homogeneously. Contrarily, in low liquid velocity, Serizawa et al. (1975) conducted that in general, bubbles are lied on the near pipe wall, so the peak of void fraction distribution graph is located near wall periphery. The lateral distribution profiles are also influenced by the bubble size. The prevoius studies were focussed on the relationship between bubble size and lateral distribution, such as Sekoguchi et. al., (1974), Zun, (1987), and Tomiyama et al. (1995). They did experiments for different bubble size and observed the bubble movement. As the results, a lift force correlation was determined.

2.3.2. Bubble forces

Bubble motion and dynamics are influenced by the bubble forces. In vertical pipe, the bubbles move not only in straightly vertical direction but also lateral even angular directions. These phenomena is strongly related with forces acting on the bubbles. Figure 2.9 represents the bubble forces which create possibilities of bubble motion in vertical and lateral directions as well.

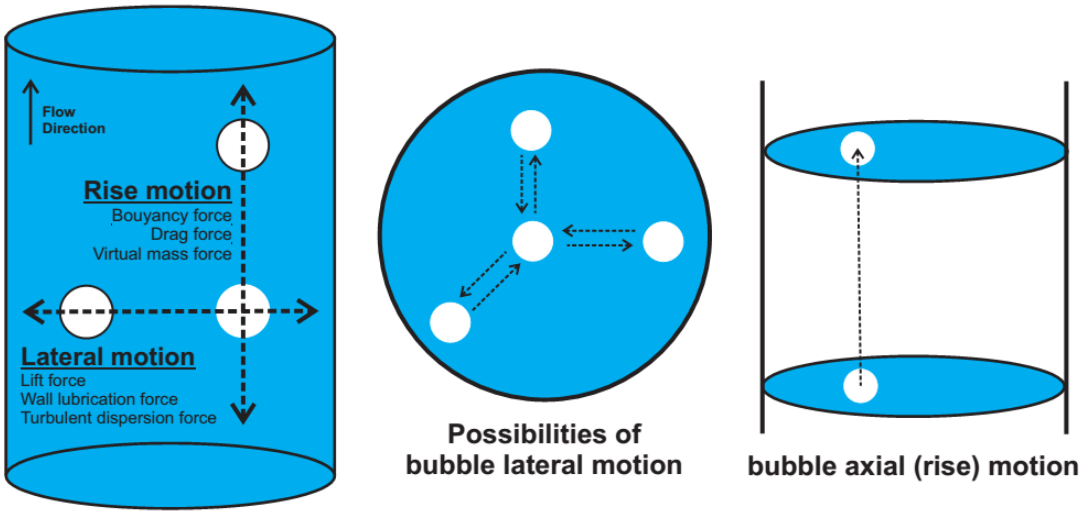

Figure 2.9. Schematic diagram of forces acting on the bubble and bubble motions.

Lucas and Krepper (2007) summarized the important forces acting on a bubble, such as buoyancy, drag, virtual mass (rise motion), lift, wall lubrication, and turbulent dispersion (lateral motion) forces. Those forces are influenced by the important physical parameters, represented as the dimensionless number such as Reynolds, Eötvös, and Morton number. Definition of each bubble forces is explained as follows:

a) Forces acting on bubble axial motion

1. Drag force

Drag force affects the axial velocity of the bubble by reflecting the resistance effects of bubble relative motion to the liquid around it. Drag force gives a limit to the bubble axial motion. When bubbles move with constant velocity it means drag force in balance with buoyancy weight of the bubble. The Schiller-Naumann (1933) equation of drag force per-unit volume are reprsented as follow:

$$\vec{F}_D = \frac{3}{4d_b} C_D \rho_l \alpha \left|\vec{w}_g - \vec{w}_l\right| (\vec{w}_g - \vec{w}_l) \tag{2.2}$$

Where C_D is the drag coefficient, proposed by Ishii and Zuber (1979), as follows:

$$C_D = \frac{24}{Re}(1 + 0.1Re^{0.75}) \tag{2.3}$$

2. Virtual mass force

Virtual mass force reflect as the replacement of the corresponding amount of fluid due to the bubble movement. In bubble acceleration or de-acceleration, a replacement of the corresponding amount of fluid is necessary and this force is given in terms of the relative acceleration of the phases.

$$\overrightarrow{F_{VM}} = C_{VM} \rho_l \alpha \left(\frac{d\overrightarrow{w_g}}{dt} - \frac{d\overrightarrow{w_l}}{dt}\right) \tag{2.4}$$

Where C_{VM} is shape and particle dependence with the value of 0.5 for single spherical particle. This force is also recognized as added mass.

3. Bouyancy forces

An important force which positively support the axial direction of bubble vertical upward motion. Bouyancy force is an interaction between bubble volume, weight, density, and gravity, as well represented in equation:

$$F_{Bou} = \rho g V \tag{2.5}$$

b) Forces acting on bubble lateral motion

1. Lift forces

The interaction of the bubble with the shear field of the liquid is represented in lift force. The force works due to difference of liquid velocity between the sides of the bubble(Patmonoaji, 2013). This difference of velocity also creates a difference of pressure between both sides thus create a force of bubbles from lower velocity to higher velocity. Lift force per unit volume is written as:

$$\overrightarrow{F_L} = -C_L \rho_l \alpha \left(\overrightarrow{w_g} - \overrightarrow{w_l}\right) \times rot\left(\overrightarrow{w_l}\right) \tag{2.6}$$

Experimental and numerical investigations from Tomiyama (1995, 1998) showed that if a considerable deformation of the bubble occurs, the direction of the lift force changes its sign. For flows of water-air at normal condition, coefficient of lift (C_L) changes its sign at a bubble diameter of d_b = 5.8 mm. Hence, Tomiyama (1998) correlation for lift-coefficient is presented as follow:

$$C_L = \begin{cases} \min[0.288\tanh(0.121Re), f(Eo_d), & for\ Eo_d < 4 \\ f(Eo_d), & for\ 4 \geq Eo_d \geq 10 \\ -0.27 & for\ Eo_d \geq 10, \end{cases} \tag{2.7}$$

Where,

$$f(Eo_d) = 0.001105Eo_d^3 - 0.0159Eo_d^2 - 0.0204Eo_d + 0.474 \tag{2.8}$$

Equation uses the modified Eötvös number, as follow::

$$Eo_d = \frac{g\left(\rho_l - \rho_g\right)d_H^3}{\sigma} \tag{2.9}$$

Here, the maximum horizontal bubble diameter is:

$$d_H = d_b \sqrt[3]{1 + 0.163Eo^{0.757}} \tag{2.10}$$

2. Wall force

Bubble oscillation movements are affected by competition and fluctuation of lift and wall forces. The presence of wall force reflects the resistance for bubble tends to move toward the pipe wall and bubble collides the wall (Patmonoaji, 2013). This force phenomenon was described in detail by Antal (1991), represented in the equation:

$$\overrightarrow{F_W} = -\frac{\rho_l}{r_b}\alpha(C_{W1} - C_{W2}\left(\frac{r_b}{y}\right))w_{rel}^2\overrightarrow{n_r} \quad (2.11)$$

where C_{W1} = -0.104 and C_{W2} = 0.147.

This force works by creates a hydrodynamic force due to asymmetry effect that swept bubble away from the wall and resist it from a collision to pipe wall. If bubble loctaed near pipe wall, the fluid drainage around bubble changes. The no-slip nature of near wall area causes a slower rate of fluid drainage (among bubble and wall) that increase drainage rate of the opposite side (Patmonoaji, 2013).

3. Turbulent dispersion force

Liquid velocity plays an important role to generate the turbulent fluctuation and the fluctuations yield the turbulent dispersion force. This force affects the sharpness of wall peak of radial gas fraction profile. Turbulent dispersion force tends to disperse the bubble to move away from pipe center in case of the negative lift force coefficient (Patmonoaji, 2013). Moreover, Lahey et al. (1993) proposed an equation to explain this force. Equation of turbulent dispersion force is presented below:

$$\overrightarrow{F_{TD}} = -C_{TD}\rho_l k_l \nabla\alpha \quad (2.12)$$

Where the coeeficient of C_{TD} = 0.1

Equilibrium of bubble lateral forces in radial direction influences the radial gas fraction distribution. However, the higher gas flow rates is possible to cause the chaotic movement even vortices that superpose the effect of bubble forces, therefore bubble forces are no longer qualified to be used as parameter for bubble movement (Patmonoaji, 2013). The condition acts as a trigger for more frequent

bubble coalescence. Tomiyama (1995) also mentioned that the larger bubble tends to move toward core area of the pipe since the coefficient of lift force change its sign. During the coalescence process, bubbles grow to be larger and they are able to occupy the total cross sectional area along axial direction. When this type of bubble exists, gas – liquid flow has transformed into slug flow.

2.3.3. Bubble rise velocity

Bubble motion in axial direction is ruled by the equilibrium between buoyancy, drag, virtual mass which consider the bubble weight itself. Kulkarni and Joshi (2005) reported factors affected bubble rise velocity. There are bubble characteristics (shape and size), fluid properties (density, viscosity, surface tension, solution concentration, and interfacial density difference), direction of liquid motion, and operating conditions (pressure, temperature, gravity).

Based on Clift et al. (1978), there are various shapes of gas bubbles including sphere, oblate ellipsoidal, spherical cap, or cylindrical. The different shapes affects the terminal or rise velocity. Commonly, small bubbles are in the form of sphere shape, so they retain their rigid spheres and also resist with agglomeration process. In general calculation, the bubble type is estimated as bubble with diameter less than estimation from Broadkey (1967), shown in Equation 2.13.

$$d_{crit} = [\frac{0.4\gamma}{\Delta\rho g}]^{1/2} \quad (2.13)$$

There are differences rise mechanism for bubbles flow in stagnant and flowing liquid. The term of terminal velocity (or also recognized as drift velocity) is referred to a velocity when bubbles are accelerated until it reaches maximum velocity. It can be also stated as the bubble velocity due to buoyancy. Rise movement of bubble is also influenced by bubble forces. The force balance among buoyancy and drag forces yields a different drift velocities for bubble in different sizes. The larger bubble has a higher bouyancy force than small size bubble, so that the larger bubble has a higher drift velocity. However, analysis of the terminal velocity is common based on the calculation for small gas bubbles as reported by Harmathy (1960). For the relatively small bubbles, he stated that terminal velocity is independent with

bubble size and effect of liquid properties more dominant. Taitel et al. (1980) conducted that for bubble with diameter larger than critical diameter of Broadkey (1967), equation from Harmathy (1960) can be implemented. Therefore, an equation to calculate the terminal velocity of small bubble in stagnant water is obtained from the Harmathy's proposed correlation, as presented in Equation 2.14, as follow:

$$U_B = 1.53\left(\frac{g\Delta\rho\gamma}{\rho_L{}^2}\right)^{1/4} \tag{2.14}$$

Clift et al. (1978) also performed the relationship between bubble size and terminal velocity, both for pure and contaminated water, shown in Figure 2.10. In this study, there were spherical, ellipsoidal, and spherical cap bubble. One notable point from this curve is shown that the effect of contaminant on terminal velocity is only presented in ellipsoidal bubble regime.

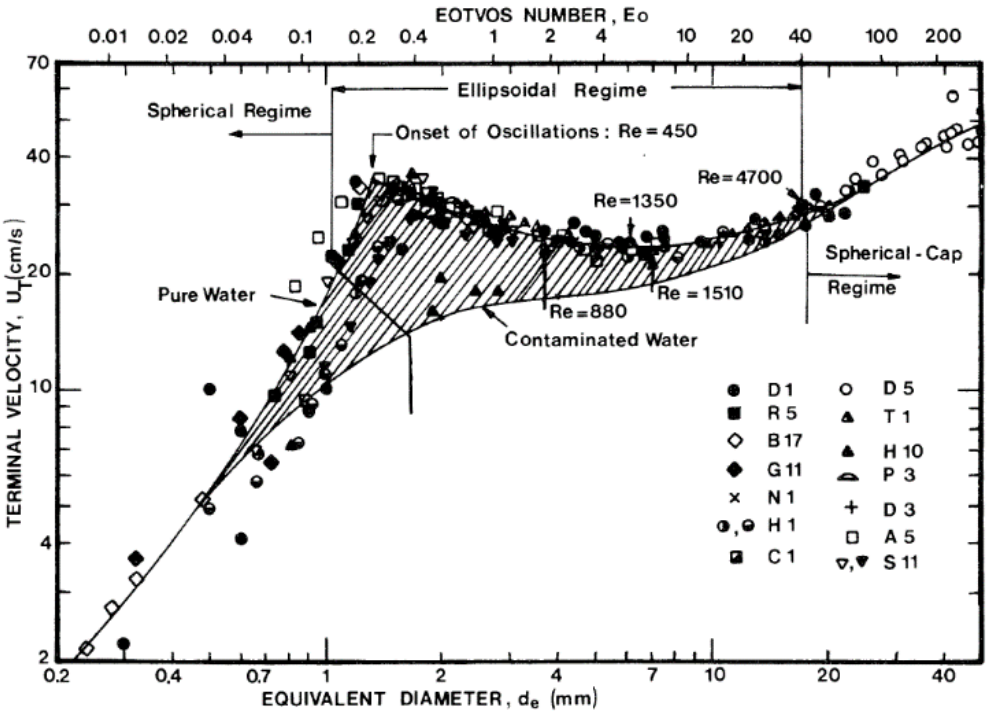

Figure 2.10. Relationship of terminal velocities and bubble size in different liquid phase (Clift et al., 1978)

2.4. Co-current upward slug flow

Slug flow is a part of gas-liquid two-phase flow regime characterized by the presence of large, long-bullet shaped gas bubble called as the elongated bubble or Taylor bubble. It can also be interpreted as the gas-slug. Due to very low density and velocity of gas-phase, the pressure difference among the bubble-nose and the tail is assumed to be small enough. Thus, the inner bubble surface is also be considered as isobaric (Orell and Rembrand, 1986).

2.4.1. Basic terminology

Slug flow is defined by the presence of large bullet-shaped bubbles, occupied in almost total area of the cross-sectional pipe and elongates for a specific length, generates a downward thin film, called as falling film region. (Taitel et al. 1980, Fernandes et al. 1983, Orell and Rembrand, 1986, Fabre and Liné, 1992). The particular flow structure gives the specific phase distribution and affects the flow behavior of each phase inside. Among the prominent features of slug flow are intermittent, irregularity, and chaotic movement. Many factors that can influence shape and hydrodynamics of vertical upward slug flow. One of them is mentioned by Zukoski (1966) that conducted that the inclination of the tube decreases, the bubble shape gradually changes and the when the tube diameter is increased, the bubble propagation rate also increase.

According to Fabre and Liné (1992) on their review, two basic approaches namely “semi-mechanistic model” and “unit-cell model” were developed at the beginning of vertical upward slug studies. The methods become a basic of the subsequent analysis. The first model worked by simplifying the slug intermittency to the periodicity, resulted an equivalent cell consisting of a long bubble (approached by a long cylindrical capsule) and a liquid slug (treated as either single phase or homogeneous bubbly flow). Griffith and Wallis (1961), Nicklin et al. (1962), who set about the long bubble motion. Next, the second model was initiated by Wallis (1969) for predicting pressure gradient from the contribution of liquid slug, main bubble body, and the end of the long bubble. The model was also developed by Fernandes et al. (1983) to describe slug flow structure in vertical

upward. An involvement of the statistical model was presented by Line (1983) which namely statistical cellular model.

Slug flow has a complex natures, so it was not easy to analyze and proposes a mechanistic model for this pattern. However, Fernandes et al. (1983) successfully introduced the relevant comprehensive model for slug flow. However, Mao and Dukler (1989) revealed the two shortcomings of the both Fernandes et al. (1983) and Orell and Rembrand (1986) models. First, the models did not involve the prediction for Taylor bubble frequency. This shortage is then improved by the emergence of Sylvester (1987) model. Second, the dissatisfactory performance of void fraction in liquid slug (α_{LS}) model.

Moreover, Araújo et al (2013) stated that hydrodynamics environment of slug flow is affected by an interaction among gravitational, interfacial, viscous, and inertial forces. In addition, Kang et al. (2010) conducted a numerical study of Taylor bubble rising in stagnant viscous liquid. The effects of dimensionless parameters that influence the Taylor bubbles dynamics were examined. The simulation overcame that density ratio and viscosity ratio gave minimal effects to the dynamics of Taylor bubble. Moreover, higher Eötvös number and Archimedes number (Ar) resulted longer tail and wake structures. Weber number was applied to explain a sudden tail extension. Under the increase of Archimedes number, the final shape of Taylor bubble was also changed into shorter and fatter bubble. As the effects, reduction of film thickness and wall shear stress occur.

Investigations on the slug flow characteristics are still become a hot topics because the unique nature and irregularity of slug flow. Besides, the presence of other regions in slug flow, caused by the dynamics of Taylor bubble, attracts the scholars to reveal the truly characteristics of them. Some studies were focused on development of measuring technique to determine flow properties. The Photochromic Dye Activation (PDA) method was introduced by Kawaji and his group, by several publications to obtain velocity profiles in slug flow. De Jesus et al. (1995) and Kawaji et al. (1997) showed results of liquid velocity profiles around Taylor bubble. Ahmad et al. (1998) also conducted liquid film and near wake region velocity profiles for single and pairs of Taylor bubbles. On the other hand, Particle

Image Velocimetry (PIV) was also used to track the profiles. For instance, Polonsky et al. (1999a) showed the velocity fields in front area of a Taylor bubble in both stagnant and flowing water. Van Hout et al. (2002) determine the velocity characteristics by analyzing the velocity field a single Taylor bubble in stagnant water. Moreover, the study by Shemer et al. (2005) also implemented PIV to obtain liquid profiles around Taylor bubble in laminar and turbulent flows. The velocity field in wake region has also conducted by Shemer et al. (2007) in various Reynold numbers and different pipe diameters. However, those above mentioned studies were mainly focus to detect and to analyze the liquid behavior, as well as the liquid velocity and liquid profiles. There were still rare studies which discuss about gas-bubble velocity or properties profiles in various region of slug flow. The understanding of bubble individual properties can give a good contribution in the studies about vertical slug flow. On the other hand, turbulence in the liquid slug is still remains as an interesting issue. According to Fabre and Liné (1992b), turbulence in the liquid slugs is dependent in the turbulence in the falling film region as wake on the length of the slugs.

2.4.2. Hydrodynamics of slug flow

The complex natures of slug flow arise from its particular structure, which is neither periodic in space nor in time (Fabre and Liné, 1992). Consequently, some focus should be focused on the phase distribution between gas and liquid, characteristics of long bubble and liquid slug, hydrodynamics, and the turbulence inside liquid slug. Generally, in order to explicate the interfacial problems of two-phase flow, four major approaches are usually used. These are the homogeneous model, the two-fluid model, the drift-flux model, and the flow pattern-based model (Sylvester, 1987). Due to the chaotic and rigorous movement of slug flow, a simplification of Hydrodynamics models of slug flow has been proposed by Fernandes et al. (1983), Orell and Rembrand (1986), and Sylvester (1987).

A model for ideal co-current vertical upward slug flow, known as “unit cell” concept, has been proposed by Fernandes et al. (1983). This model treats the slugs as equilibrium, isothermal, low-pressure and steady flow with axisymmetric and

one-dimensional forms. A schematic preview of this model is depicted in Figure 2.11.

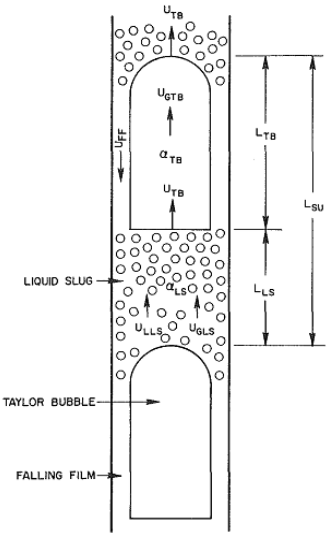

Remarks:

L_{SU} Length of the slug unit
L_{TB} Length of the Taylor bubble
L_{LS} Length of the liquid slug

α_{SU} Void fraction of the slug unit
α_{TB} Void fraction of the Taylor bubble
α_{LS} Void fraction of the liquid slug

U_{TB} Velocity of the Taylor bubble
U_{GTB} Velocity of the gas inside the Taylor bubble
U_{FF} Velocity of the liquid film around Taylor bubble

U_{GLS} Velocity of the gas in the liquid slug
U_{LLS} Velocity of the liquid in the liquid slug

Figure 2.11. A slug unit
(picture taken from Sylvester (1987) – with modification)

However, the previous work of Mao and Dukler (1989) stated that the models by Fernandes et al (1983) and Orell and Rembrand (1986) have two shortcomings, the Taylor bubble frequency has not involved in both models and the proposed models of void fraction. Another explanation from Fabre and Liné (1992), the prediction of the average void fraction both in the long bubbles and the liquid slugs involves (a) the distinct momentum interaction in separated flow and bubbly flow and (b) the phase exchange between the long bubbles and liquid slugs.

An explanation of wall-shear stress has been conducted by Mao and Dukler (1989). The found that at the top of the liquid slug, the wall-shear stress value is positive due to the penetration of falling film into the liquid. But, this value gradually drops into negative as the influence of the upward flow of liquid in the body of liquid-slug. The sign of τ_w changes twice in around the Taylor bubble nose (where the falling film is formed) and at the top of liquid slug. The initiation of flow reversal point is located in small distance below the bubble nose by the increase τ_w.

2.4.3. Shape and characteristics of Taylor bubble

An early study of Davies and Taylor (1949) conducted that a round shape of lenticular shape of Taylor bubbles is influenced by the pressure distribution around them. Due to the movement of large bubbles, a layer running down around the bubble recessive area. Dumitrescu (1943) investigated analytically on the movement of a single large elongated bubble in a stagnant water by attempting potential flow theory. He divided shape of the bubble into the nose region and the film region. From the visual observation, Ahmad et al. (1998) conducted that the Taylor bubble movement is influenced by the large waves flow. These waves may cause lateral motion of the Taylor bubble which is alternately pushed side to side changing the film thickness.

When a Taylor bubble moves, the liquid-phase around it is penetrated, inflicts a movement of falling film between the long bubble and the pipe wall. A liquid jet-like is injected into the liquid region behind the elongated bubble region, as a result of the generation of that falling film. Figure 2.12 illustrates the mechanism of the falling film movement which generates the entrainment behind the Taylor bubble. Moreover, it also shows the small bubble coalescence near nose.

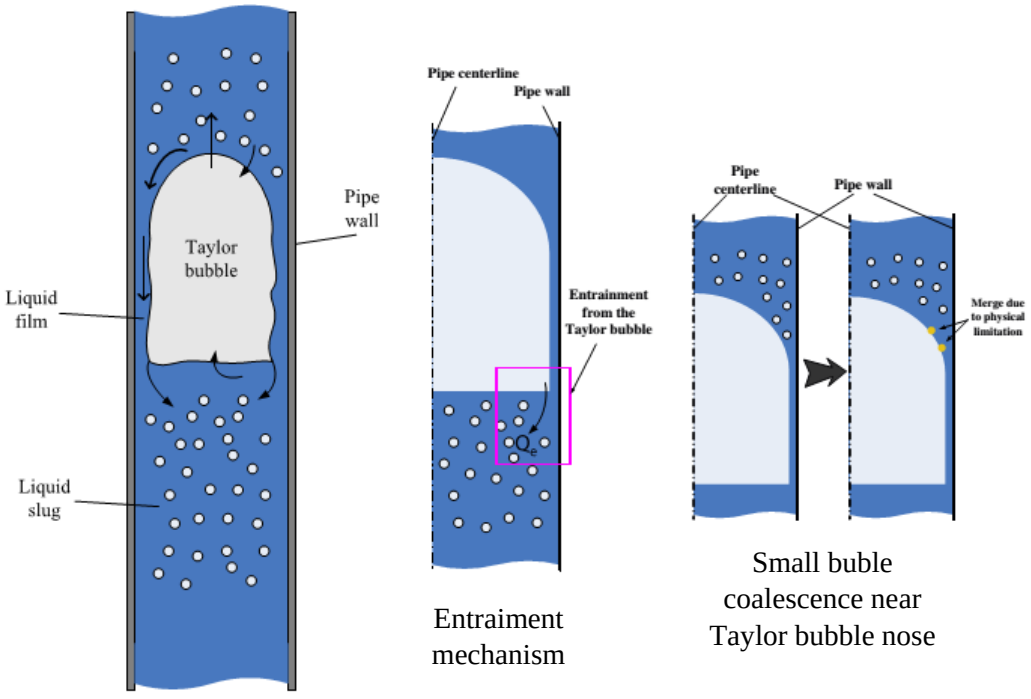

Figure 2.12. Preview of unit cell model for slug flow (Yan and Che, 2011)

Since the presence of falling film, the small bubbles tends to decelerate, shoved toward the pipe wall, and trailed by the falling film region at the side of the Taylor bubble. Due to the geometry limitation, Yan and Che (2003) stated that for the most part of those small bubbles are arduous to pass thru the thin liquid film. This reason causes a coalescence between them with the elongated bubbles that is transpired at near of the Taylor bubble nose region.

Basically, shape of Taylor bubble nose is rounded-oval. However, it can be formed in various shapes, depend on the surroundings ahead the Taylor bubbles. Moreover, during the Taylor bubble motion, the nose tip can be move straightly following the main axis of pipe center or tends to pipe wall (swaying motion). Reason of the swaying motion are also strengthened by Mayor et al. (2008) who conducted that the nose follows the fastest portion of fluid ahead, resulted in continuous elongations and relaxations of the bubble shape. Moreover, Taylor bubble shape is varying and the bubble nose sways from one to other sides because most dispersed bubbles in the liquid slug are consumed by the elongated bubbles, but some of them penetrate into the liquid (Shemer et al., 2003)**.** The small bubble coalescence to nose mechanism has been explained by Yan and Che (2011) as the result of re-coalesces back action due to out-of-controlled wake and vortices in liquid slugs. Since the 1960's, properties of Taylor bubble have been investigated, focusing on the topology, structure, and factors which contributed. Barnea et al. (1993) proposed the correlation for Taylor bubble and liquid slug length. It was strengthened by Khatib and Richardson (1984) on the bubble length.

In the previous studies, there were still rare studies which firmly mention the quantitative definition of a Taylor bubble. Mainly, those only stated the qualitative description about large and elongated bubble. Mandal et al. (2007) mentioned that Taylor bubble an elongated bubble that has length exceeds 1.5 times the tube diameter or its diameter is greater than 60% of the tube diameter, as well supported by the studies from Zukoski (1966) and Tomiyama et al. (1998). In the term of bubble equivalent diameter distribution, Taylor bubble can be defined as an elongated bubble which has an equivalent diameter more than a tube diameter (Krussenberg et al., 1999; Prasser et al., 2001; Lucas et al., 2003, 2005).

Relationship between consecutive Taylor bubbles has been presented by some researchers. Among them are Moissis and Griffith (1962), Pinto et al. (1996, 1998), Alajdem Talvy et al. (2000), Van Hout et al. (2001), Mayor et al. (2008), and Guo-dong et al. (2009). Additionally, Hasanein et al. (1996) also did an experiment in laminar regime with air-kerosene flow. Rise velocity of Taylor bubble was related to the length of separation distance in front of the preceding Taylor bubble. It can be stated that under the lower separation distance, the normalized Taylor bubble rise velocity tends to be higher. Table 2.2 mentions some correlations for the consecutive Taylor bubble. In this table, U_2 is addressed as velocity of the leading Taylor bubble whereas U_1 is velocity of the trailing one. The length of liquid slug (L_{LS}) is the separation length between the leading and trailing Taylor bubbles. Pinto et al. (1996) set a minimum stable length, called as L_{min}, when velocity of trailing bubble similar with the leading one.

Table 2.2. Correlations for the consecutive Taylor bubbles

Moissis and Griffith (1962)	$U_2 = U_1\left[1 + 8\, e^{\left(-1.06\frac{L_{LS}}{D}\right)}\right]$	(2.15)
Hasanein et al.	$U_2 = U_1\left[1 + 3\, e^{\left(-0.85\frac{L_{LS}}{D}\right)}\right]$	(2.16)
Pinto et al. (1996)	$U_2 = U_1\left[-11.4\,\frac{D}{L_{min}} + 4.24\right] for\ \frac{D}{L_{min}} < 0.24$ $U_2 = U_1\left[2.01 - 1.96\,\frac{D}{L_{min}} + 4.24\left(\frac{D}{L_{min}}\right)^2\right] for\ \frac{D}{L_{min}} > 0.24$	(2.17)
Van Hout et al. (2001)	$U_2 = U_1\left[a + 8\, e^{\left(-1.5\frac{L_{LS}}{D}\right)} + \frac{D}{L_{LS}}\right]$ $a = 1$ for narrower column; $a = 1.2$ for larger column	(2.18)
Mayor et al. (2008)	$U_2 = U_1\left[1 + 2.4\, e^{\left(-0.8\frac{L_{LS}}{D}\right)^{0.9}}\right]$	(2.19)
Guo-dong et al. (2009)	$U_2 = U_1\left[1 + 4.5\, e^{\left(-0.65\frac{L_{LS}}{D}\right)}\right]$	(2.20)

Additionally, Ahmad et al. (1998) observed by a visual study on the the successive Taylor bubbles movement in stagnant air-kerosene flow. The trailing

Taylor bubble tends to rise faster and eventually coalescence due to the the wake effect behind the leading bubble. Near the agglomeration, the trailing Taylor bubbles had larger velocity during a closer separation distance between two bubbles.

2.4.4. The Taylor bubble rise velocity

A Taylor bubble rises through stagnant liquid with a velocity which is affected by several factors. Tudose (1997) stated that the rising velocity of a bubble comes as the result of the forces acting on it, such as its own buoyancy, liquid inertia, viscosity, and surface tension. Therewith, Yan and Che (2011) conducted that the viscous, inertial, and interfacial forces play an important role when a Taylor bubble raises in a stagnant liquid. The other finding from Brown et al. (1965) also stated that as long as pressure inside the gas-bubble is assumed constant, the contributing factors can be expressed in general relationship in Equation 2.21.

$$U_\infty = C_\infty \left(N_f, E_o, \theta\right)\sqrt{g'D} \tag{2.21}$$

It can be noted that *Eötvös* number represents the inverse of dimensionless surface tension and N_f represents the dimensionless inverse viscosity. Zukoski (1966) stated that the upward motion of long bubble in stagnant liquid is relatively stable against the perturbations and its shape. He also appended θ as the representation of pipe inclination and put g' to involve density, so that $g' = \frac{g\,\Delta p}{\rho_L}$. The dimensional analysis has been used by White and Beardmore (1962) to show that Froude number ($Fr = U_\infty/\sqrt{gD}$) is a function of Eötvös number and inverse viscosity number (N_f), where N_f is a function of Morton number (M_o), as well presented in this explanation:

$$N_f = \left(\frac{Eo}{Mo}\right)^{1/4} = \frac{\rho\sqrt{gD}}{\mu} \tag{2.22}$$

The relationship between the Froude number as a function of Eötvös number and Morton number is well presented by White and Beardmore (1962). The

experiment used various types of liquids and diverse properties for single cylindrical air bubble which is assumed to have the similar characteristics with Taylor bubble. They explained that non-dimensional numbers, such as Froude number, *Eötvös* number, and Morton number were suitable to be applied for referring the Taylor bubble rise velocity. In addition, they also overcame different type of correlations depending on the force involved.

Another empirical correlation to obtain either Froude number or Taylor bubble rise velocity that was provided by Wallis (1969). This correlation is applicable for the liquid with inertial, viscous, and interfacial forces, such as:

$$C_\infty = Fr = 0.345 \left[1 - e^{\left(-\frac{0.01\,N_f}{0.345}\right)}\right] \left[1 - e^{\left(\frac{3.37-Eo}{m}\right)}\right] = \frac{U_\infty}{\sqrt{gD}} \qquad (2.23)$$

where the value of m is depended on the value of inverse viscosity number (N_f) which defined as $\frac{\sqrt{gD^3}}{\vartheta}$, showed in Table 2.3:

Table 2.3. Criteria of m value

$N_f < 18$	$m = 25$
$18 < N_f < 250$	$m = 69\,{N_f}^{-0.35}$
$N_f > 250$	$m = 10$

The early studies of gas-bubble rising in a vertical tube were conducted by Dumitrescu (1943) and Davies and Taylor (1950), who investigated a single Taylor bubble rising in a stagnant liquid (non-viscous and without surface tension liquid). Both presented that the rise velocity of Taylor bubble was influenced by the terminal velocity of rise of bubble in a vertical pipe, where took account in several value, as well presented in Table 2.4.

Table 2.4. Proposed correlations of constant C for the stagnant liquid cases

Reference	***C***	**Methodology**
Dumitrescu (1943)	0.351	Analytical
Davies and Taylor (1949)	0.328	Analytical

Laird and Chisholm (1956)	0.328	Experimental
Brown (1965)	0.303	Analytical
Campos and De Carvalho (1988a,b)	0.350	Experimental
Polonsky *et al.* (1999)	0.351	Experimental

However, the value of 0.35 is often used, based on the values of 0.346 (empirical) and 0.351 (theoretical) by Dumitrescu and 0.328 for Davies and Taylor. The general value of $C_\infty = \mathrm{Fr} = 0.35$ was then accepted if $N_f > 250$ (White and Beardmore, 1962). In stagnant liquid, rise velocity of Taylor bubble is influenced by the presence of dimensionless number, namely Froude number, as the relation between interia and gravity force.

$$Fr = \frac{U_\infty}{\sqrt{gD}} \tag{2.24}$$

The Taylor bubble rise velocity can be presumed as steady when it is prevailed as a fully developed slug flow. Nowadays, there are a great number of proposed correlations to describe the rising velocity of Taylor bubbles in a flowing loquid. Basically, this case is a result of a great extent on the mixture velocity and the rising velocity in stagnant liquid. Nicklin et al. (1962) proposed an empirical correlation for the Taylor bubble rising velocity (U_N) that comes as the contribution of mixture superficial velocity (J_m) and terminal raise velocity in a stagnant liquid (U_{TB}).

The investigations of the Taylor bubble motion were developed in different cases when the bubbles move inside the non-stagnant liquid. Consequently, the movement of liquid-phase should be considered. The co-current movement of Taylor bubbles inside a moving liquid can be prescribed as the combination of the rising velocity in stagnant liquid (U_∞) and a component related to the liquid motion or can be expressed as the mean liquid velocity (Nicklin et al., 1962). This relation can be expressed as:

$$U_{TB} = U_\infty + C\,\bar{U}_L \tag{2.25}$$

where $\overline{U}_L$ is defined as mean liquid velocity and C an empirical coefficient due to liquid condition. Nicklin et al. (1962) reported that the component due to the liquid motion is 1.2 times greater than mean liquid velocity ($C = 1.2$) for fully turbulent flow (Re > 8000 and $\overline{U}_L \geq 1$ ft/s). The coefficient value was also confirmed by some experiments from the others investigators, such as Bendiksen (1984) – for turbulent flow with Reynolds numbers of 6000 - 104000 and Polonsky et al. (1999b), which suitable for Reynolds numbers in the range of 2300-6300. Moreover, the value of 0.35 was accepted to be general Froude number value based on the explanation above and White and Beardmore (1962) study. Thus, the equation side for terminal velocity is defined as $0.35\sqrt{gD}$.

$$U_{TB} = 1.2\,\overline{U}_L + 0.35\sqrt{gD} \tag{2.26}$$

The Taylor bubble rise velocity can be presumed as steady (continuous slug flow) when it is prevailed as a fully developed slug flow. Consequently, there is no relative motion between the slugs and the motion of liquid between gas and liquid phase gives a contribution to the rising velocity of the gas-slug. Griffith and Wallis (1961) proposed an approach by exerting a continuity theory and suggested that mixture velocity should be included to replace liquid velocity. By implicating those findings, Nicklin et al. (1962) proposed an empirical correlation, as follows:

$$U_{TB} = U_\infty + C\,\overline{U}_m \tag{2.27}$$

Therefore, Nicklin et al. (1962) suggested the correlation for rise velocity of the continuous slug, represented as follow:

$$U_{TB} = 1.2\,\overline{U}_L + 0.35\sqrt{gD} \tag{2.28}$$

Fernandes et al. (1983) and Sylvester et al. (1987) proposed slight modification of C, proposed correlation 1.29 due to larger pipe diameter (52 mm) than be used by Nicklin et al. (1962) of 1.02 inch. Beside of them, there are some

of proposed correlations to describe the rising velocity of Taylor bubbles in a flowing liquid. The equation is represented as follow:

$$U_{TB} = 1.29\,\bar{U}_L + 0.35\sqrt{gD} \tag{2.29}$$

2.4.5. Hydrodynamics parameter of slug flow regions

The rise movement of Taylor bubbles affects the liquid around it to be put away or swept towards the pipe wall and freely flows in downward direction, relative to the rise movement of Taylor bubble at the narrow annular channel between the Taylor bubble and the tube wall. Dumitrescu (1943) and Nicklin et al. (1962) classified the slug flow into two regions, namely nose region and film region.

Investigation on the thin film around the Taylor bubble movement become an interesting topic since the past. De Jesus et al. (1995) asserted that gravity forces, wall shear stress, interfacial shear stress, inertia, and pressure gradient is involved in regard to the flow in the film. They also briefly resumed the investigation stage on the falling film which among them was began by Dumitresu (1943), Brötz (1954), Brown (1965), and Fernandes et al. (1983). The initial statement of Dumitrescu (1943) was revealed that the flow in the falling film region can be assumed as inviscid and it was re-categorized by Brown (1965) into two radial sections (near Taylor bubble nose and further below) and treated it as laminar and fully developed flow. Moreover, Fernandes et al. (1983) improved this relation for turbulent flow condition. A correlation to calculate the film thickness was proposed by Brötz (1954) by assuming the film thickness was uniform. To simplify the calculation, the interfacial shear was neglected. By obtain this equation, Fernandes et al. (1983) developed a proposed correlation for calculating velocity of the falling film:

$$U_{FF} = 9.916\left[gD(1-{\alpha_{TB}}^{1/2})\right]^{1/2} \tag{2.30}$$

In film region, liquid accelerates freely under gravity, viscous forces are negligible and liquid film in which can be obtained by Bernoulli theorem and lower

region, in which gravity is balanced by wall shear forces and the constant film thickness. A specific study on the hydrodynamics and velocity profiles of slug flow falling film region was conducted by Ahmad et al. (1998). When the axial distance from the nose increases (positive reference below the nose), the thinner liquid film was represented and gives effect to the increase of liquid film velocity. For calculating falling film velocity, Ahmad et al. (1998) also suggested a theoretical prediction based on continuity which was confirmed by result of the experiment to determine falling film velocity. In the calculation, Taylor bubble shape and velocity were considered, shown in Equation 2.31.

$$U_{FF} = U_{TB} \frac{A_{TB}}{A_{FF}} \tag{2.31}$$

Regarding the depth of falling film penetration, Kawaji et al. (1997) reported that penetration of falling film rapidly decays once it leave the tail of Taylor bubble due to vigorous mixing and circulation of fluid occurred. Penetration of falling film surprisingly does not increase in increase of Taylor bubble length greater than 6 cm. Falling film mixing took place less than 1 tube diameter to 1.25 tube diameters.

The presence of small dispersed bubbles in liquid slug region attracts some interests, especially regarding the turbulent mechanisms, the mixing phenomena, the wakes, and the vortices. One example is the crowded situation around the Taylor bubble tail region. Movement and dynamics of the Taylor bubble wake region are related to the velocity profile of the liquid slug, which possible to determine the extent of the interaction between consecutive bubbles (Mayor, 2007).

In the study of the small bubbles dispersion in liquid slug, several authors have adduced the mechanisms. The early study of the wake region behind the Taylor bubble is begun, among them by Moissis and Griffith (1962) and Maxworthy (1967). Moreover, Van Hout et al. (1992) noted that the small bubbles dispersion in the liquid slug is affected by the tearing of Taylor bubble tail, as well stated by Fernandes et al. (1983) for vertical flow. In agree with the previous statement, Fabre and Liné (1992) enriched it by their statement which stated that

the existence of small bubbles in the liquid slugs are caused by the bubble tail fragmentation, the entrainment out of the bubble wake, and the drift relative to the mean flow. It was also stated that the dynamic interaction due to small bubbles and wake in the liquid slug influenced the Taylor bubble motion. Additionally, Mao and Dukler (1985) found that the increased of Taylor bubble rise velocity affected the existence of small bubbles in liquid slugs. Movement of falling film is able to penetrates and generate a vortex. De Jesus et al. (1995) addressed that the different size of vortices are generated due to the liquid film penetration, so the penetration produces greater velocity range.

In stagnant liquid, the study from Campos and De Carvalho (1998b) resulted a model of liquid mixing due to the Taylor bubble movement in different pipe diameters by measuring the tracer concentration. The wake length (L_W) and wake volume (Vol_{wake}) were also measured by Equation 2.32 and 2.33, respectively:

$$\frac{L_{Wake}}{D} = 0.3 + 1.22\, x\, 10^{-3}\, (Nf) \tag{2.32}$$

$$\frac{Vol_{wake}}{D^3} = 7.5 \times 10^{-4}\, \left(N_f\right) \tag{2.33}$$

Campos and De Carvalho (1988a) also recognized three different flow patterns in the Taylor bubble wakes, based on the each shape from the visual study and quantitative classification depend on N_f:

- Laminar → closed axisymmetric wakes with $N_f < 500$
- Transition → closed un-axisymmetric wakes with $500 < N_f < 1500$
- Turbulent → opened wake flow with $N_f > 1500$

Mao and Dukler (1989) used Radio Frequency Probe (RFP) to determine a new methods for carrying out the average void profiles in liquid slugs. They found that gas void fraction is very high just at the beginning of slug, just behind the Taylor bubble, and it decays with the distance, then drops quickly through the wake. In the study, average void fraction is obtained for different axial (h/D) and radial position of each measurement. In addition, the presence of liquid film is related to

the vortexes generation in wake region. The condition agrees with Fernandes et al. (1983) and De Jesus et al. (1995).

Another interesting study on wakes and vortices was revealed by van Hout et al. (1992). In this study, the region inside the liquid slug can be classified into three regions called wake region, intermediate region, and developed region, depicted in Figure 2.13.

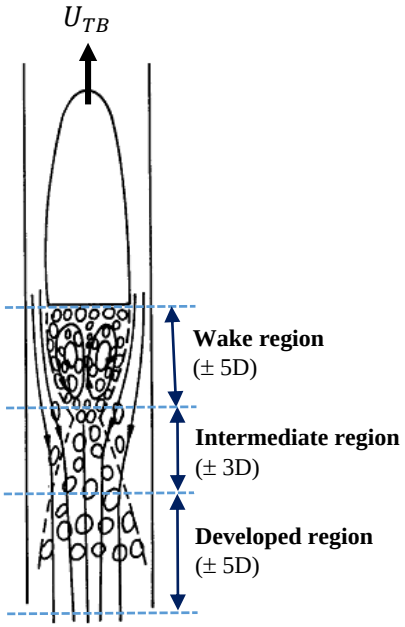

Figure 2.13. Classification of regions behind the Taylor bubble tail region (picture taken from: Van Hout et al. (1992) – with modification)

Wake region is characterized by strong vortices and turbulences which result in high void fraction in area directly behind Taylor bubble. Intermediate region is region where bubbles are injected in the center area of this region which results in peak void fraction in pipe center. Developed region is a region where high vortices and turbulences from Taylor bubble have been neutralized. Hence, radial void fraction distribution resembles the same character with bubble flow.

Measurement of velocity field becomes an important step to determine the wake region of slug flow. Van Hout (2002) stretched up the previous study by using PIV technique. An important result of this study revealed that toroidal vortexes are extended about 2 pipe diameters behind Taylor bubble. The result has in line agreement with the observation by PDA technique from Ahmad et al. (1998).

Moreover, Nakoryakov et al. (1986, 1989) observed that there was an independent relation between the Taylor bubble vortexes. In their observation, the vortex was extended in approximately 2 pipe diameter for all cases. Results of velocity field observation by PIV technique for regions around Taylor bubble are shown in Figure 2.14.

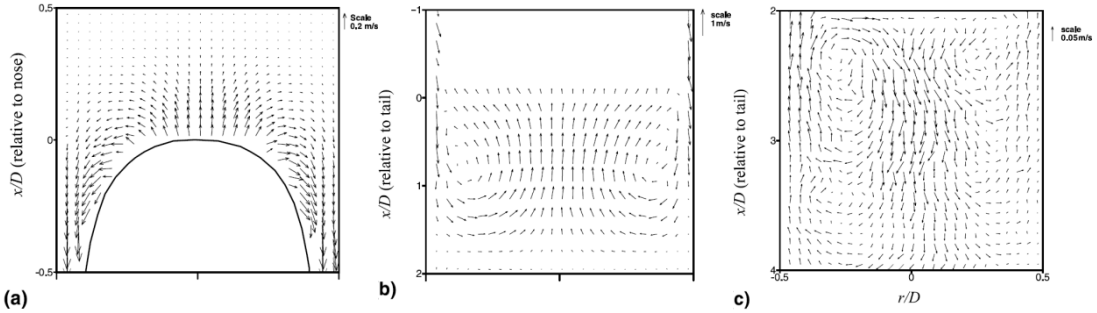

Figure 2.14. PIV observation of the regions around Taylor bubble (van Hout et al., 1992)

The random movements of slug flow potentially affect the liquid mixing around the surroundings. Campos and De Carvalho (1998a) has denoted two contributing factors of mixing in the liquid movements. First, the liquid circulation mechanism which is influenced by the large scale movement of the liquid bulk. Second, the liquid displacement in the vicinity of rising bubble (recognized as mixing induced by gas-slugs/Taylor bubbles - for the slug flow cases).

The presence of turbulence in the liquid slugs depends on the turbulence in the falling film as well as in the length of liquid slugs (Fabre and Liné, 1992). Basically, the falling film penetration to the wake producing a mixing zone (Ahmad et al., 1998). In a stagnant liquid, De Jesus (1995) stated that velocity of the penetrating film rapidly decays due to the mixing and yields a counter-clockwise vortex at the tail. This statement was proved by the obtained velocity vector field result from Photochromic Dye Activation measurement and confirmed by video observation.

At the Taylor bubble tail, a secondary flow mechanism potentially occurs. Liquid penetration caused a wake move counter-currently to the bulk liquid flow and creating vortices of different sizes. These facts are shown by a study of velocity

profiles by De Jesus et al. (1995). As the effect, secondary flow occurs and the liquid flow return to essentially its stagnant initial state. Ahmad et al. (1998) observed that the waviness of the velocity profile increases for the longer bubbles. They revealed the two contributing factors were:

- Greater shear between the film and rising near wall liquid core due to the higher velocity of falling film for longer bubbles
- Shearing and entrainment of small bubbles at the Taylor bubble tail which enhance mixing in the wake

This observation also suggested the critical film velocity that causes shearing and bubble entrainment appears in about 1 m/s.

For the average rise velocity of bubble in liquid slugs, Fernandes et al. (1983) proposed a relation which comes as the combination of the average velocity of liquid-slug and bubble terminal velocity (U_O), stated in the Equation 2.34.

$$U_{GLS} = U_{LLS} + U_O \tag{2.34}$$

where Harmathy (1960) equation of single bubble drift velocity can be implemented to determine U_O. However, the presence of gas fraction inside the liquid flow demands a necessity to consider the gas void fraction in liquid slug. As stated by Fernandes et al. (1983) and Sylvester (1987), Zuber and Hench (1965) modified the equation for the drift velocity calculation by adding $(1-\alpha_{LS})^{1/2}$. Hence, the bubble velocity in liquid slug is represented in equation 2.35, as follow:

$$U_{GLS} = U_{LLS} + 1.53\left[\frac{\gamma g(\rho_L - \rho_G)}{{\rho_L}^2}\right]^{1/4}(1-\alpha_{LS})^{1/2} \tag{2.35}$$

CHAPTER III
RESEARCH METHODOLOGY

3.1. Experimental setup

Experiments were carried out at the **T**ransient Tw**o** **P**hase **Flow** (TOPFLOW) facility at the Institute of Fluid Dynamics of Helmholtz-Zentrum Dresden-Rossendorf (HZDR), Germany. The institute concerns on experimental and the development of advanced measurement techniques (such as special multiphase flow sensors and foremost imaging techniques) with high accuracy in space and time.

3.1.1. Working fluid

In the present experiment, air and water were used as the working fluids. The fluid properties were taken when the gas is injected. For the air-water experiments, the test conditions were in maximum pressure (p_{max}) at 0.4 MPa (4 bar) and temperature at 30^o C (303 K). The fluid properties of water and air (taken at 30^o C) are described in Table 3.1, as follows:

Table 3.1. Properties of water and air (*Engineering Toolbox - accessed in 2014*)

Parameter	Value	Unit
Air (gas-phase)		
Density (ρ)	1.165	kg/m^3
Interfacial Surface tension (γ)	7.12 x 10^{-2}	N/m
Kinematic viscosity (υ)	16.04 x 10^{-4}	m^2/s
Dynamic viscosity (μ)	1.983 x 10^{-5}	Ns/m^2
Parameter	**Value**	**Unit**
Water (liquid-phase)		
Density (ρ)	995.7	kg/m^3
Interfacial Surface tension (γ)	7.12 x 10^{-2}	N/m
Kinematic viscosity (υ)	0.801 x 10^{-6}	m^2/s
Dynamic viscosity (μ)	0.798 x 10^{-3}	Ns/m^2

3.1.2. TOPFLOW research facility

The TOPFLOW test facility provides a multipurpose thermo-hydraulic test facility for the investigations on stationary and transient problems of gas-liquid two-phase flow. The facility is available to conduct either air-water or steam-water two-phase flow experiments. The air-water experiments are usually conducted at temperature of 30^{o}C and maximum pressure of 4 bars. Otherwise, a steam-water experiment with the operation pressure up to 6.5-7 MPa at the saturation temperature of about 281-286^{o}C can also be carried-out.

Measurement of the steady-state and transient two-phase flow phenomena in both adiabatic and non-adiabatically operation can be carried-out. Inside this facility, there are three test rigs, a steam generator module, and the necessary auxiliary systems. General explanations of the facility were described by Prasser et al. (2006) and Scaffrath et al. (2001). A schematic diagram of the TOPFLOW technical system is depicted in Figure 3.1.

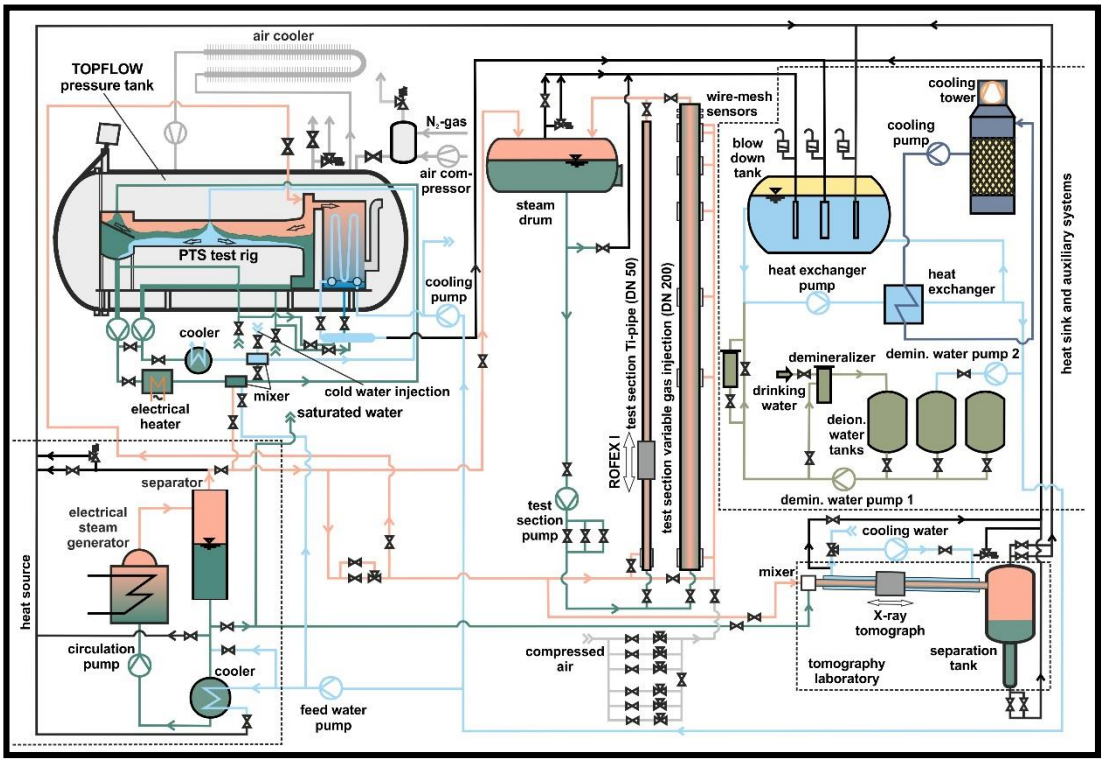

Figure 3.1. Schematic diagram of TOPFLOW facility
(source: https://www.hzdr.de/db/Cms?pNid=1004)

ROFEX–a unique ultrafast X-ray tomography device is installed at the vertical test section DN-50 of TOPFLOW facility. A vertical titanium pipe with inner diameter (ID) of 54.8 mm and total length of 6 m was installed in the test section. During the X-ray measurement, the available length for the tomography is about 3.3 m from gas injection point. The use of titanium material is useful for carrying out the experiments by ultrafast X-ray at high pressure and high temperature. It also gives advantage of the reduction of radiation attenuation possibility by accommodate a better signal to noise ratio. Moreover, for steam-water experiments, the titanium pipe gives a benefit in wall thickness reduction, up to 1.6 mm for operation pressure of 7 MPa. Figure 3.2 (a) and (b) show the test section both in schematic view and real images, respectively.

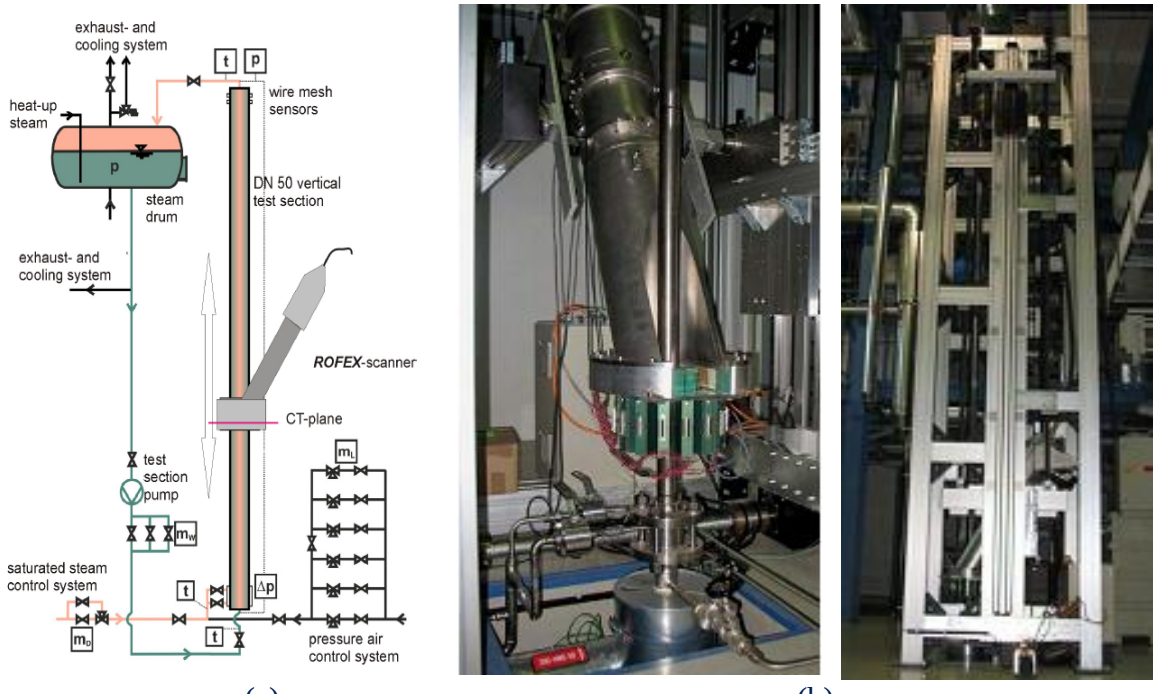

(a) (b)

Figure 3.2. Schematic d of DN-50 test section, (a) schematic; (b) real images (source: Banowski et al., 2013; Fischer and Hampel, 2010)

A special casing, made by lead with 6 mm thickness, is assembled enclose around the scanner and the elevator. This is used as the radiation protector by restraining any radiation penetration to undesired direction. A variable gas injection, specially designed to find out both upward and downward flow direction, can be mounted either at the upper or at the lower end of the test section.

Various gas injection modules can be used to provide experiments in different flow direction and wide range combinations of gas-liquid flow rates. The devices are made by stainless steel and consisted by a complex weldment. To adjust amount of gas bubble, the device is comprised by 40 cannulae. These are feed with gas from several ring chambers that can be activated separately (Fischer and Hampel, 2010). For co-current upward flow, a type of gas injection module, called as L-14, is used for low gas flow rates, shown in Figure 3.3 (a). A different type of gas injection module that is used for high air flow rate, called as L-18, shown in Figure 3.3 (b). To obtain less homogeneous gas phase distribution, another gas injection module is also used, shown in Figure 3.3 (c). As the result, a faster flow development is performed by less homogeneous gas-phase distribution than a homogeneous gas-phase distribution.

(a) (b) (c)

Figure 3.3. Various kinds of gas injection modules
(source: https://www.hzdr.de/db/Cms?pNid=1004)

3.1.3. ROFEX measuring principles

As an ultrafast X-ray tomography device, ROFEX has some advantages as a noninvasive and nonintrusive imaging tool, which is capable to penetrate an opaque tube wall. Moreover, it powerful to observe the structure of the inherent multiphase flows in opaque material. The device is able to work with the maximum frame rates of about 7000-8000 cross-sectional images per second at a spatial

resolution of about 1 mm. A schematic preview of the ROFEX-ultrafast X-ray tomography is depicted in Figure 3.4.

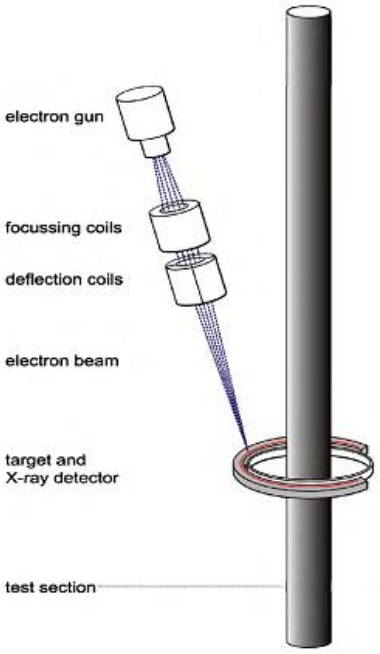

Figure 3.4. Schematic diagram of ROFEX working principle
(Fischer and Hampel, 2010)

Basically, the working principle of X-ray Computed Tomography (X-ray CT), which is commonly used for medical purposes and material testing, is adapted as the measuring principle of the ultrafast X-ray tomography. An X-Ray CT works by a radiation attenuation which passes through an object, in accordance with the Beer-Lambert law on "*the exponential attenuation of a light as it travels through an object"*. Subsequently, a detector records the intensity change of the attenuation. However, for air-water flow, the high measurement frequency is required. Thus, the mechanical rotating parts should be avoided to reach the necessity of high frequency. Therefore, a scanned electron beam technology plays an important role to solve that problem. At the first, Boyd and Lipton (1983) and Gould (1992) introduced a scanned electron beam technology for the medical application. Therefore, ROFEX works by implicating the scanned electron beam principle (Hampel et al., 2005).

An electron beam with maximum beam current of 65 mA at 150 kV acceleration voltage is produced by an electron beam gun. The beam is focused and

centered on a circular tungsten target at the far end of the beam column. At the same time, the deflection coils periodically deflects the beam in x-y direction with a high frequency. Hence, a moving X-ray source with less than 1 mm diameter and Maximum sweeping frequency amounts to 10 kHz is produced. A horse shoe with 250 mm diameter and semi-circular ring of 240^o is employed as the X-ray metal target. The X-ray detector, composed by 240 CZT detector elements each of 1.5 mm x 1.5 mm x 1.5 mm for each detector, is established in a circular manner along the horse shoe inner wall of enclosure in 360^o. The current design allows imaging objects until the diameter of 120 mm by tilt the target up to 30^o of inclination angle to the beam axis (Fischer and Hampel, 2010). The basic explanation of ROFEX is presented by Fischer et al. (2008) and Fischer and Hampel (2010). Additionally, the detail information of an ultrafast electron beam CT-scanner is performed in Table 3.2.

Table 3.2. Properties of an ultrafast electron beam computed tomography scanner (Fischer et al., 2008)

Parameter	**Value**
Electron beam gun	
Perveance (beam widening)	1.1×10^{-9}
Max. acceleration voltage	150 kV
Max. beam current	65 mA
Max. beam power	10 kW
Wehnelt voltage	3 kV
Auxiliary supply for electron bombardment	1 kV
Filament heating current	8 A
Max. deflection frequency	10 kHz
Max. deflection angle	±17.5°
Beam generating system	Rogowski
Dimensions	650 mm length, 273 mm dia.
Gas pressure	10^{-6} mbar
Detector and electronics	
Number of detector elements	240
Size of detector elements	1.5 mm × 1.5 mm × 1.5 mm
Detector material	Cadmium zinc telluride (CZT)
Maximum sampling rate	1 MSample s^{-1}
RAM size	4 GB
Operating parameters	
Max. frame rate	7000 fps
Focal spot size	1.1 mm
Spatial image resolution	0.51 lp mm^{-1} at 10% MTF

In order to investigate the gas-bubble velocities, the dual measurement planes are used. These planes, equipped by using dual planes targets and also two pixel rings detectors measurement, are particularly placed in an axial distance of 10.2 mm from each other. The construction of dual measurement planes is shown in Figure 3.5. For air-water experiments, each measurement is commonly taken during 10 seconds with 1000-2500 Hz frame rates, depending on the gas and liquid flow rates (Banowski et al., 2003).

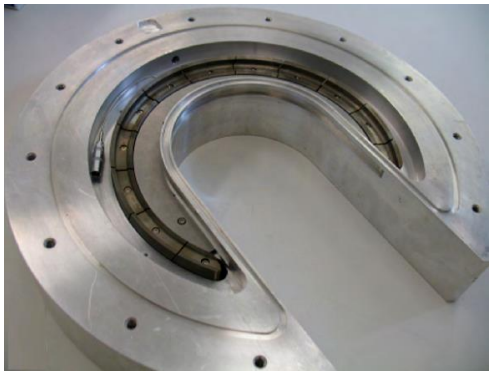

Figure 3.5. Dual plane target (Fischer and Hampel, 2010)

3.2. Test matrices and measurement stations

The present study is focused on the slug flow and transition regime (spherical cap bubble flow). The experimental conditions for investigated slug flow involves the gas-superficial velocities of 0.219 and 0.534 m/s and liquid-superficial velocity ranging from 0.045 to 1.017 m/s, shown in Table 3.3.

Table 3.3. Measurement set matrix

	Superficial Gas Velocity (m/s)																				
Superficial Water Velocity (m/s)	0.003	0.004	0.006	0.01	0.015	0.024	0.037	0.057	0.09	0.14	0.219	0.342	0.534	0.835	1.305	2.038	3.185	4.975	7.772	12.14	18.97
4.047	11	22	33	44	55	66	77	88	99	110	121	132	143	154	165	176	187	198	209	220	231
2.554	10	21	32	43	54	65	76	87	98	109	120	131	142	153	164	175	186	197	208	219	230
1.611	9	20	31	42	53	64	75	86	97	108	119	130	141	152	163	174	185	196	207	218	229
1.017	8	19	30	41	52	63	74	85	96	107	118	129	140	151	162	173	184	195	206	217	228
0.641	7	18	29	40	51	62	73	84	95	106	117	128	139	150	161	172	183	194	205	216	227
0.405	6	17	28	39	50	61	72	83	94	105	116	127	138	149	160	171	182	193	204	215	226
0.255	5	16	27	38	49	60	71	82	93	104	115	126	137	148	159	170	181	192	203	214	225
0.161	4	15	26	37	48	59	70	81	92	103	114	125	136	147	158	169	180	191	202	213	224
0.102	3	14	25	36	47	58	69	80	91	102	113	124	135	146	157	168	179	190	201	212	223
0.0641	2	13	24	35	46	57	68	79	90	101	112	123	134	145	156	167	178	189	200	211	222
0.0405	1	12	23	34	45	56	67	78	89	100	111	122	133	144	155	166	177	188	199	210	221

= data matrices for this present study
L18 - gas injection module

In order to observe the flow evolution along the vertical pipe, there are 6 dimensionless axial stations (z/D) from the gas injection point along the available measurement length, shown in Table 3.4.

Table 3.4. Axial stations

z/D	Height Position (mm)	Position Label
0.3	16	A
1.13	62	D
3.12	171	G
7.94	435	J
23.3	1271	M
59.7	3270	P

3.3. Data processing of ultrafast X-ray tomography

3.3.1. Image reconstruction

Measurement by ultrafast X-ray resulted the tomography data which are contained attenuation value of X-ray distribution, called as “sinogram”. The data represented the detector number in the horizontal direction and the projection angle in the vertical direction. Example of data matrices (sinogram), for empty-pipe (a), water-filled (b), and unknown gas-fraction inside pipe (c) are shown in Figure 3.6.

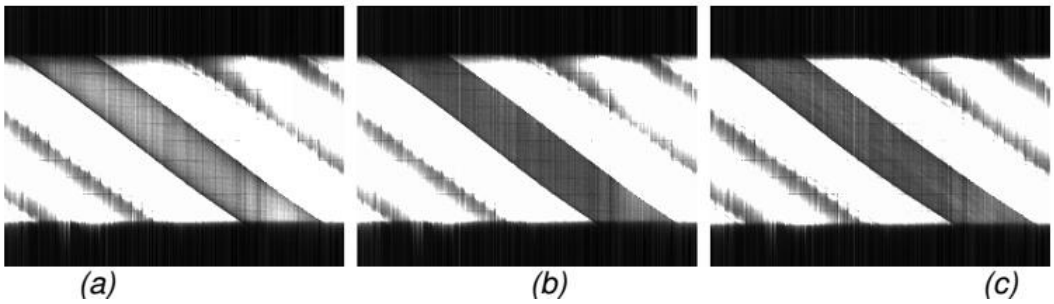

Figure 3.6. Example of resulted sinograms, (a) empty-pipe; (b) water-filled; (c) filled by unknown gas-fraction (Banowski et al., 2013)

The data were then reconstructed as the cross-sectional image stacks that is captured by detector ring is processed by means of filtered back projection algorithm, as mentioned by Kak and Slanley (1988) in their book. The process results the 3D arrays of gray values that were scaled up to represent gas and liquid

phase distribution based on the pixel ratio. Array dimensions are 108 x 108 pixels and the array length is depended on selected frequency and measurement time. The cross sectional cut of reconstructed image is shown Figure 3.7.

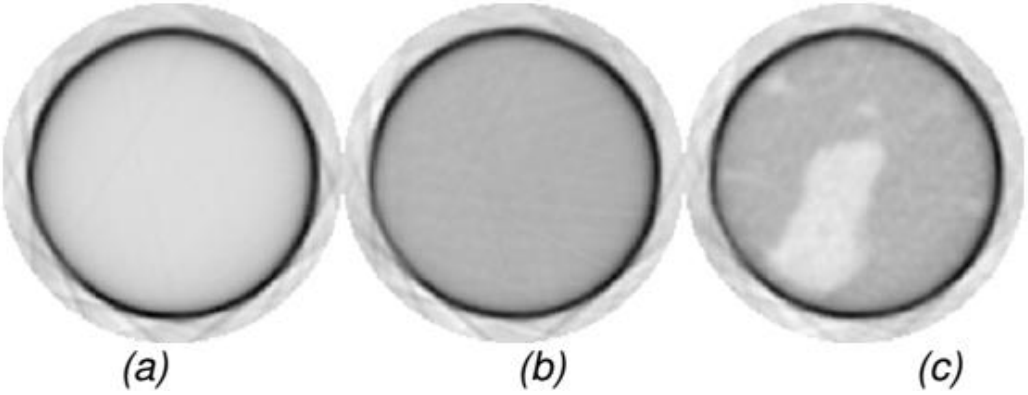

Figure 3.7. Example of reconstructed cross-sectional images, (a) empty-pipe; (b) water-filled; (c) filled by unknown gas-fraction (Banowski et al., 2013)

3.3.2. Image segmentation

The bubble parameters can be revealed after the gray value arrays are binarized, shown in Figure 3.8. Binarization process was needed to obtain interfacial boundaries among gas and liquid.

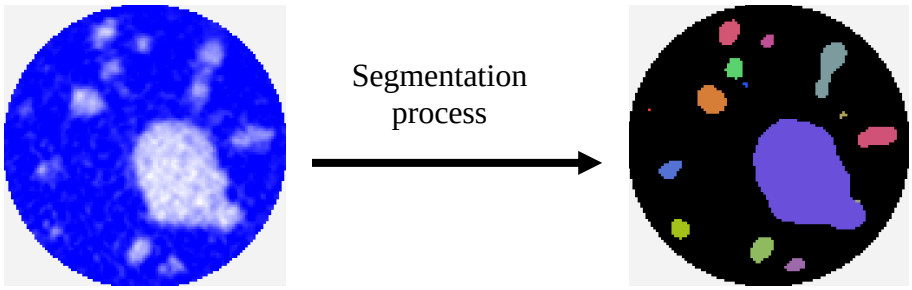

Figure 3.8. Preview of bubble segmentation process (Patmonoaji, 2014)

However, an improvement of segmentation method was needed for a better result of bubble segmentation. Banowski et al. (2013) developed a new algorithm for bubble segmentation from ROFEX database. Detail of the working principle of the algorithm can be carried out in their report. The segmentation process yields important parameters of gas bubble, such as bubble number, detected time of bubble

at front, center of mass, and back, bubble coordinate in x and y directions, bubble size, and maximum radius in cross sectional direction. The segmentation process becomes an existing data processing, as well noted by Patmonoaji (2014), which mainly did by Banowski et al. (2013) as the previous steps of research methodology for this present work.

3.4. Bubble pair algorithm

In order to obtain more accurate results of bubble velocities and bubble properties as well, an individual recognition based on the highest bubble probabilities is obtained, called as bubble pair algorithm. This method is a new data processing which processed by Patmonoaji (2014) and adopted in this present work. The algorithm works by an assumption of looking for highest similarity of detected bubble at lower and upper measurement planes. The other assumption considers small possibilities of bubble coalescence and breakup possibility due to very short distance between both measurement planes.

By finding the same bubble that was detected on both measurement planes, bubble time travel and bubble movement from both measurement planes were obtained. Therefore, from these parameters, bubble velocities such as axial velocity, horizontal velocity, 3D velocity, radial velocity, and azimuthal velocity were able to be calculated. This method is able to be performed for ROFEX measurement database because ROFEX is non-invasive and non-intrusive measurement device. The advantages of this method is the individual recognition of each bubble. It gives a benefit to study more about detail desired properties of each bubble. Figure 3.9 illustrates how the bubble pair method works. The “similar” bubble is recognized in a similar bubble colors.

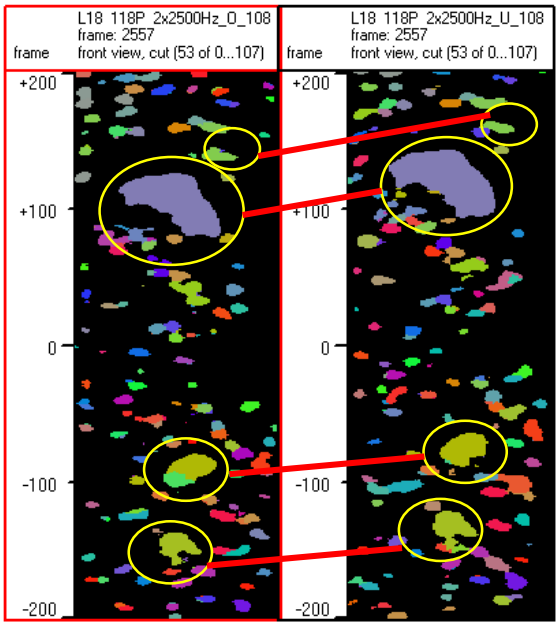

Figure 3.9. Illustration of the bubble pair choosing.

The possible "paired" bubble is bubbles with the the highest probabilities of of volume, position, and expected axial velocity prediction in lower and upper planes. In the method, bubble was sorted from larger to smaller bubbles to ease the bubble recognition then easier to be solved. Detail of the concept of this algorithm can be obtained in Patmonoaji (2014).

3.4.1. Bubble rise velocity probability

3.4.1.1. Calculation of expected velocity

The velocity of a bubble in flowing liquids is a superposition of its terminal velocity and the component due to liquid flows. For bubbly flow case, it follows the power-law distribution equation, as originated proposed by Bankoff (1960) and formed by Beyerlin et al. (1985). Theoretical prediction from Bankoff (1960) is used because all of the processed flows were in turbulent regimes while theoretical prediction from Harmathy (1960) can be used because range of detected bubble size was mainly larger than critical diameter given by Broadkey (1967).

A modification of the equation with the use of terminal velocity equation by Harmathy et al. (1960) was obtained for expected velocity of bubbly flow case, written as:

$$U_B = 1.2\,(J_G + J_L)(1 - \frac{r}{R})^{1/6} + 0.53\left[\frac{g\Delta_\rho \gamma}{\rho_L}\right]^{0.25} \quad (3.1)$$

For the special case of slug flow, the different flow regions were defined. There are Taylor bubble, falling film, extension of falling film (referred as "swelling" region), wake region, and developed bubble region – a region which similar characteristics with bubbly flow. Illustration of the slug flow sub-regions was depicted in Figure 3.10.

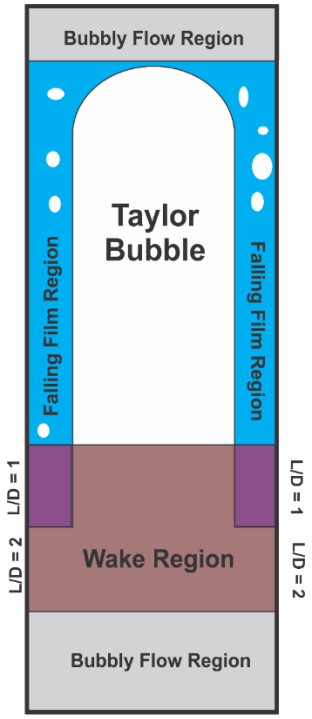

Figure 3.10. Preview of divided zone in around Taylor bubble

Detail explanations of expected velocities that applied to each bubble region are summarized as follows:

a) Taylor bubble

By considering the different behaviors of Taylor bubble, the correlation by Nicklin et al. (1962) was used as the expected velocity.

$$U_{exp} = 1.2\ (J_G + J_L) + 0.35\ (gD)^{1/2} \quad (3.2)$$

In this algorithm, Taylor bubble was defined as bubble with maximum cross-sectional diameter more than 35 mm and equivalent diameter more than 40 mm.

b) Falling film region

Falling film region, located between pipe wall and Taylor bubble, wraps around Taylor bubble from bubble nose until the end of Taylor bubble tail. For the expected velocity approximation, theoretical prediction which proposed by Ahmad et al. (1998) were used as velocity approximation. By considering the continuity equation, considering the Taylor bubble rise velocity and downward movement of falling film relative to the Taylor bubble, the expected velocity equation for this region is shown in equation 3.3.

$$U_{exp} = 1.2\ U_{avg}\ (1 - \frac{r}{R})^{1/6} + 1.53(\frac{g\ \Delta\rho\ \gamma}{\rho_L})^{0.25} - (U_{TB} - U_m)\frac{A_{TB}}{A_{FF}} \quad (3.3)$$

c) Extension of falling film region (swelling region)

The falling film region extends until 1-pipe diameter length and creates "swelling" motion inside (Ahmad et al., 1998; Kawaji et al., 1997). Specification of one pipe diameter after Taylor bubble tail follows the description of falling film penetration by Kawaji et al. (1997). Bubbles in this region using the specified criteria when $I_{back\text{-}TB} \leq I_m \leq I_{back\text{-}TB\ +\ (1D/Uexp\text{-}TB)}$ and bubble radial position is more than $r_{xymax\text{-}TB.}$ For the expected velocity calculation, a similar calculation method with the case of falling film, as in Equation 3.4 was used to obtain the expected velocity.

$$U_{exp} = U_{exp\text{-}Falling\ film\ region} \quad (3.4)$$

d) Wake region

Wake region lies on around 2 pipe diameter behind the Taylor bubble (Van Hout et al., 2002). In this calculation, wake region was described as region that is not assigned as falling film region and located from Taylor bubble tail until two

pipe diameter behind Taylor bubble tail. For calculation of expected velocity, the general expected velocity for bubbly flow was also used (Equation 3.1).

$$U_{wake} = U_B \tag{3.5}$$

e) Developed bubble region (bubbly flow)

During this flow region, bubble moves in rectilinear or zigzag motion depending on bubble size. Vortices and wake effects during the flow are so minor. Bubble only moves slightly in horizontal direction and rises due to surrounding flow and buoyancy force. For calculation of expected velocity, surrounding flow velocity is approached with theoretical prediction of turbulent flow velocity profile by Bankoff (1960) in Beyerlin et al. (1985) and Ishii et al. (2004). However bubble expected velocity is approached as shown in Equation 3.1 above.

3.4.1.2.Calculation of velocity probability

In this method, bubble was expected to move according to theoretical prediction of liquid flow velocity and bubble drift velocity itself, shown in the equations above, depends on which region the bubbles are located. After estimating the expected bubble velocity, the difference between the calculated axial velocity of the possible bubble pair and expected velocity was first determined, called as bubble pair velocity (U_{BP}). The velocity range was then calculated by criteria of 0.375 U_{exp} and the drift velocity. Determination of velocity probability considered these specified criteria:

Table 3.5. Criteria for velocity range in velocity probability calculation

Criteria	Velocity range	
0.375 $U_{exp} > U_{drift}$	$U_{range} = 0.375\ U_{exp}$	(3.6)
else	$U_{range} = U_{drift} = 0.2502$	(3.7)

The velocity probability was then determined by using the calculated U_{BP} and U_{range}, as in Table 3.6.

Table 3.6 Determination of velocity probability

Criteria	Velocity probability ($\emptyset_{vel}$)	
0.375 $U_{BP} < U_{range}$	$\emptyset_{vel} = 1$	(3.8)
$U_{range} \leq U_{BP} < 2\ U_{range}$	$\emptyset_{vel} = 2 - \frac{U_{BP}}{U_{range}}$	(3.9)
else	$\emptyset_{vel} = 0$	(3.10)

3.4.2. Bubble volume probability

The highest bubble volume probability could be generated by considering the most identical volume between bubble pair candidates using the Gaussian distribution. The equation involves volume difference and sigma parameter which can be represented as:

$$\emptyset_{vol} = e^{-0.5\left(\frac{\Delta_{vol}}{\sigma_{vol}}\right)^2} \tag{3.11}$$

To determine the bubble volume, a multiplication of virtual volume, symbolized as v_b (mm^2.ms), with the bubble axial velocity was needed. It was because the obtained volume from the measurement still in virtual volume, so the multiplication with axial velocity bring into volume unit (mm^3). This can be written as:

$$vol \quad = v_b\ U_{axial} \tag{3.12}$$

Therefore,

$$\Delta_{vol} = |\ (\Delta_{vol}\ )_O - (\Delta_{vol}\ )_U\ | \tag{3.13}$$

After the volume was calculated, the bubble equivalent diameter or Sauter mean diameter, was able to be determined, as presented in Equation 3.14.

$$d_{equiv} = \sqrt[3]{\frac{6\ vol}{\pi}} \tag{3.14}$$

For the calculation of σ_{vol}, the criteria were set to give the tolerance ranges, based on the bubble size. These criteria were used to anticipate the volume or size difference of detected bubbles in upper and lower planes. If the volume difference occurs, it need to be considered that the reconstruction process did not always result

a similar gray value for same bubble at both planes. Thus, it gave effect in segmentation process, as well. However, for larger bubble, such as Taylor bubble and spherical cap bubble, the possibility to be wrong volume detection in both planes is smaller than small bubbles. The different criteria for small and large bubbles are presented in Table 3.7.

Table 3.7. Criteria for sigma volume in Gaussian function

Criteria	Sigma volume (σ_{vol})	
	d_{equiv} + 0.5 mm	
d_{equiv} < 5 mm	$\sigma_{vol} = \left[\frac{\pi}{6}(d_{equiv} + 0.5)^3\right] - vol_{equiv}$	(3.15)
	10 % (d_{equiv})	
else	$\sigma_{vol} = \left[\frac{\pi}{6}(1.1 \times d_{equiv})^3\right] - vol_{equiv}$	(3.16)

In order to prevent coalescence problems and chaotic movements in wake region of slug flow, it was used 2 x σ_{vol} which was implemented only for this case.

3.4.3. Bubble radial position probability

A similar statistical method (Gaussian function) was also implemented to find position probability.

$$\emptyset_{pos} = e^{-0.5\left(\frac{\Delta_{pos}}{\sigma_{pos}}\right)^2} \quad (3.17)$$

The difference of bubble position (Δ_{pos}) was obtained from the horizontal position difference between bubble center of mass in both planes.

$$\Delta_{pos} = \sqrt{(j_{m_O} - j_{m_U})^2 + (k_{m_O} - k_{m_U})^2} \quad (3.18)$$

This method used an assumption that bubble with higher axial velocity has less possibility to horizontally moves due to short gap of measurement planes and time to move upward, and vice versa. Thus, the calculation of σ_{pos} followed the

ratio of constant value 2.5 mm^2/ms and axial bubble velocity (Patmonoaji, 2014). This coefficient came from the empirical value.

$$\sigma_{pos} = \frac{2.5\ mm^2/ms}{U_{axial}} \tag{3.19}$$

After all probabilities were calculated, the total probability was determined by multiplication of three probability types. The velocity and volume probabilities consider the bubble movement from lower-to-upper as well as upper-to-lower plane.

$$\emptyset_{total} = \emptyset_{vel(UO)} . \emptyset_{vel(OU)} . \emptyset_{vol(UO)} . \emptyset_{vol(OU)} . \emptyset_{pos} \tag{3.20}$$

3.5.Data analysis

3.5.1. Calculation of bubble velocities

The instantaneous bubble velocity was obtained by bubble displacement (from lower to upper measurement layer) in a particular time. Some criteria were used to determine time-lag of each bubble displacement, based on the maximum radius of cross sectional area (r_{xymax}). These criteria are summarized in Table 3.8.

Table 3.8. Criteria for time determination

Bubble size	Time used
r_{xymax} < 3 mm	Time in center of mass (I_m)
3 mm < r_{xymax} < 10 mm	Interpolation virtual time (I_{vir})
r_{xymax} > 10 mm	Time in front region (I_{front})

This criteria were set by considering the small bubble coalescence especially for larger bubble. It was common and relevant to use the detected time in center of mass in velocity calculation for small bubbles. However, for large bubble, including Taylor bubbles, coalescence was unavoidable in rear area (tail region) and sometimes occurred along the body (influenced by falling film). Hence, the detected time in front region was more relevant to be implemented in the calculation, considering the nature of Taylor bubble nose which straightly move upward and had a relatively small possibility of bubble coalescence than rear or

center area. For intermediate size bubbles, a linear interpolation between I_m and I_{front} was used, recognized as virtual time. Therefore, the three dimensional velocities can be determined by using bubble pair result and segmentation file database.

a) Three-Dimensional (3D) velocity

Bubble three-dimensional velocity is a composition of both movements in axial and horizontal directions:

$$U_{3D} = \sqrt{{U_{axial}}^2 + {U_{hor}}^2} \tag{3.21}$$

The explanation for each velocity component is expressed as follow:

- Axial velocity (U_{axial})

  The axial bubble velocity was derived from the division of the distance between measurement planes (10.2 mm) to the time differences

$$U_{axial} = \frac{10.2mm}{(\Delta I)_{O \to U}} \tag{3.22}$$

- Horizontal velocity (U_{hor})

During the rising movement, bubbles can also move laterally in horizontal direction. Hence, the horizontal velocity was calculated based on the coordinate differences in x (j) and y (k) directions:

$$U_{hor} = \frac{(\Delta pos)_{hor}}{(\Delta I)_{O \to U}} = \frac{\sqrt{(j_o - j_u)^2 + (k_o - k_u)^2}}{(\Delta I)_{O \to U}} \tag{3.23}$$

- Polar angle (α°)

  The angle between bubble axial and horizontal movements is defined as a polar angle. According to the trigonometry function, the polar angle was defined as follow:

$$\alpha^\circ = tan^{-1}\left(\frac{U_{hor}}{U_{axial}}\right) \tag{3.24}$$

b) Radial velocity

The bubble lateral movement influences by lift force, which has either direction to pipe core region or wall region. Radial velocity considers the bubble movement from inter-cross sectional radius area. Hence, bubble tendency to move can also be determined. In calculation, the radial position difference and the travel time between lower to upper measurement planes were considered, as in Equation 3.24.

$$U_{rad} = -\left(\frac{(\Delta pos)_{rad}}{(\Delta I)_{O\rightarrow U}}\right) = -\left(\frac{r_o - r_u}{(\Delta I)_{O\rightarrow U}}\right) \tag{3.25}$$

where the bubble radial position was calculated in Equation 3.25 below,

$$r = \sqrt{(j-R)^2 + (k-R)^2} \tag{3.26}$$

For the radial velocity, negative sign was used to define the bubble tendency. Thus, positive value of radial velocity means bubble moved toward pipe center region and vice versa.

c) Azimuthal velocity

A simple analogy of tangential velocity was used to determine azimuthal velocity.

$$(U_{azm})_{U\rightarrow O} = \varnothing \frac{\beta}{(\Delta I)_{O\rightarrow U}} r_u \tag{3.27}$$

where $\varnothing$ is a symbol for movement direction {-1,0,1} by obtaining the lowest angle possibility between two-radial distances and β is an azimuthal angle (°) which is obtained from Equation 3.28.

$$\beta = cos^{-1}\left[\frac{\overrightarrow{r_o}\cdot\overrightarrow{r_u}}{|\overrightarrow{r_o}||\overrightarrow{r_u}|}\right] = cos^{-1}\left[\frac{(j_o j_u) + (k_o k_u)}{\sqrt{{j_o}^2 + {k_o}^2}\sqrt{{j_u}^2 + {k_u}^2}}\right] \tag{3.28}$$

It should be noted that in this present calculation, the counter-clockwise movement is initialized by positive sign. For the sake of clarity, illustration of the explained velocities are depicted in Figure 3.11 below.

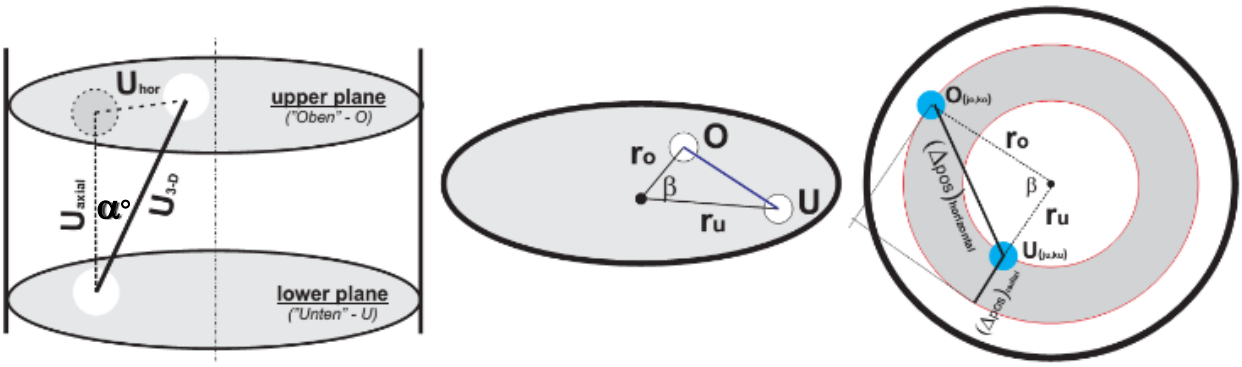

(a) (b) (c)

Fig. 3.11 (a) Preview of bubble three-dimensional rising movement; (b) Bubble azimuthal movement; (c) Bubble horizontal and radial velocities.

3.5.2. Taylor bubble and liquid slug length

The individual Taylor bubble length can be determined by the multiplication of Taylor bubble axial velocity and the time detection difference in each measurement layer. The liquid slug length behind a Taylor bubble is also determined by the same procedure using the velocity of leading Taylor bubble by using an asuumption of constant bubble nose and tail velocity. This method was used to simplify the problems related to the difficulty of defining the rear area of the Taylor bubble due to the presence of swarm dispersed bubbles, as well strengthened by Guo-dong et al., (2009). Therefore, the length calculations are shown, as follows:

Taylor bubble length is defined as:

$$L_{TB} = U_{axial}\,(I_{back} - \Delta I_{front})_{O\ or\ U} \tag{3.29}$$

Liquid slug length is defined as:

$$L_{LS} = U_{LS}^{axial}\left[(I_{front})_{TB\ i+1} - (I_{back})_{TB\ i}\right] \tag{3.30}$$

Using the assumption of,

$$U_{LS}^{axial} = (U_{axial})_{TB\ i-1} \tag{3.31}$$

3.5.3. Bubble frequency

Bubble frequency was calculated by addressing the number of encountered bubbles per measurement time. Hence, it is stated in bubble/s unit.

$$f = \frac{number\ of\ encountered\ bubbles}{measurement\ time} \quad \text{[bubble/s]} \tag{3.32}$$

3.5.4. Averaged cross-sectional void fraction

The time-series data shows the cross-sectional averaged void fraction. Measurements were capable to produce time-series data from upper and lower planes in the form of void fraction signal in time domain. In this case, void fraction was defined as the averaging of gas fraction in each cross-sectional image. The use of simple statistic method of mean and standard deviation were used to analyze.

3.5.5. Calculation of discretization error in temporal resolution

The discretization error in temporal resolution was calculated by considering the obtained time from Nicklin et al. (1962) theoretical value. This error was calculated in order to understand the frame or temporal difference compared to the time from theoretical value. Discretization may contributes to erase some desired or add undesired information. Hence, it affects the inappropriate detected time when Taylor bubble rises. It was also suspected to be a reason for velocity distribution. The steps of calculation is presented as follows:

Calculation of time from Nicklin et al. (1962) equation:

$$t = \frac{10.2\ mm}{U_{nicklin}\ 1000\ mm} \tag{3.33}$$

After time was obtained, involving the measurement frequency or frame rate (fr), the number of frame was calculated as follow:

$$n = t\ x\ fr \tag{3.34}$$

Therefore, the time difference was carried out and assumed as the discretization error in temporal resolution.

$$\Delta t = \frac{1}{n} 100\ \% \tag{3.35}$$

CHAPTER IV
RESULTS AND DISCUSSION

4.1. Qualitative observation

In this present study, Taylor bubble properties and and slug flow characteristics were qualitatively and quantitatively studied. Measurements by an ultrafast X-ray tomography, continuing by a series of data processing processes, (reconstruction and segmentation) were useful to reveal the qualitative appereances of Taylor bubbles. The apparent characteristics of slug flow were defined by the presence of large, long, and rounded-shaped-nose bubbles, namely Taylor bubble. In between of each successive Taylor bubble, the liquid slugs that contain small dispersed bubbles were presented. The front area of Taylor bubble is commonly called as ”nose”, whereas the so-called ”tail” for the rear-bubble-area. Visualization of a Taylor bubble and liquid slug (as a ”unit cell”), sub-regions of slug flow, and scope of this study are presented in Figure 4.1.

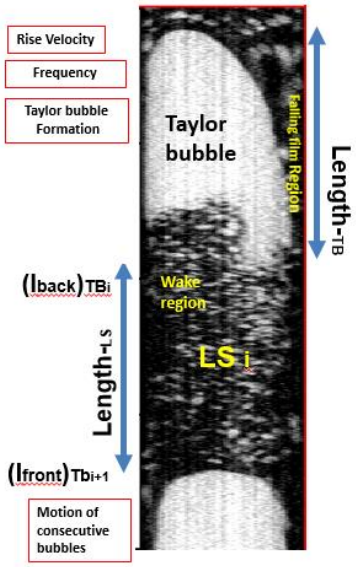

Figure 4.1. Visualization of a single-cell unit of slug flow
and scope of this present study

Since the presence of Taylor bubble, the sub-regions around a Taylor bubble were generated. Each region had specific characteristics and reasons behind their formation. Therefore, this phenomenon enacted slug flow as a the most complex

nature of flow pattern, so it attracted more attention to study. Specifically, those sub-regions could be described as follow, as well by a qualitative observation:

a) Falling film region – a thin liquid film that located in between Taylor bubble and pipe wall. It lengthwises until near rear-area of a Taylor bubble. In this region, a few number of bubbles were existed. They flowed along narrow gap between Taylor bubble and pipe wall and sometimes were found coalesced with the Taylor bubbles.
b) Wake region – a region that was located behind the Taylor bubble tail. In this region, small bubbles were circulated due to torroidal vortices and turbulent movement. Bubbles were seen dense and swarm at specific distance from the Taylor bubble-rear area.
c) Developed bubble region – a region when bubbles had similar characteristics with bubbly flow. The wake effects did not influence the bubble-characteristics anymore. In this region, bubbles were looked discreted and dispersed, similar to the bubbly flow characteristics.

Due to their formation process, Taylor bubbles exist on various shapes. Some examples of the unique shapes are depicted in Figure 4.2.

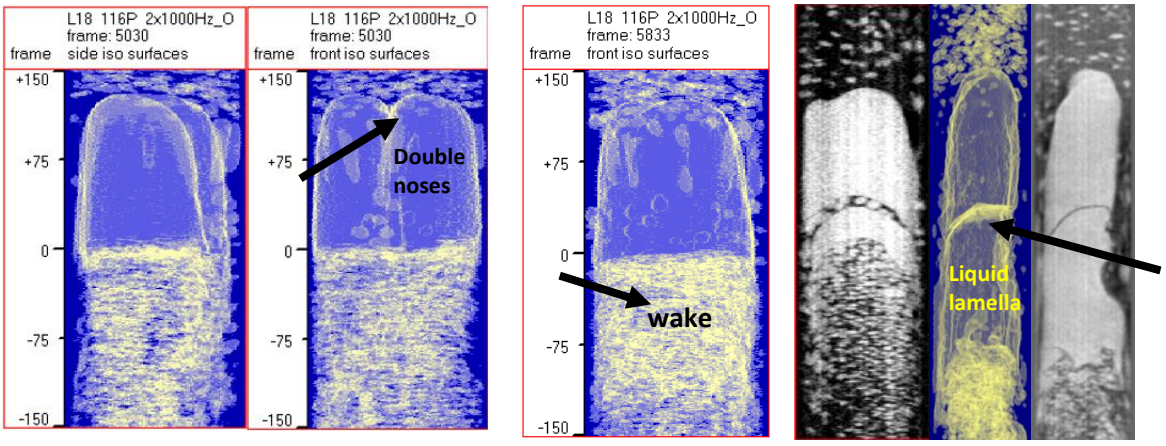

(a) (b) (c)

Figure 4.2. Visual images of Taylor bubble unique shapes (a) double-noses (b) natural shape (c) liquid-lamella (J_L=0.405 m/s and J_G=0.219 m/s)

By using tomography technique, more detail shapes of Taylor bubble were able to be highlighted. Those pictures were taken from reconstructed images of the

available data. However, the observations of Taylor bubble unique shapes had been also conducted by the previous investigators by using an ultrafast X-ray at HZDR-Germany. Hence, this chapter is also aimed to affirm the previous study on the qualitative interpretation of Taylor bubble shapes.

In those pictures, there are three examples of Taylor bubble shapes. The middle picture of Figure 4.2 (b) shows a natural Taylor bubble shape with rounded-shaped nose. The visual appearance of dense bubbles in wake region is also showed. A few number of bubbles flow in between pipe-wall and Taylor bubbles, inside a thin falling film region. Additionally, there are a quite swarm bubbles in front of the Taylor bubble nose.

Figure 4.2 (a) and (b) present a unique double-noses and liquid-lamella shapes, respectively. Considering the developing condition of slug flow, it is believed that those contours represent the coalescence and formation process to be developed Taylor bubble. Those pictures seem to demonstrate "unfinished" coalescence process of two Taylor bubbles. The "double-noses" phenomenon comes from a "competition" between two-bubbles to flow together and then agglomerates and captured to be double-noses bubble. On the other hand, the presence of "liquid lamella" ascertains that Taylor bubble may be formed from two successive large bubbles. The preceding bubble hit the leading one and the coalesce point was captured as a thin liquid lamella, alike the thin layer between them. Phenomena of agglomeration of smaller to be larger bubble were still continuing to grow to be larger Taylor bubbles.

Quantitatively, the Taylor bubble is be defined as an elongated bubble which has an equivalent diameter more than a tube diameter (Krussenberg et al., 1999; Prasser et al., 2001; Lucas et al., 2003, 2005) with length longer than 1.5 times of the tube diameter as stated by Zukoski (1966) and Tomiyama et al. (1998) which reported by Mandal et al. (2007). After the quantitative parameters were stated, classification of bubble types can be apparently derived, including Taylor bubble, spherical cap bubble, or the natural bubble. In this present study, the three observed bubble types were observed, shown in Table 4.1. There were spherical

cap bubbles, Taylor bubble, and bubble flow. Based on those criteria, they could be clearly derived.

Table 4.1. Example of bubble types in slug flow region

Bubbly flow	Spherical caps bubble	Taylor bubble
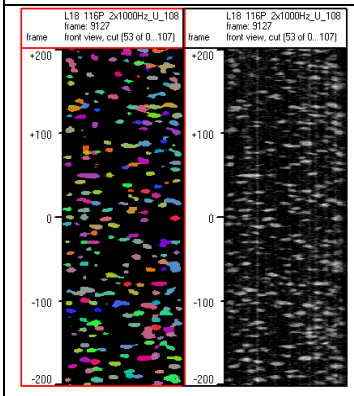	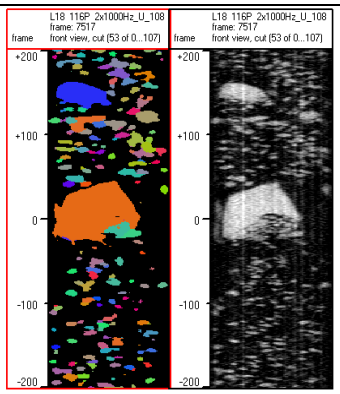	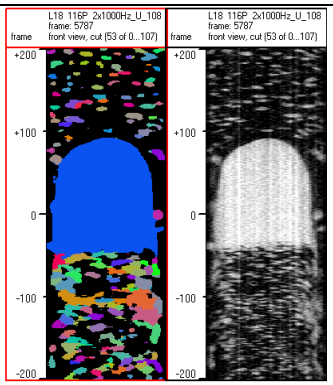

4.2. Slug flow general characteristics

4.2.1. General characteristics from time-series data

Measurement by ultrafast X-ray tomography also revealed averaged time-series void-fraction data during 10 second measurement time. Figure 4.3 depicts the examples of the time-series data in whole measurement time (10 seconds) in every measurement layer and various axial stations.

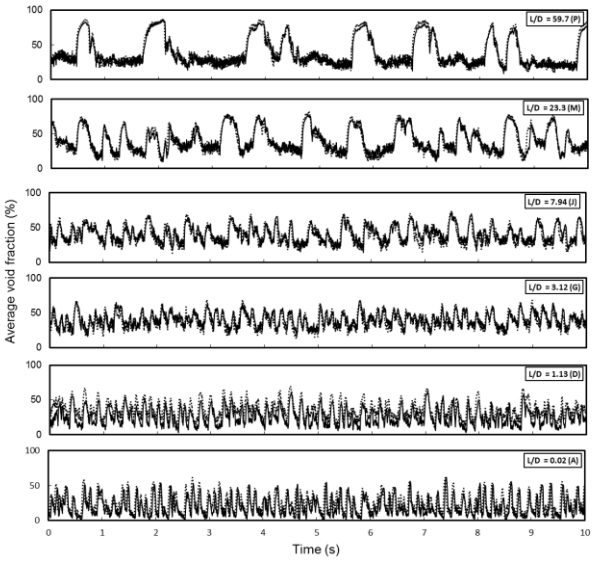

Figure 4.3. Time series of void fraction in J_L = 0.161 m/s and J_G = 0.219 m/s. The sign of (---) indicates lower measurement plane and (—) indicates upper measurement plane

This obtained results draw the averaged void-fraction characteristics of each axial stations, from A (z/D = 0.3) to P (z/D = 60) stations. Time-series data of matrix point 114 (J_L = 0.161 m/s and J_G = 0.219 m/s) shows a different type of void fraction from low and tight gap (cross sectional average void fraction was laid from 0.78 % to 62.03 % at A-station) to be larger value with an intermediate gap in D (z/D =1.13) and G (z/D = 3.12) stations and finally become wider when Taylor bubbles clearly appear in P-station (cross sectional average void fraction was laid from 8.58 % to 85.28% at A-station). Since the presence of Taylor bubbles and spherical cap bubbles, P station has larger standard deviation than A-station. The irregular characteristics of slug flow also visible from the bubble distribution. Thus, void fraction distribution and standard deviation change.

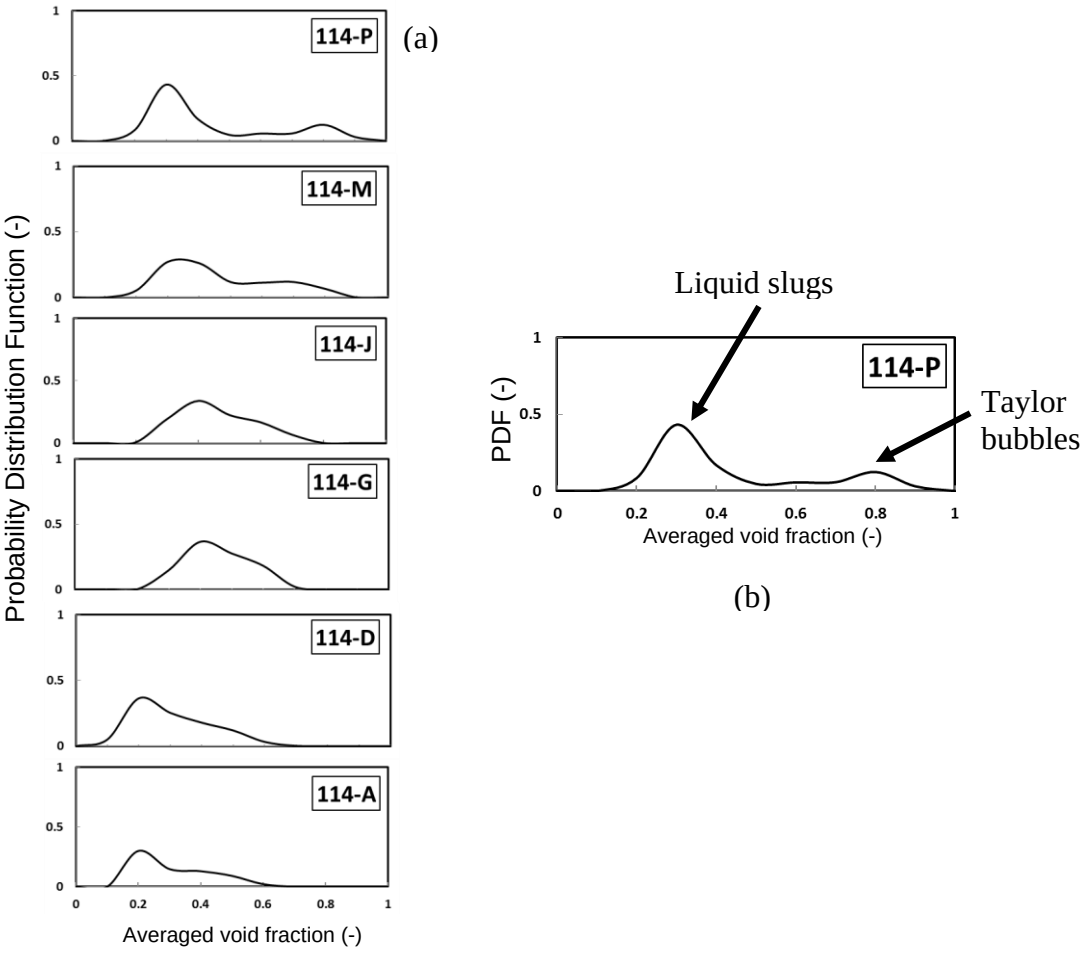

Figure 4.4. Void fraction measurement along the vertical position (a) in different axial station (b) description of double-peaks plot of void fraction (J_L = 0.161 m/s and J_G = 0.219 m/s)

Figure 4.4 (a) points out an example of void fraction distribution in the form of Probability Distribution Function (PDF) plots. Slug flow pattern is characterized by the presence of bimodal void fraction distribution curve. This statement was in agreement with Costigan and Whalley (1997), Kaji et al., (2009), and Khatib and Richardson (1984) who also conducted that double-peaked void fraction curves identified the existence of slug flow, which the higher one is belong to liquid slugs and the lower one is Taylor bubble. By showing probability density curves of each axial station, it can be performed that a flow transition occurred by the presence of large void fraction and bimodal probability density curves.

In the data of matrix point 114 (J_L = 0.161 m/s and J_G = 0.219 m/s), the stand out transition from lower to higher average void fraction is occurred in J (z/D = 8) station. Moreover, at the M (z/D = 23) and P (z/D = 60) stations, the bimodal curves are shown. It is in accordance with the visual images (see the Appendix 1) and quantitative results which stated that Taylor bubbles exist since J to P stations. It can be referred that to be a developed slug, initialized by the presence of large-elongated bubble, bubble need a particular time to develop and caused by the coalescence and bubble agglomeration along the pipe. Therefore, this data confirmed the bubbly to slug transition proposed by Taitel et al. (1980), Lucas et al. (2005), and Kaji et al. (2009).

Gas and liquid superficial velocities certainly influence the void fraction characteristics. Figure 4.5 presents the effects of gas and liquid superficial velocities to void fraction distribution at the highest station (P-station with z/D = 60). Under the liquid superficial velocity increases, the higher peak (bubbles in liquid slug) tends to be left-shifted. Therefore, the increase of J_L gives the higher dominancy of liquid-slugs. At this point, Taylor bubble formation tends to be more difficult. As the increase of J_L, the second peak of Taylor bubble is also not presented. It is strengthen by the qualitative observation in run 118 that dominated by spherical cap bubble and without Taylor bubbles. On the other hand, when J_G increases in constant J_L, the peak for Taylor bubbles tend to appear. A higher value of J_G gives a trigger to produce the larger bubbles including Taylor bubbles. Hence, more

Taylor bubbles are formulated, characterized by the presence of second peak for Taylor bubbles.

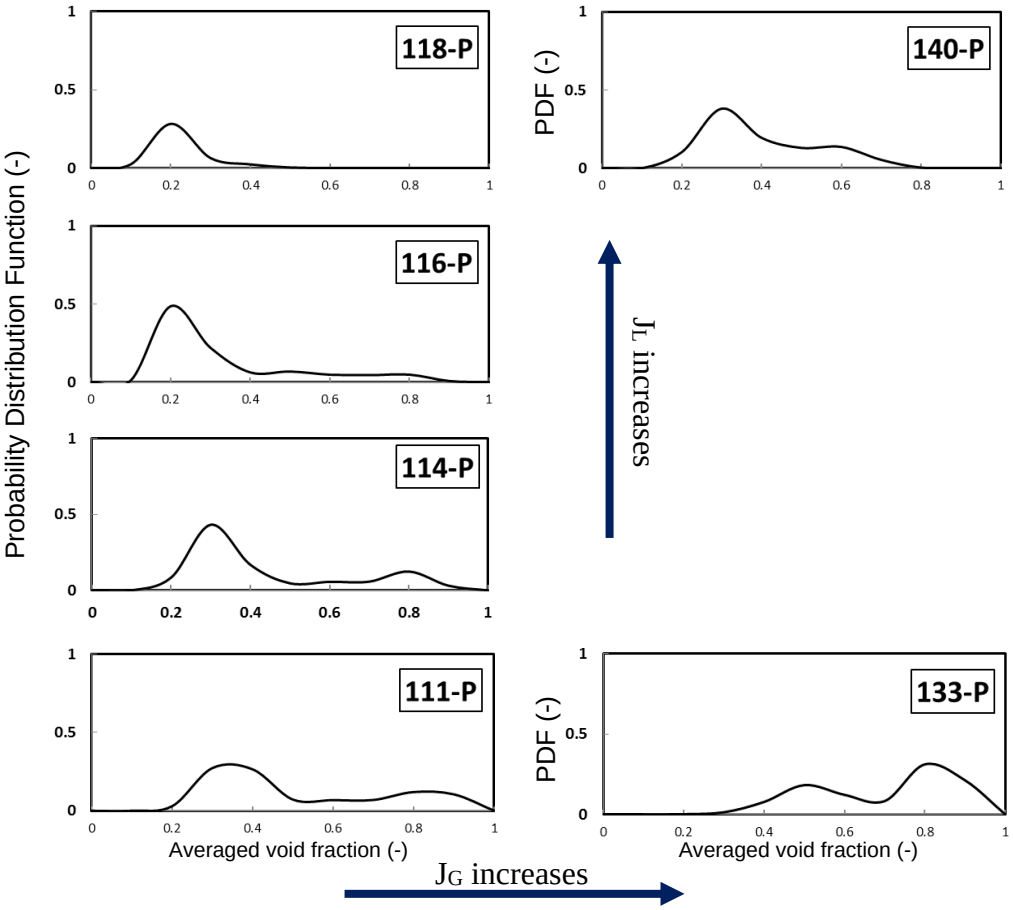

Figure 4.5. Effects of superficial velocities to void fraction distributions | at the highest axial station (P station - z/D = 60)

At the different axial station of developing areas, the void fraction distribution curves show a different shape. Figure 4.6 presents the void fraction distributions in the developing area especially in D (z/D = 1.13) and G (z/D = 3.12) stations. When bubbles still in the process to be a developed slug flow, there is only one-peak distribution curves. For each transition from D-station to G-station, the curves are right-skewed. If the effects of the gas and liquid superficial velocities are compared for the similar axial station, peak of the distribution curves tends to left. Typical of void fraction distribution in developing zone is characterized by the existence uni-modal curve of left-skewed curves (D-station) to nearly normal-distribution (G-station). A condition when liquid superficial velocity become

dominant (data 118 with J_L=1.017 m/s) shows the lowest value of maximum void fraction. The combination of gas and liquid superficial velocities give a turbulence effect (can be counted by the Reynolds number). Each liquid and gas phase find the dominancy at the same area. Hence, at the maximum J_L, transition and flow development from bubbly flow to slug flow also become the slowest and can be stated as most difficult condition.

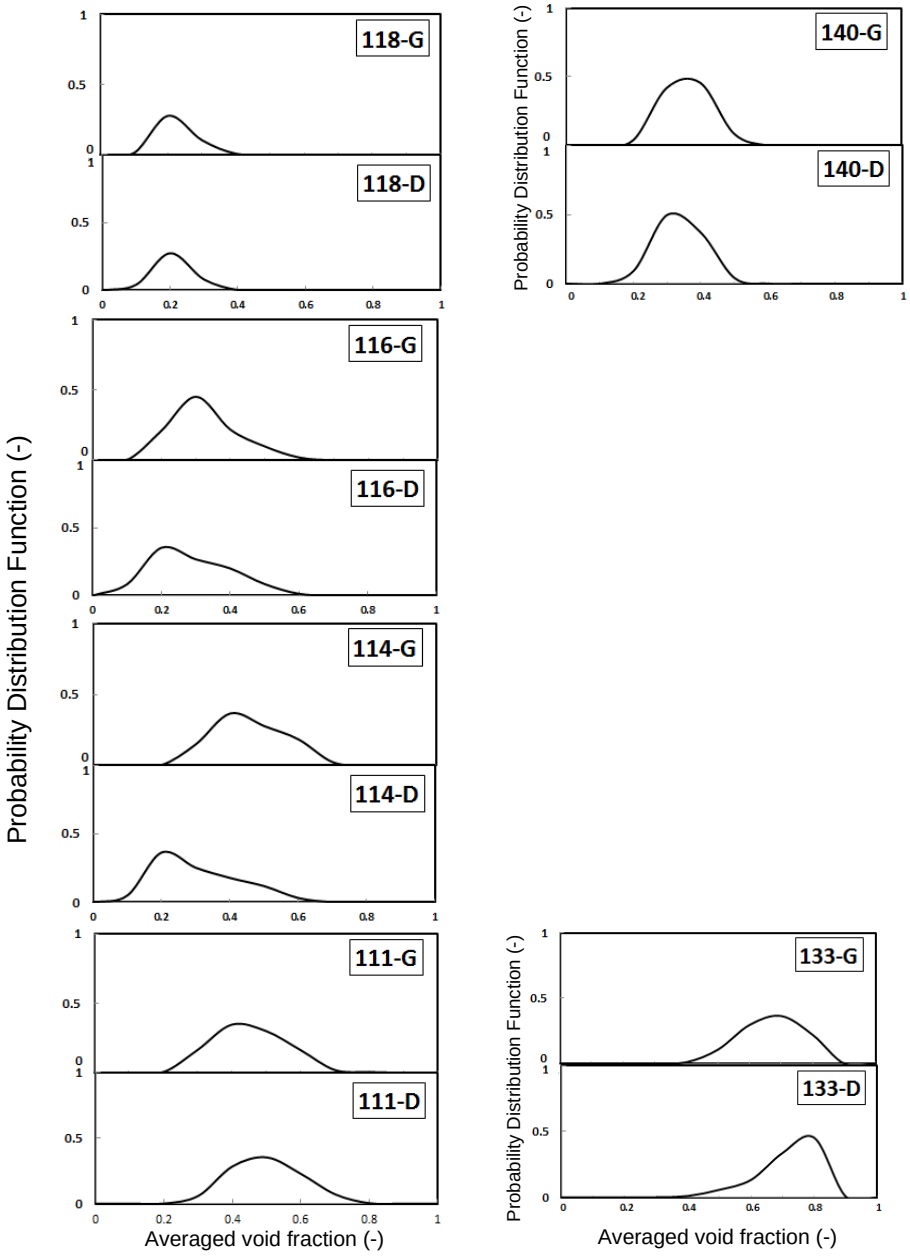

Figure 4.6. Effects of superficial velocities to void fraction distributions | at developing zone (z/D = 10 (G) and 5.5 (D))

4.2.2. Averaged void fraction

Effects of the gas and liquid superficial velocities to the averaged void fraction are presented in Figure 4.7. (a) and (b), respectively. The bars show the standard deviation of the measurement. As the liquid superficial velocity increases, the average void fraction also decreases. Otherwise, the increase of gas superficial velocity also increases the value of average void fraction. It should be remembered that void fraction is the representation of gas volume fraction comparison to the total volume of gas and liquid mixture. Hence, the more dominant value of gas (the increase of gas mass flow rate, as well the J_G) gives the higher void fraction. When liquid flow rates becomes more dominant (J_L or liquid mass flow rate increase), the average void fraction decreases.

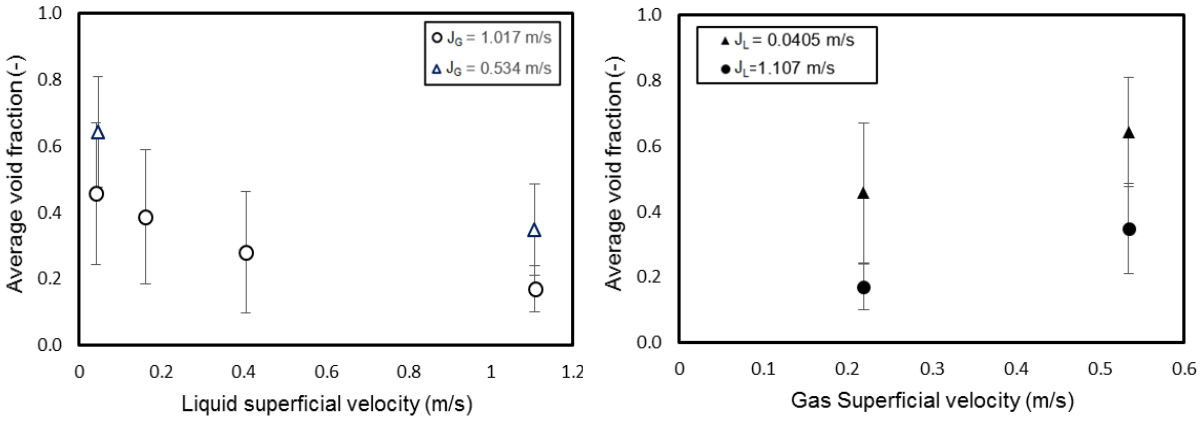

(a) (b)

Figure 4.7. Effects of superficial velocities to averaged void fraction, (a) liquid superficial velocity; (b) gas-superficial velocity

4.3. Properties of Taylor bubble

4.3.1. Rise velocity

Axial velocity of Taylor bubble was obtained by the superposition of liquid velocity and terminal velocity in stagnant liquid (Nicklin et al., 1962). Figure 4.8 shows the averaged axial velocities of 5 data which contain Taylor bubbles in P (z/D = 60) axial station. In this figure, average axial velocity follows the Nicklin's and Fernandes' equations but little bit under-predicted. As the mixture velocity increases, the averaged axial Taylor bubble velocity increases.

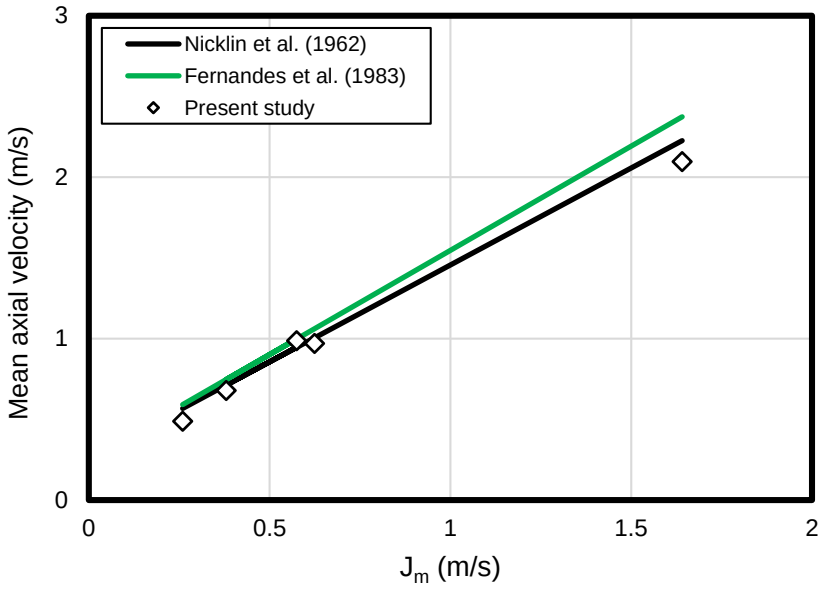

Figure 4.8. Comparison of Taylor bubble axial velocity to theoretical predictions

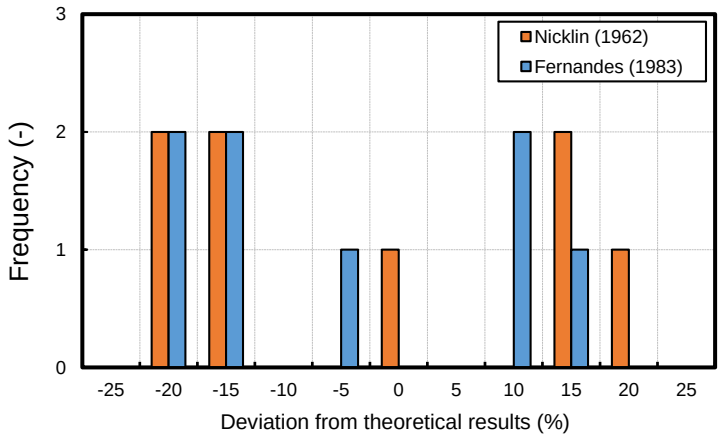

Figure 4.9. Velocity distribution of each Taylor bubble
(J_L = 0.161 m/s and J_G = 0.219 m/s, z/D = 60)

It is important to investigate the reasons of under-and over-predicted results and the distributed axial velocities. Theoretically, when the high velocity distribution of Taylor bubble still occurs, flow is not yet developed (as fully developed slug flow). In a fully developed slug flow, the rise velocity of the Taylor bubble can be regarded as steady (Nicklin et al., 1962; White and Beardmore, 1962). Each Taylor bubble velocity difference and under-predicted result might be caused by the less high axial station (not yet stable slug) and the existence of small

dispersed bubbles in the liquid slug separation distances, respectively. Van Hout et al. (2002) also conducted that the small bubbles in between successive Taylor bubbles may cause velocity distribution. It is also believed that a different behavior of those small bubbles affects the rise velocity of each Taylor bubble.

The presence of small bubbles in around Taylor bubble nose can be a reason of velocity distribution. For such cases, the dense bubbles in slug flow region caused the specific difficulties in segmentation process. As the result, artificial coalescence around Taylor bubble nose could be one of the reasons of the velocity distribution. This phenomenon affected wrong detected time (I_{front}) of the velocity determination. Hence, the velocity was scattered among each other and Nicklin et al. (1962) prediction.

A systematic error in visual study, namely discretization error in temporal resolution might also be a reason of the velocity distribution. Table 4.2 shows the discretization error of temporal resolution. The discretization is various from 6.99 to 9.86 %. In the visual study, the discretization may contributes to form a discrete grids to obtain the image analysis. Therefore, there were some erased information as well as the small measurement points which actually become the important desired information which should be referred as the initial scanned point, for example. In this study, the temporal variable from experiment was compared to obtained time from Nicklin et al. (1962) velocity equation.

Table 4.2. Discretization error in temporal resolution

		J_G (m/s)	
		0.219	**0.534**
J_L (m/s)	**1.107**	7.25 %	8.73 %
	0.405	9.86 %	
	0.161	6.99 %	
	0.0405	5.57 %	9.27 %

4.3.2. Taylor bubble length

After individual velocity of Taylor bubbles was obtained, the individual Taylor bubble length could be carried out. It was interesting to find out the relationship between Taylor bubbles length and their axial velocity. The relation is

presented in Figure 4.10, for the data at 114-P (at z/D = 60). A slight increase of velocity is performed as the increase of Taylor bubble length. The length increase gives an effect to the volume increase which also contributes to the increase of drift velocity due to buoyancy forces. The experiment result was agree with experiment by Polonsky et al. (1999) on the influence of different Taylor bubble lengths to Taylor bubble axial velocity.

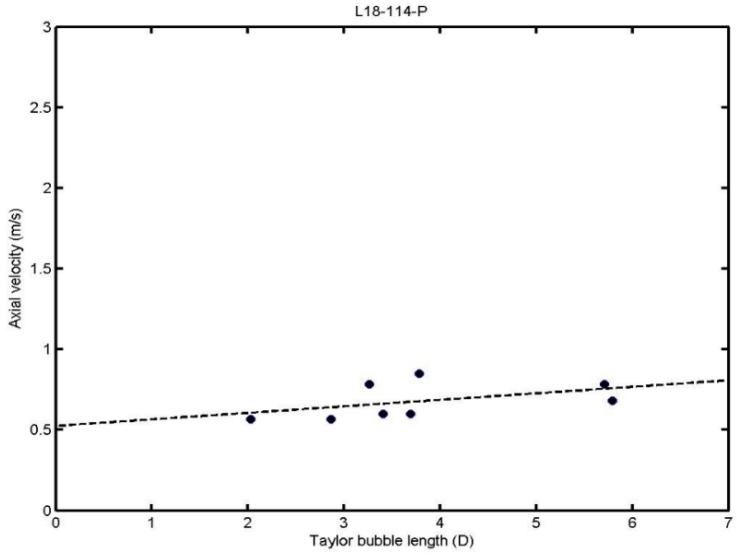

Figure 4.10. Relationship between Taylor bubble length and its axial velocity (J_L = 0.161 m/s and J_G = 0.219 m/s, P-station)

In the major results, measurements of Taylor bubble length showed the satisfied results by the deviation of relative length among upper and lower measurement is about -10% and 10%, as well depicted in Figure 4.11, for the case of J_L = 0.161 m/s and J_G = 0.219 m/s at P-station. In this figure, the relative lengths to lower-plane are presented. However, there are still a few differences on the Taylor bubble length between lower and upper measurement planes. One of the problems was the presence of small bubbles in rear-area of Taylor bubbles. It caused a specific difficulty in the segmentation process. Therefore, it was difficult to define I_{back} as the detected rear area of Taylor bubble and about the presence of small bubble which stuck to the nose. In this case, the expansion effects were neglected due to the short gap of measurement planes. Hence, the length differences were

only assumed as the measurement effect or the presence of sticky bubble in around rear or front areas.

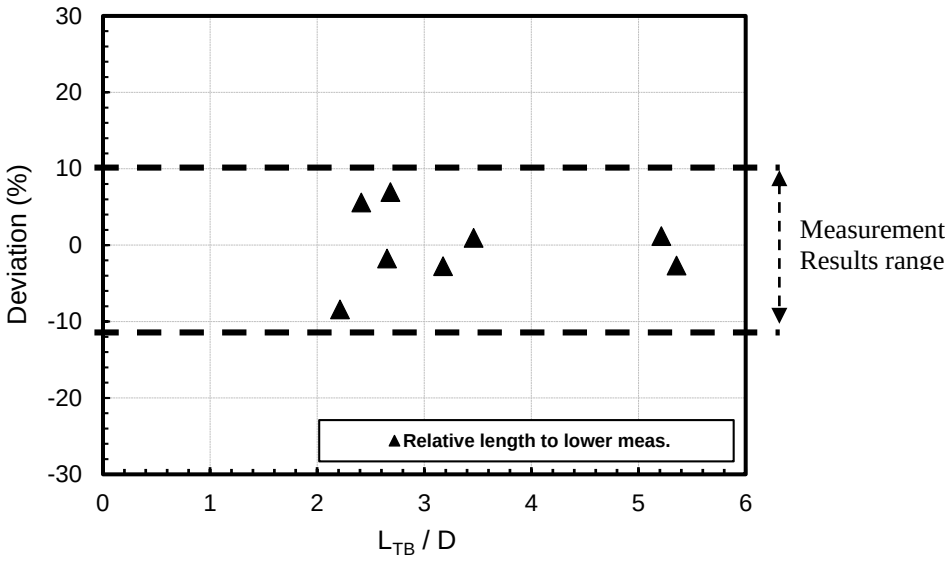

Figure 4.11. Length measurement between upper and lower planes
(J_L = 0.161 m/s and J_G = 0.219 m/s, P-station)

Length distribution of Taylor bubbles is shown in Figure 4.12. According to the figure, Taylor bubbles have different length. There were 8 detected Taylor bubbles in data of 114 at P station.

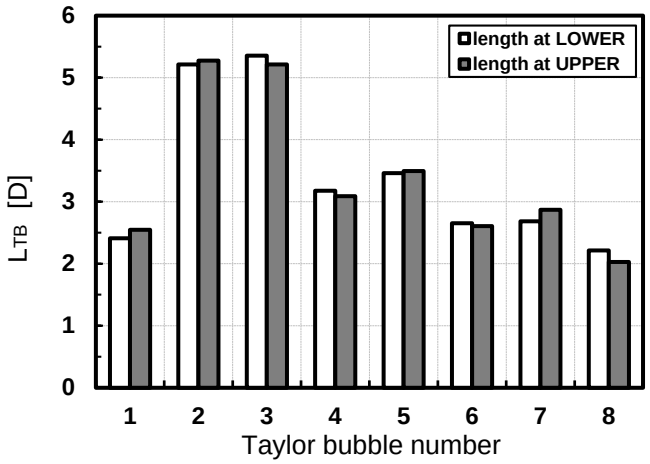

Figure 4.12. Distribution of Taylor bubble length
(J_L = 0.161 m/s and J_G = 0.219 m/s, P-station)

Due to the limited measurement period (10 seconds) for each measurement, the data had a lack of statistical result. Thus, this data did not comprehensively represent the type of length distribution. Theoretically, the Taylor bubble length distribution follows the normal-distribution curves (Barnea et al., 1993; Zheng et al., 2006; Khatib and Richardson, 1984). However, in the present study, the Probability Distribution Function (PDF) of Taylor bubble length was not presented because there are only small number of Taylor bubbles during the limited measurement time. Hence, PDF analysis cannot represent the general distribution. The similar Taylor bubble length is only reached when the stable slug (Nicklin et al., 1962). In these results, the length distribution presents the developing slug flow condition. The tendency of Taylor bubbles to be longer (by coalescence) and maintain their dimension is also depended on the velocity profile in front of each Taylor bubble.

4.4. Effects of the different axial station to the flow properties

In this present study, slug flow was observed at various axial stations. It gives an advantage to understand the effects of different axial station in related with both flow development and Taylor bubble properties and bubbles in other regions.

4.4.1. Bubble frequency at various axial stations

Experiments of vertical slug flow involved 6 axial stations to observe the flow development as well the flow pattern transition from bubbly to slug flow. Figure 4.13 presents the bubble frequency of Taylor bubble and spherical cap bubbles.

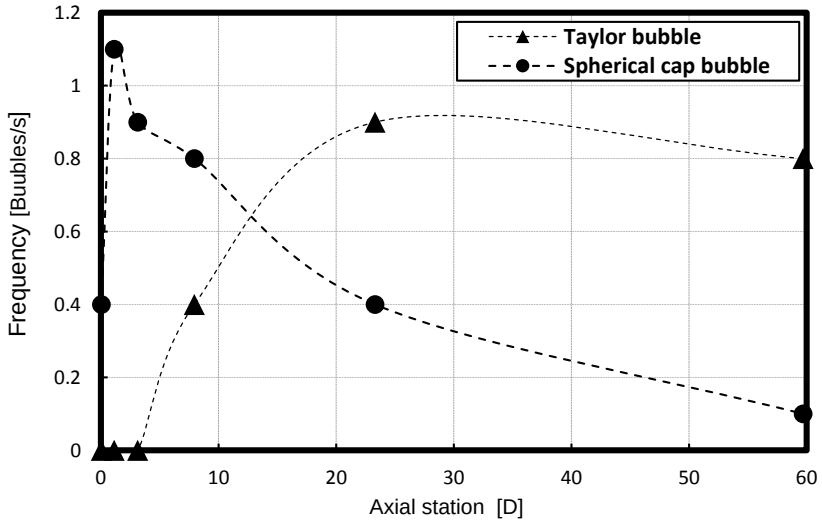

Figure 4.13. Relationship between bubble frequencies to different axial station (J_L = 0.161 m/s and J_G = 0.219 m/s)

The presence of large-skirted bubble is usually known as "spherical cap bubbles" (Joseph et al., 2003). In this present study, a large bubble with $20\ mm \leq d_{equiv} \leq D_{pipe}$ was defined as spherical cap bubble. According to Figure 4.13 above, the development of cap bubbles and Taylor bubbles can be interpreted.

In that figure, the larger bubbles grow from D-station (z/D – 1.13). Again, they develop to be cap bubbles that located at pipe center because there are lower rate of turbulence dissipation and lower shear rate than in around pipe wall, as well stated by Lucas and Krepper (2007) and Krepper et al. (2008). Since the J-station (z/D = 8), Taylor bubbles start to grow and cap bubbles frequency is decreased because of the coalesce intention to the Taylor bubbles or the other cap bubbles. Contrarily, Taylor bubble numbers through J and M stations are increased. The bubble agglomeration results more bubbles with $d_{equiv} > d_{pipe,}$ which is recorded by the algorithm as a Taylor bubble. Next, the Taylor bubble is still going to become larger and longer again, as long as the increase of axial stations. Although P-station is the highest station, bubble coalescence still occurs there. Hence, a slight frequency decrease is shown in P-station (z/D = 60). A qualitative observation is showed in Figure 4.14. Transition from smaller into larger bubbles is shown by the series from large cap to spherical cap bubbles. During the increase of axial stations,

they agglomerates into larger spherical caps and Taylor bubbles in highest axial station.

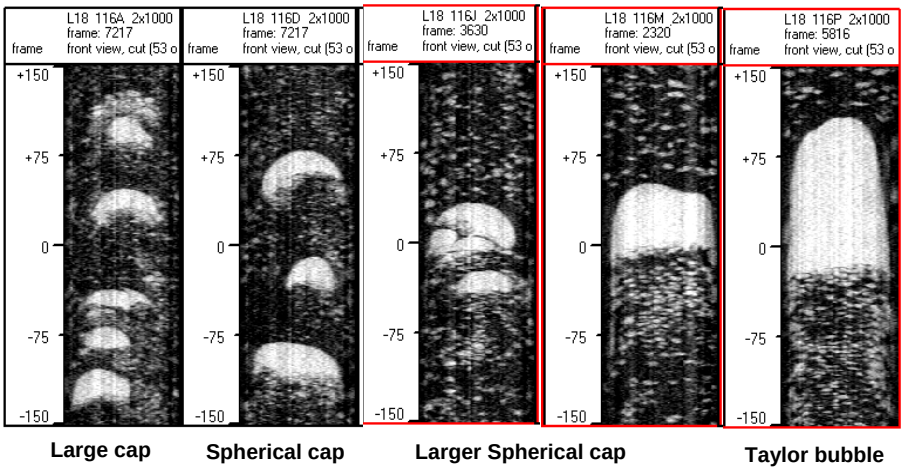

Figure 4.14. Transition from spherical cap to Taylor bubble
(J_L = 0.405 m/s and J_G = 0.219 m/s)

In general, the transition performs a similar pattern if the data of matrix point 114 is compared to the other matrix points (118 and 140). The difference is in the onset of slugging. Figure 4.15 (a) points out the bubble frequencies in matrix point 118 with no detected Taylor bubbles. There is only spherical cap bubble in P-station (z/D = 60). Under a constant J_L = 1.017 m/s, as the highest observed value of liquid superficial velocity, the matrix point 140 has a higher J_G than 114 with higher Taylor bubble frequency.

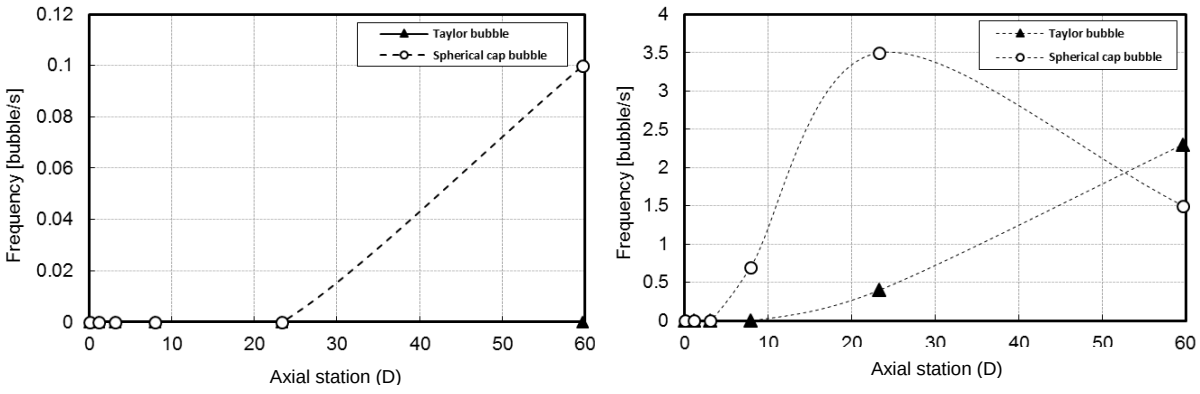

(a) (b)

Figure 4.15. Effects on difference stations to spherical cap bubble and Taylor bubble frequencies. (a) 118 (b) 140

In a constant J_L, the influence of higher gas volume flow rates (represented as higher J_G) more than 2 times than matrix point 118 gives different number of Taylor bubbles. For matrix point 140, Taylor bubble are appeared since M-station (z/D = 23), slower than matrix point 114 (observed since J-station). It should be noted that the data matrix 140 has a quite high J_L which liquid dominancy is stronger than gas-phase. The observed flow evolution were agree with Van Hout (2001, 2002), Lucas et al. (2005), and Kaji et al. (2009). As well stated by Krepper et al. (2008), basically, the transition from dispersed bubbles at low gas rates to slug flow requires a process of agglomeration or coalescence. It is determined by a complex interaction between the bubble forces, caused by a lateral bubble migration and bubble coalescence also bubble breakup.

4.4.2. Effects of the different axial station to Taylor bubble rise velocity

Figure 4.16 presents the effect of the different axial station to the Taylor bubble rise velocity. As the increase of axial station, Taylor bubble velocity is not strongly influenced, but the velocity seems a slightly decrease. Certainly, a higher mixture velocity gives higher Taylor bubble axial velocity.

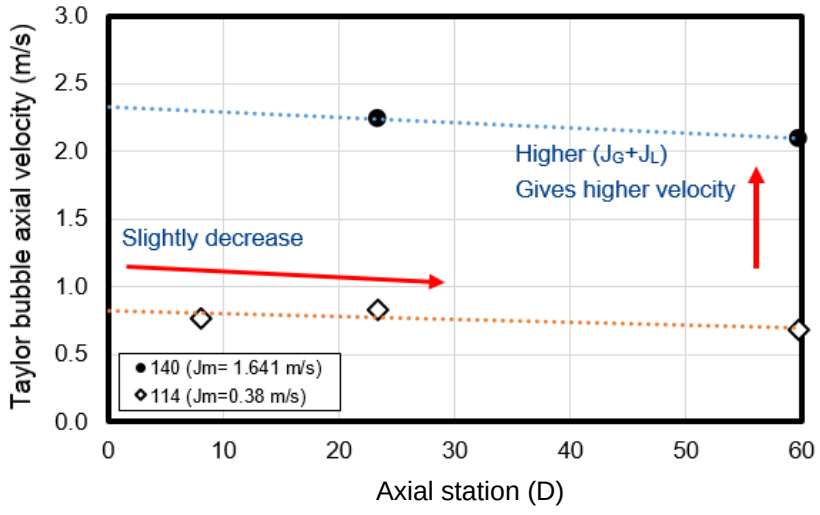

Fig. 4.16. Effects of the different axial station to Taylor bubble rise velocity

This phenomenon was in a good agreement with experiment in 54 mm pipe diameter by Van Hout et al. (2001). In this experiment, Taylor bubble velocity was normalized by Nicklin's equation. However, only experiments in z/D = 16.8 and

50.4 could be used as comparison. According to Van Hout et al. (2001), translational velocity tends to decrease first in the developing stations and increase at z/D = 88.7 to 127. Measurements in points 140 and 114 show the similar trends, but Taylor bubbles are only formed and detected since axial station J.

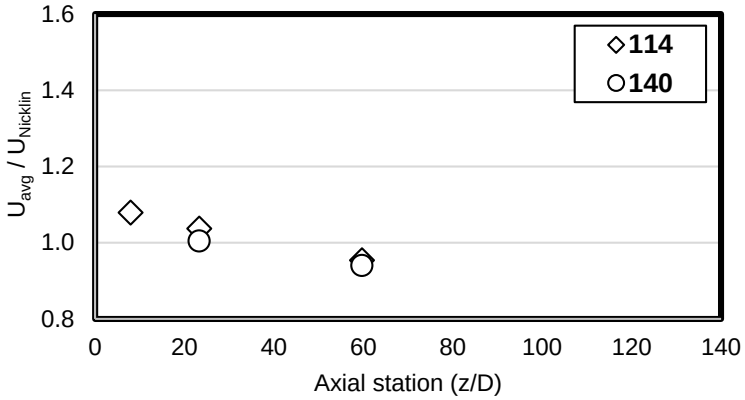

Fig. 4.17. Effects on axial station on Taylor bubble axial velocity

4.4.3. Effects of the different axial station to Taylor bubble length

Averaged length of Taylor bubble and liquid slug in various axial stations were measured, shown in Figure 4.18. During the developing process, both of Taylor bubble tend to be longer. For each measurement point, at the highest axial station (z/D = 60), the longest Taylor bubble is found and perhaps still developed to be longer bubble due to coalescence and agglomeration from the cap bubbles or the dispersed bubbles. The results were in agreement with Mi et al. (2001) who reported that Taylor bubble length is gradually increased along the axial stations.

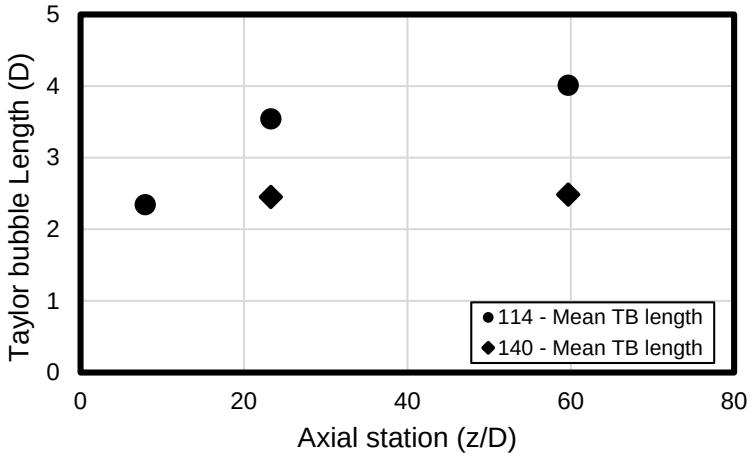

Figure 4.18. Length measurement between upper and lower planes

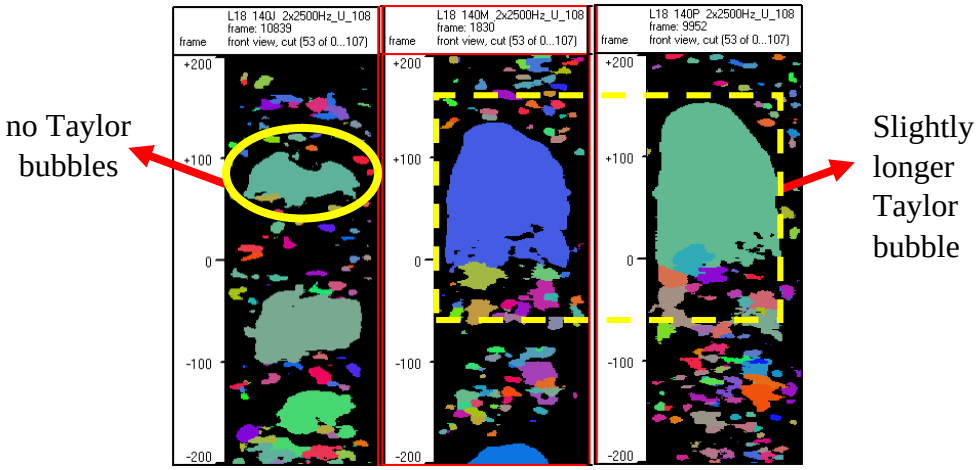

Figure 4.19. Taylor bubble length comparison of matrix point 140
140 (J_L=1.017 m/s and J_G=0.534 m/s)

Figure 4.19 depicts a qualitative evidence from front-cut view of the Taylor bubbles in J-M-P stations of J_L = 1.017 m/s and J_G = 0.534 m/s. This figure explains the data of Taylor bubble length for matrix point 140 in Figure 4.18 above. In this data-point, Taylor bubbles are observed since M-station (z/D = 23.3) and there is no Taylor bubbles founded in lower stations since the higher liquid superficial velocities. Consequently, the shorter Taylor bubbles are shown, compared with data-point 114 (J_L = 0.161 m/s and J_G = 0.219 m/s) which has lower J_L. In M and P-stations, the average length is almost similar. It is believed that the dominancy of liquid-phase higher than gas-phase, so that it resist the bubbles to be longer.

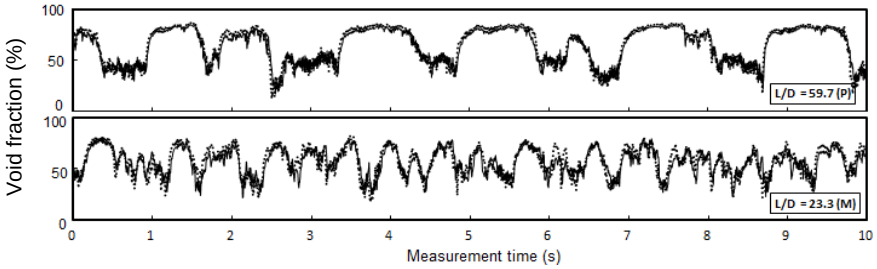

Figure 4.20. Example of time-series data in different axial station
(J_L = 0.0405 m/s and J_G = 0.534 m/s at P and M stations)

When the trend is compared with result of time-series data, higher axial station affects longer and wider time durations of high-void fraction peak and the separation distance, shown in Figure 4.20. In this diagram, the averaged void

fraction signal for matrix point 133 P and M are presented. It is obviously shown that the highest station is consisted of longer and wider "signal" rather than the lower stations. Additionally, the matrix point 133 is the lowest liquid superficial velocity which generates much longer Taylor bubble due to the gas-phase dominancy in two-phase flow.

4.4.4. Effects of different axial station to the bubble properties in other regions

In slug flow case, bubble pair algorithm was able to identify bubbles in different slug flow regions, based on the previous criteria. As the result, bubble frequency could be calculated. Figure 4.21 (a) performs the frequency of solved dispersed bubbles in liquid slug region along 10 seconds measurement time for 114-P matrix data. In this figure, classified bubbles that located in wake and swelling (falling film extension) regions are appeared since at the D-station. Not only Taylor bubble, but also spherical cap bubbles generates small wake and falling film effects.

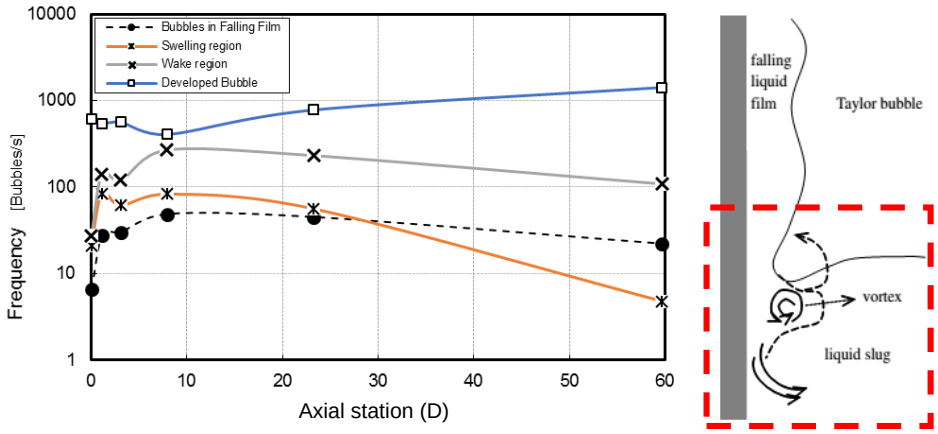

(a) (b)

Figure 4.21. (a) Effect of axial station on the small bubbles frequency in liquid slug for point 114; (b) Entrainment formation in the behind area of Taylor bubble (taken from Zheng et al., 2006)

Frequencies of bubbles in falling film, swelling region, and wake region seems decrease along J-M-P stations. The appearance of Taylor bubble (since J-station) generates the vortices (Figure 4.21 (b)) and more chaotic condition in rear Taylor bubble area rather than at the lower stations. As the effect, bubble collision

and coalescence become more frequent. Consequently, the bubble frequency decreases and there is a little increase of bubble diameter, as well shown in Figure 4.22 as the agglomeration effects.

Figure 4.22 represents the observation results of equivalent diameter. The data were taken as the averaged value. In this diagram, it can be stated that along the lower stations such as A-D-G stations, diameter of the dispersed bubbles in other slug flow region increases whereas in the next stations has a relatively flat trend. Specifically, there are a different pattern for wake and swelling region. It can be interpreted that an increasing trend occurs as the increase of the axial stations. The mixing and turbulence effects in those region are contributed to generate swarm and dense bubbles. Basically, the segmentation process was an important process which was able to contribute in the next process. Hence, it is fair to say a slightly increase of the bubble equivalent diameter occurs for bubbles in wake and swelling regions. When the segmentation process was not perfect, it also caused the inappropriate diameter detection, especially in around Taylor bubble rear area. It is important to note that the value is averaged value, hence not all bubbles segmented to had "higher" diameter.

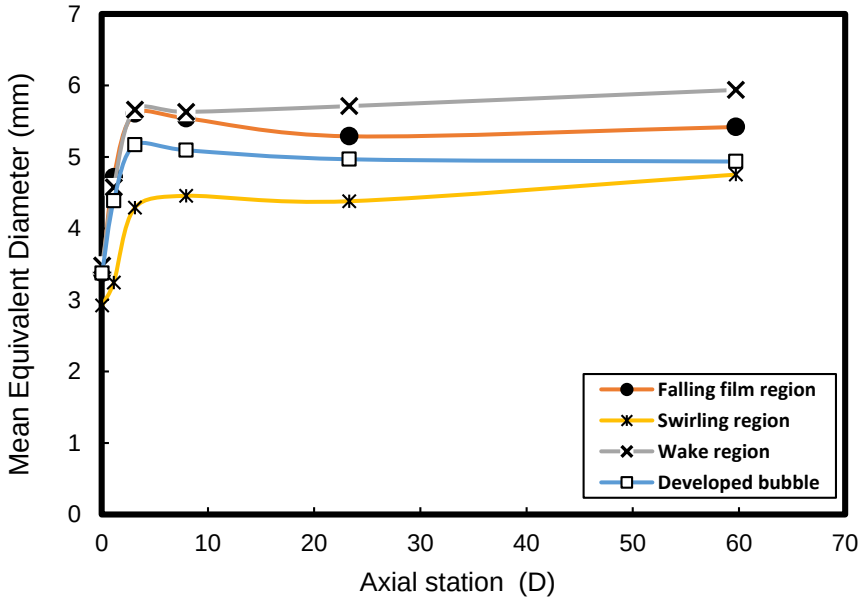

Figure 4.22. Effects on axial station on bubble size in other regions

4.5. Relationship between the consecutive Taylor bubbles

The consecutive relation between the leading and the trailing Taylor bubble is also performed in Figure 4.23 for J_L = 0.161 m/s and J_G = 0.219 m/s at P-station. There is a specific relation between Taylor bubble rise velocity and length of liquid slug ahead. Comparing with of the other experimental results (Moissis and Griffith, 1962 and Guo-Dong et al., 2009), the result represents a good agreement by showing a good data trend.

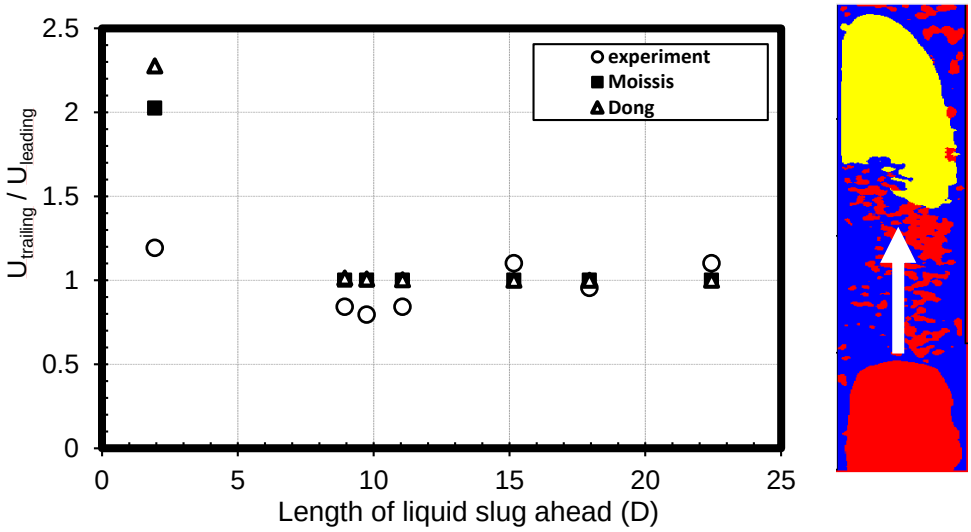

Figure 4.23. Relationship between the consecutive Taylor bubbles
(J_L = 0.161 m/s and J_G = 0.219 m/s, z/D = 60)

Commonly, after reach the stable liquid slug length (10-20 D), the trailing and leading Taylor bubbles are in the similar velocity. In the present result, fluctuation still occurs at about 15 D and 23 D because Taylor bubble flows in a developing slug flow. It is also remembered that measurement of point 114, with medium J_L and J_G, was conducted in z/D=60 that had not have fully developed nature of slug flow yet whereas the compared data were commonly taken at quite higher axial stations. Theoretically, the coalescence mechanism is also influenced by the liquid profile and bubble behavior in separation distance ahead the Taylor bubble.

4.6. Characteristics of bubbles in other slug flow regions

4.6.1. Bubbles in falling film region

Axial velocities of small bubbles in falling film, normalized by each Taylor bubble velocity are illustrated in Figure 4.24. As an example, there are 8 bubbles in the case of 114-P with J_L = 0.161 m/s and J_G = 0.219 m/s. According to the figure, most bubbles are located in near pipe wall (relative radial positions starting from 0.7 to 0.9) due to swept effect of Taylor bubble rises. Due to the smaller size than Taylor bubble, the small bubble velocity was expected to be less than Taylor bubble velocity (or the value is less than 1.0). Taylor bubble velocity should be faster than the bubbles in surrounding since the larger buoyancy force. Moreover, the bubble diameter distributions are ranging around 3-6 mm and 6-10 mm in near wall and slightly pipe centered, respectively.

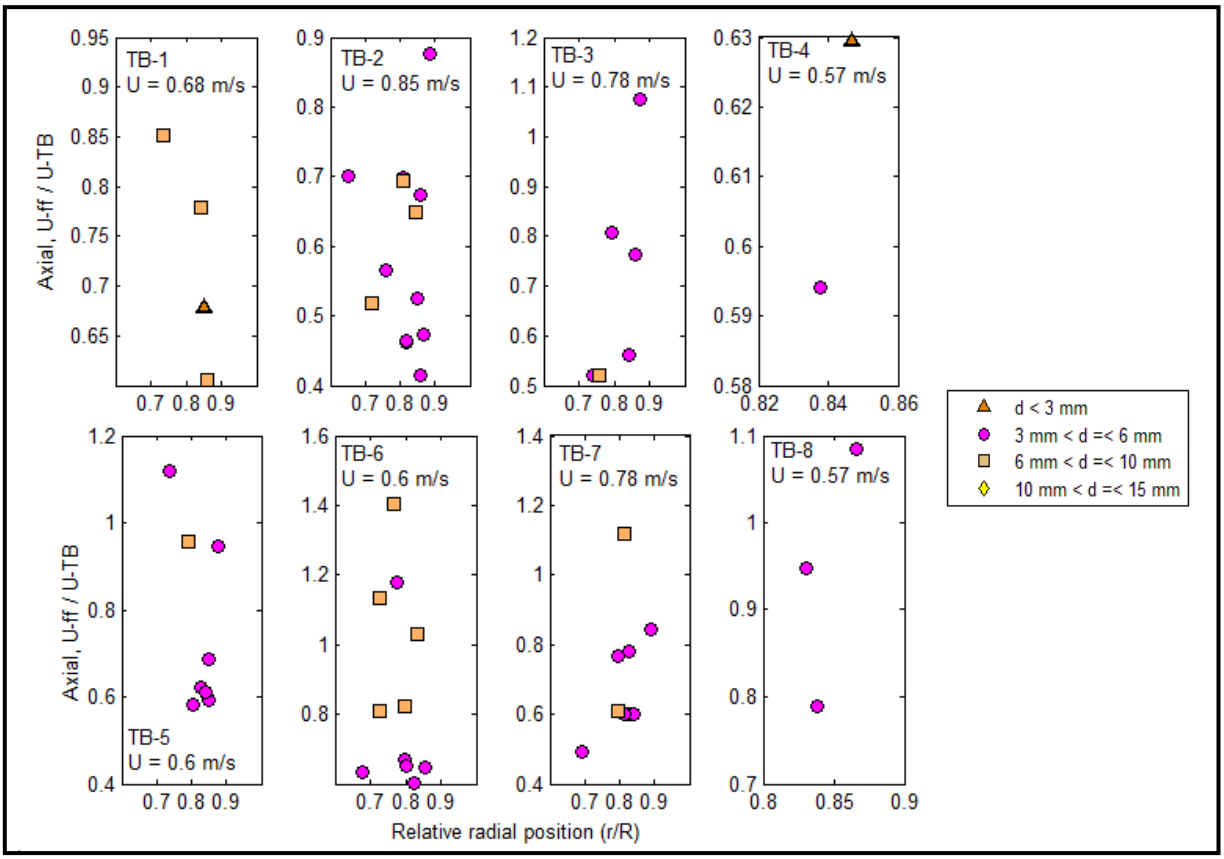

Figure 4.24. Small bubbles in falling film region
(J_L = 0.161 m/s and J_G = 0.219 m/s)

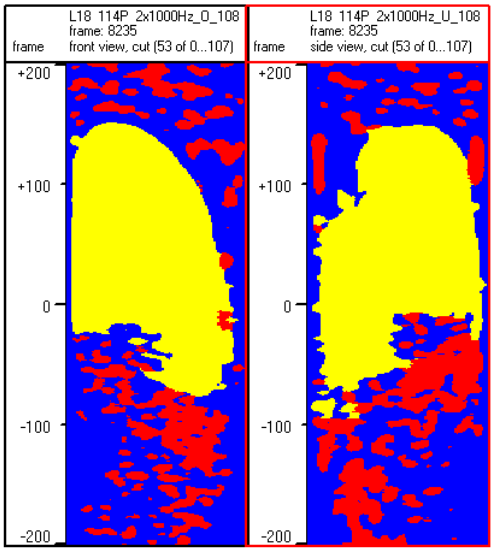

Figure 4.25. Visualization of bubbles in falling film region

However, bubbles with larger velocity are might be a result of an artificial coalescence to the Taylor bubble body or nose which detected has a same or even larger velocity with the Taylor bubble. Figure 4.25 illustrates the example of a case when small bubbles tend to stick in Taylor bubble body or nose. This phenomena might be the reason of wrong detected time in velocity measurement.

4.6.2. Bubbles in wake region and developed bubble region

Previously, the individual characteristics of small dispersed bubble in liquid slug were still rarely to be characterized. The high dense flows, swarm dispersed bubbles with high shear stress in Taylor bubble rear area, and also the generated vortices by wake region were contributed to the difficulties of the segmentation process. They also became the reasons of the visual limitations.

Figure 4.26 presents the distributions of bubble sphere equivalent diameter in wake region. A larger bubble distribution is occurred in wake region. However, the larger diameters were possibly caused by artificial coalescence due to the difficulties to define interface boundaries in very small and chaotic movements of bubbles in wake region. Bubble pair algorithm was able to detect individual velocity and equivalent diameter as well. Thus, the better prediction for small bubble diameter is expected, as long it is supported by a good performance of

reconstruction and segmentation processes. Additionally, in this present study, the wake regions were classified as the laminar wake, according to Campos and De Carvalho (1988b) criterion that based on inverse viscosity number (N_f).

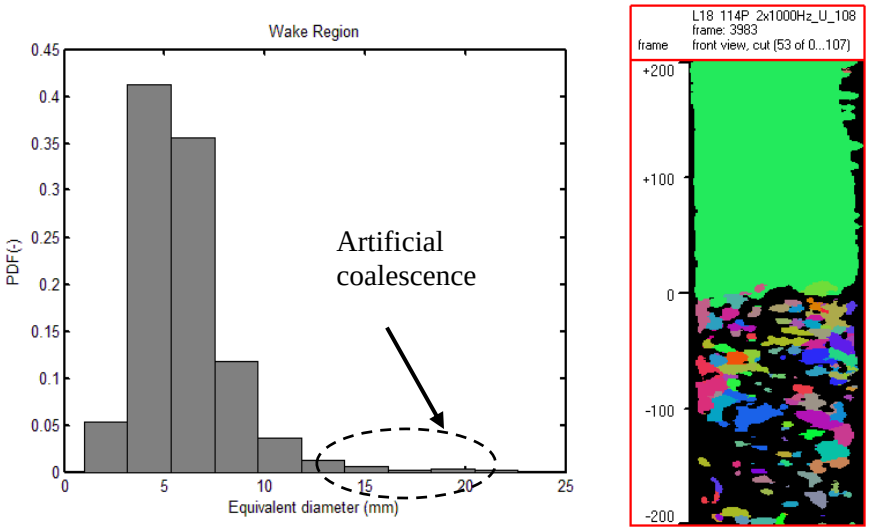

Figure 4.26. Distribution of bubble equivalent diameter in wake region (J_L = 0.161 m/s and J_G = 0.219 m/s)

Probability Distribution Function of bubble sphere equivalent diameter for developed bubble region is depicted in Figure 4.27. The average diameter is reached around 5-5.5 mm.

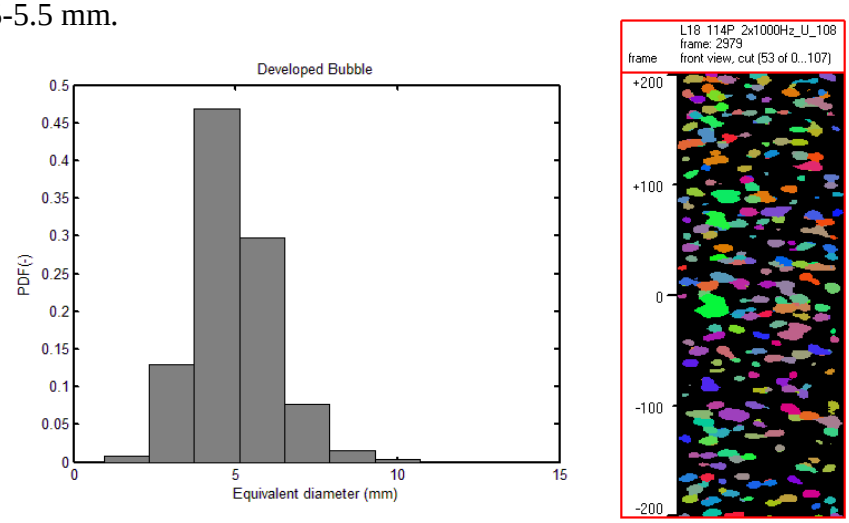

Figure 4.27. Distribution of equivalent diameter in developed bubble region (J_L = 0.161 m/s and J_G = 0.219 m/s)

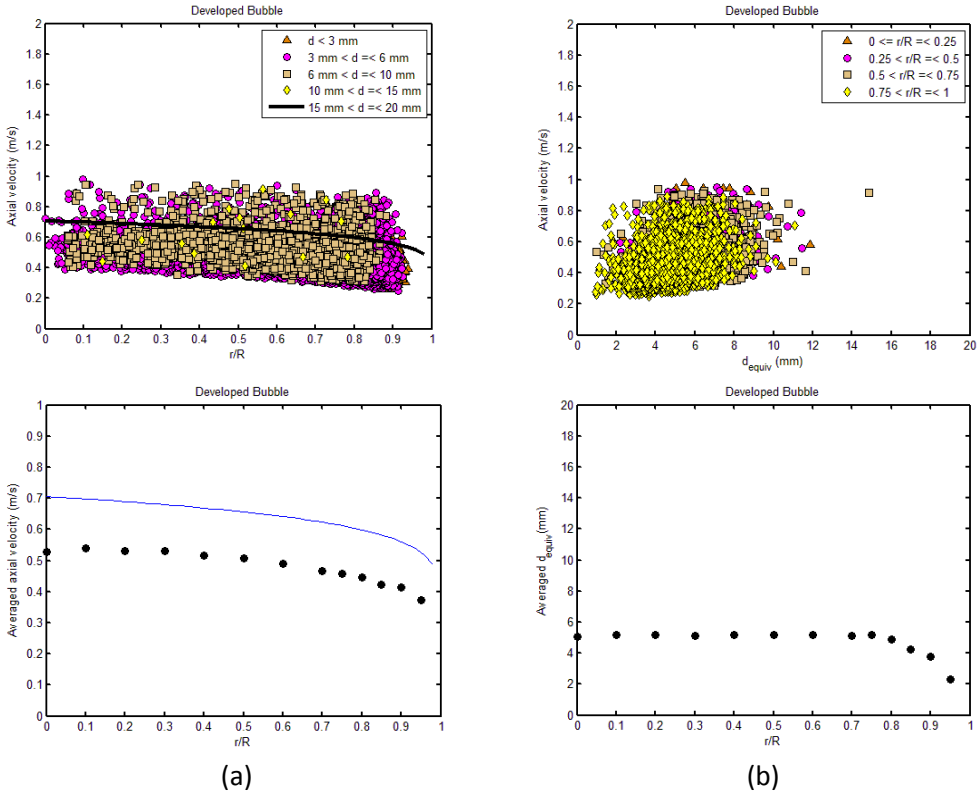

(a) (b)

Figure 4.28. Axial velocity in developed bubble region,
(a) radial distribution; (b) diameter-based distribution
(J_L = 0.161 m/s and J_G = 0.219 m/s, z/D = 60)

Figure 4.28 (a) and (b) depict the bubble axial velocity in developed bubble region in the form of radial distribution and diameter-based, respectively. Plots of individual bubble velocity, considering the diameter, are presented. However, the mean axial velocity diagrams is also shown for obtaining the better interpretation of the data. Basically, the axial profile follows the Power Law Distribution curves by slightly decrease velocity at the near pipe-wall. In near pipe wall, the bubble diameters decrease so that this area is occupied by smaller bubble diameters. The smaller bubbles certainly have lower velocity than the larger bubble due to buoyancy forces. The mean axial velocity follows power-law distribution curve which represents the nature of bubbly flow.

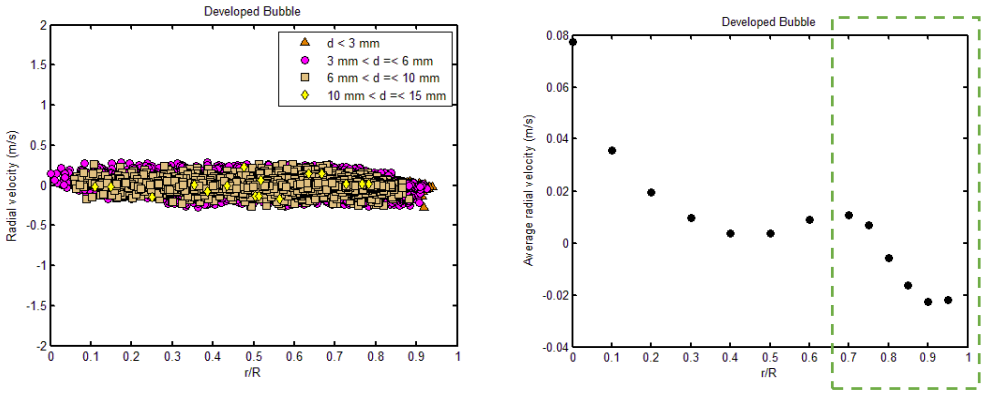

Figure 4.29. Radial velocity in developed bubble region,
(a) individual velocity; (b) average velocity distribution
(J_L = 0.161 m/s and J_G = 0.219 m/s, z/D = 60)

Figure 4.29 (a) presents the bubble individual radial velocity in the developed bubble area. Moreover, to get better interpretation, the averaged value of radial velocity distribution profile are explained in Figure 4.29 (b). In general, the value exists in very small range (-0.02 to 0.08 m/s) but there is an "oscillating" profile. It should be noted that minus (-) sign is an identity for bubble direction which tends to pipe wall. Almost similar characteristics of bubbly flow, the oscillating pattern is ruled by lift and wall force. During the rise movement of Taylor bubble, it gives a swept effect to the bubbles in the surroundings.

Finally, bubble pair algorithm showed a good performance to reveal slug flow characteristics, as well as the Taylor bubble properties and characteristics of bubbles in liquid slug. Detail analysis of the algorithm performance has been presented by Patmonoaji (2014) as well the velocity field profile. This study ensure that the algorithm was suitable enough for observing important flow properties which have not been processed before by obtaining ultrafast X-ray tomography and bubble pair method.

CHAPTER V
CONCLUSION AND FUTURE WORKS

5.1. Conclusion

1. Taylor bubble properties and their reactions to the surroundings are investigated from the experimental database of an ultrafast X-ray tomography
2. General characteristics of slug flow were explained in the form of qualitative observation and quantitative explanation of void fraction. In higher J_L, slug flow was not observed and only spherical cap bubbles were presented.
3. Taylor bubble properties such as the velocity, frequency, and length were observed. This study was also included the results of:
    a. Reasons of velocity distribution are studied.
    b. The presence of Taylor bubble generates different flow behaviors for small bubbles around it such as bubbles in falling film region and behind area of the Taylor bubble.
4. Transition from bubbly to slug flow pattern gives an important understanding of flow development and evolution. In related with Taylor bubble properties and slug flow, there are some conclusion, stated as follow:
    a. The increase of axial measurement station influences flow pattern, void fraction, and properties of Taylor bubble and liquid slug as well.
    b. Taylor bubble formation is quantitatively shown and caps bubble grow to be Taylor bubble along the higher stations.
    c. Slug flow need a certain distance to be a fully developed flow characteristics (stable slug).
5. Bubble pair method was capable to reveal the Taylor bubble properties and slug flow characteristics. A relevant agreement between the previous studies was carried-out.

5.2. Future works

1. More accurate segmentation data, especially in wake region are needed
2. Wider data range (J_G-J_L) and effects of other properties (fluids) can be applied for more comprehensive studies
3. Collaboration with other measurement technique, such as Particle Image Velocimetry (PIV) and wire-mesh sensor should be applied to obtain accurate velocity profiles
4. The present work generates some possibilities to obtain the future works, such as:
    a. Deeper study on bubble characteristics in liquid-slug region.
    b. Investigation of velocity profiles and velocity vector field, especially around bubble nose, liquid slug, and Taylor bubble rear-area.
    c. Turbulence effects and swelling movements in liquid slugs and entrainment formation in between falling film regions

BIBLIOGRAPHY

Ahmad, W.R., De Jesus, J.M., and Kawaji, M., 1998, Falling film hydrodynamics in slug flow, *Chem. Eng. Sci*, 53, pp. 123-130.

Alajdem Talvy, C., Shemer, L. and Barnea, D., 2000, On the interaction between two consecutive elongated bubbles in a vertical pipe. *Int. J. Multiphase Flow* 26: pp. 1905-1923.

Antal, S.P., Lahey, R.T., and Flaherty, J.E., 1991, Analysis of Phase Distribution in Fully Developed Laminar Bubbly Two-Phase Flow, *International Journal of Multiphase Flow*, 17, pp. 635-652.

Araújo, J.D.P., Miranda J.M., Campos, J.B.L.M., 2013, Flow of two consecutive Taylor bubbles through a vertical column of stagnant liquid – A CFD study about the influence of the leading bubble on te hydrodynamics of the trailing one, *Chemical Engineering Science*, 97, pp. 16-33.

Bankoff, S. G., 1960, A variable density single-fluid model for two-phase flow with particular reference to steam-water flow, *J. Heat Transfer*, 82 (2), pp. 265-270.

Banowski, M., Lucas, D., Hoppe, D., Beyer, M., Szalinski, L., Hampel, U., 2013, Segmentation of ultrafast x-ray tomographed gas-liquid flows in a vertical pipe at different flow regimes, *Proceeding of WCIPT7 2013*, Poland:Krakow.

Bendiksen, K. H., 1984, An experimental investigation on the motion of long bubbles in inclined tubes, *Int. J. Multiphase Flow,* 10 (4), pp. 467-483.

Beyerlein, S.W., Cosmann, R.K., Richter, H.J., 1985, Prediction of Bubble Concentration Profiles in Vertical Turbulent Two-Phase Flow, *Int. J. Multiphase Flow*, Vol. 11, No. 5, pp. 629-641.

Boyd, D.P., Lipton, M.J., 1983. Cardiac computed tomography. *Proc. IEEE 71*, pp. 298–307.

Brauner and Barnea, 1986, Slug/churn transition in upward gas-liquid flow, *Chem. Engng Sci*. 41, pp. 159-163.

Broadkey, R.S., 1967, The Phenomena of Fluid Motions, *Addison-Wesley Press*.

Brötz, W., 1954, Uber die Vorausberechnung der Absorptions geschwindigkeit von Gasenin Stromenden Flussigkeitsschichten, *Chem. Ing. Tech.*, Vol. 26, pp. 470. (in German language)

Brown, R. A. S., 1965, The mechanics of large gas bubbles in tubes. I - Bubble velocities in stagnant liquids, *Canadian Journal of Chemical Engineering*, 43: pp. 217-223.

Campos, J.B.L.M., De Carvalho, J.R.F.G., 1988a, Mixing Induced by Air Slugs Rising in Narrow Column of Water, *Chemical Engineering Science*, Vol 43. No. 7, pp. 1569-1582.

Campos, J.B.L.M., De Carvalho, J.R.F.G., 1988b, An experimental study of the wake of gas slugs rising in liquids, *J. Fluid Mech*., Vol. 196, pp. 27-37.

Clift, R., Grace, J.R., dan Weber, M.E., 1978, Bubbles, Drops, dan Particles, *Academic Press Inc.*, New York.

Costigan, G., Whalley, P.B., 1997, Slug flow regime identification from dynamic void fraction measurements in vertical air–water flows, *Int. J. Multiphase Flow*, 23 (2), pp. 263–282

Deendarlianto, Höhne, T., Lucas, D., Vierow, K., 2011, Gas–liquid countercurrent two-phase flow in a PWR hot leg: A comprehensive research review, *Nuclear Engineering and Design*, 243, pp. 214 – 233.

De Jesus, J.M., Ahmad, W.R., Kawaji, M., 1995, Experimental Study of Flow Structure in Vertical Slug Flow, *Advances in Multiphase Flow*, pp. 105 – 118.

Dukler, A.E., Taitel, Y., 1986, Flow pattern transitions in gas-liquid systems: measurement and modelling, *Multiphase Science and Technology*, Vol. 2, (Edited by Hewitt, G.F., Delhaye J.M., Zuber, N.), pp. 1-94, Hemisphere, Washington, DC.

Dumitrescu, D.T.Z., 1943, Strömung an Einer Luftblase im Senkrechten Rohr, *Z. angew. Math. Mech*., 23, pp. 139. (in German language)

Engineering Toolbox, http://www.engineeringtoolbox.com, *Accessed on July 2014*,

Fabre, J. and Liné, A., 1992, Modeling of two-phase slug flow, *Ann. Rev. Fluid Mech.*, 24, pp. 21-46.

Fernandes, R.C., Semiat, R., dan Dukler, A.E., 1983, Hydrodynamic Model for Gas-Liquid *Slug* Flow in Vertical Tubes, *American Institute of Chemical Engineering Journal*, 29, pp. 981-989.

Fischer, F., Hoppe, D., Schleicher, E., Mattausch, G., Flaske, H., Bartel, R., and Hampel, U., 2008, An Ultra Fast Electron Beam X-ray Tomography Scanner, *Measurement in Science and Technology*, 19.

Fischer, F. and Hampel, U., 2010, Ultra Fast Electron Beam X-ray Computerd Tomography for Two-Phase Flow Measurement, *Nuclear Engineering and Design*, 240, pp. 2254-2259.

Ghiaasiaan, S.M., 2008, Two-Phase Flow, Boiling and Condensation in Conventional and Miniature Systems, *Cambridge University Press*, England: Cambridge.

Gould, R.G., 1992, Principles of ultra fast computed tomography, In: Stanford, W., Rumberger, J.A., Ultrafast (Eds.), Computed Tomography in Cardiac Imaging: Principles and Practice. *Futura Publishing Co., Inc., Mount Kisco, NY*.

Govan, A. H., Hewitt, G. F., Richter, H.J., Scott, A, 1991, Flooding and churn flow in vertical pipes, *Int. J. Multiphase Flow*, 17, pp. 27-44

Griffith, P. and G.B. Wallis, 1961, Two-Phase Slug Flow, *Transactions of the ASME Journal of Heat Transfer*, Vol. 83, No. 3, pp. 307-320.

Guo-dong, X., Zhen-zhen, C., Qing, L., 2009, A model for liquid *slug* length distribution in vertical gas-liquid *slug* flow, *Journal of Hydrodynamics*, 21 (4), pp. 491-498.

Hampel, U., et al., 2005, Experimental ultrafast X-ray computed tomography with a linearly scanned electron beam source, *Flow Measurement and Instrumentation*, 16, pp. 65–72.

Harmathy, T.Z., 1960, Velocity of Large Drops and Bubbles in Media of Infinite or Restricted Extent, *American Institute of Chemical Engineering Journal*, 6, 281.

Hasanein, H. A., Tudose, G. T., Wong, S., Malik, M., Esaki, S., Kawaji, M., 1996, Slug flow experiments and computer simulation of slug length distribution in vertical pipes, *AIChE Symposium Series*, 92 (310), pp. 211-219.

Hewitt, G.F., Roberts, D.N., 1969, Studies of Two-Phase Flow Patterns by Simultaneous X-ray and Flash Photography, *AERE-M 2159*, HMSO.

Hewitt, G.F. and Hall-Taylor, N.S., 1970, Annular Two-Phase Flow, *Pergamon Press.*

HZDR Official Website, Schematic diagram of gas injection modules: https://www.hzdr.de/db/Cms?pNid=1004 , *Accessed on July 2014.*

HZDR Official Website, Schematic diagram of TOPFLOW facility: https://www.hzdr.de/db/Cms?pNid=1004 , *Accessed on July 2014.*

Ishii, M., Zuber, N., 1979, Drag coefficient and relative velocity in bubbly, droplet or particulate flows, *AIChE J.*, 25, pp. 843–855.

Jayanti, S., Hewitt, G.F., 1992, Prediction of the Slug-to-Churn Flow Transition in Vertical Two-Phase Flow, *Int. J. Multiphase Flow*, Vol. 18, No. 6, pp. 847-860.

Joseph, D., 2003, Rise velocity of a sherical cap bubble, *J. Fluid Mech*., 488, pp. 213–223.

Kaji, R., Azzopardi, B.J., Lucas, D., 2009, Investigation of flow development of co-current gas–liquid vertical *slug* flow, *International Journal of Multiphase Flow*, 35, pp. 335–348.

Kak, A. C. and Slaney, M., 1988, Principles of computerized tomographic imaging, *IEEE Press.*

Kang C-W., Quan, S., Lou, J., 2010, Numerical study of a Taylor bubble rising in stagnant liquids, Phys. Rev. E, Vol. 81, Iss. 6, 066308.

Kawaji, M., DeJesus, J.M., dan Tudose, G., 1997, Investigation of flow structures in vertical *slug* flow, *Nuclear Engineering dan Design*, 175, pp. 37-48.

Khatib, Z., Richardson, J.F., 1984, Vertical co-current flow of air dan shear thinning suspensions of kaolin, *Chem. Eng. Res. Design*, 62, pp. 139-154.

Kirsner, W., 1998, Steam Condensation Induced Waterhammer, http://www.kirsner.org/pages/condInduceWatHamText.html, *Accessed on July 2014.*

Krepper, E., Lucas, D., and Prasser, H.-M., 2005, On the modeling of bubbly flow in vertical pipes, *Nuclear Engineering and Design*, 235, pp. 597-611.

Krepper, E., Lucas, D., Frank, T., Prasser, H.-M., Zwart, P.J., 2008, The inhomogeneous MUSIG model for the simulation of polydispersed flow, *Nuclear Engineering dan Design*, 238, pp. 1690–1702.

Krüssenberg, A.-K., Prasser, H.-M., Schaffrath, A., 1999, A new criterion for the bubble slug transition in vertical tubes, *Proceeding of 9th International Topical Meeting on Nuclear Reactor Thermal Hydraulics (NURETH-9)*, USA: San Francisco CA, 3–8 October.

Kulkarni, A.A., Joshi, J.B., 2005, Bubble Formation and Bubble Rise Velocity in Gas-Liquid Systems: A Review, *Ind. Eng. Chem. Res.*, 44, pp. 5873-5931.

Lahey Jr., R.T., Lopez de Bertodano, M., and Jones. O.C., 1993, Phase Distribution in Complex Geometry Conduits, *Nuclear Engineering and Design*, 141, pp. 177-201.

Laird, A.D.K., Chisholm, D., 1956, Pressure and Forces along Cylindrical Bubbles in a Vertical Tube, *Ind. Eng. Chem.*, 48 (8), pp. 1361–1364.

Liao, Y., Lucas, D., 2009, A literature review of theoretical models for drop and bubble breakup in turbulent dispersions, *Chemical Engineering Science*, 64, pp. 3389 – 3406.

Liao, Y., Lucas, D., 2010, A literature review on mechanisms and models for the coalescence process of fluid particles, *Chemical Engineering Science*, 65, pp. 2851–2864

Liu, T.J., 1997. Investigation of the wall shear stress in vertical bubbly flow under different bubble size conditions. *Int. J. Multiphase Flow* 23, pp. 1085–1109.

Lucas, D., Krepper, E., Prasser, H.-M., 2003, Evolution of flow patterns, gas fraction profiles and bubble size distributions in gas–liquid flows in vertical tubes, *Trans. Inst. Fluid-Flow Mach.*, 112, pp. 37–46.

Lucas, D., Krepper, E., Prasser, H.-M, 2005, Development of co-current air–water flow in a vertical pipe, *International Journal of Multiphase Flow*, 31, pp. 1304–1328.

Lucas, D., Krepper, E., 2007, CFD Models for Polydispersed *Bubbly* Flow, *HZDR Technical Report FZD-486*, Dresden: HZDR-Germany.

Maley, L.C., Jepson, W.P., 2000, Wall shear stress and differential pressure in large diameter horizontal multiphase pipelines, *J. Energy Res. Technol.*, 122, pp. 193–197.

Mao, Z.S., Dukler, A.E., 1989, An experimental study of gas-liquid slug flow, *Experiments in Fluids*, 8, pp. 169-182.

Maxworthy, T., 1967, A note on the existence of wakes behind large, rising bubbles, *J. Fluid Mech*. 27 (2), pp. 367-368.

Mayor, T.S., 2007, Hydrodynamics of gas-liquid flows in Slug Flow regime, *Ph.D. dissertation in Chemical and Biological Engineering, Faculdade de Engenharia Universidade do Porto,* Porto - Portugal

Mayor, T.S., Ferreira, V., Pinto, A.M.F.R., Campos, J.B.L.M., 2008, Hydrodynamics of gas–liquid slug flow along vertical pipes in turbulent regime – An experimental study, *Int. J. Heat Fluid Flow*, 29, pp. 1039-1053.

McQuillan, K.W, Whalley, P.B., 1985, Flow patterns in vertical two-phase flow. *Int. J. Multiphase Flow*, ll, pp. 161-175.

Mi, Y., Ishii, M., Tsoukalas, L.H., 2001, Investigation of vertical slug flow with advanced two-phase flow instrument, *Nucl. Eng. Design* 204, pp. 69–85.

Mishima, K., Ishii, M., 1984, Flow regime transition criteria for upward two-phase flow in vertical tubes, *Int. J. Heat Mass Transfer*, 27, pp. 723–737.

Moissis, R., Griffith, P., 1962, Entrance effects in a two-phase *slug* flow, *J. Heat Transfer*, 84, pp. 29-39.

Nakoryakov, V.E., Kashinski, O.N., and Kozmenko, B.K., 1986, Experimental Study of Gas–Liquid Slug Flow in a Small Diameter Vertical Pipe. *Int. J. Multiphase Flow* 12, pp. 337–355.

Nakoryakov, V.E., Kashinski, O.N., Petukhov, and A.V., Gorelik, R.S., 1989, Study of Local Hydrodynamic Characteristics of Upward Slug Flow., *Exp. Fluids*, 7, pp. 560–566.

Nicklin, D.J., Davidson, J.F., 1962, The onset of instability in two phase slug flow. *Presented at a Symp. on Two-phase Flow,* Inst. Mech. Engrs, London, paper no. 4.

Nicklin, D.J., Wilkes, J.O., dan Davidson, J.F., 1962, Two-Phase Flow in Vertical Tubes, *Trans. Inst. Chem. Engrs*, 40, pp. 61.

Orell, A., Rembrand, R., 1986, A Model for Gas-Liquid Slug Flow in a Vertical Tube, *Ind. Eng. Chem. Fundam*., 25, pp. 196-206

Patmonoaji, A., 2013, Development of Numerical Algorithms for the Determination of Gas Bubble Velocities from Experimental Data Obtained by Ultrafast Two-Layer Electron Beam X-Ray Tomography, *Bachelor Thesis,* Gadjah Mada University, Indonesia.

Patmonoaji, A., 2014, Investigation of gas-bubble velocities from experimental data of ultrafast two-layer electron beam X-ray tomography, *Master Thesis*, Gadjah Mada University, Indonesia.

Patmonoaji, A., Banowski, M., Lucas, D., Deendarlianto, 2013, Investigation of gas-*bubble* velocities from experimental data of ultrafast two-layer electron

beam X-ray tomography, *Proceeding of The 12th Annual National Seminar of Mechanical Engineering (SNTTMXII), Bandar Lampung-Indonesia*, pp. 1374-1383.

Pinto, AMFR, Campos, JBLM, 1996, Coalescence of two gas slugs rising in a vertical column of liquid, *Chemical Engineering Science*, Vol. 51, 1, pp. 45-54.

Pinto, A. M. F. R., Pinheiro, M. N. C. and Campos, J. B. L. M., 1998, Coalescence of two gas slugs rising in a co-current flowing liquid in vertical tubes, *Chem. Eng. Sci.*, 53 (16), pp. 2973-2983.

Polonsky, S., Shemer, L., Barnea, D., 1999a, The relation between the Taylor bubble motion and the velocity field ahead of it, International Journal of Multiphase Flow, 25, pp. 957-975.

Polonsky, S., Barnea, D., Shemer, L., 1999b, Averaged and time dependent characteristics of the motion of an elongated *bubble* in a vertical pipe, *Int. J. Multiphase Flow*, vol. 25, pp. 795–812.

Prasser, H.-M., Beyer, M., Carl, H., Manera, A., Pietruske, H., Schütz, P., Weiβ, F.-P., 2006, The multipurpose thermal-hydraulic test facility TOPFLOW : an overview on experimental capabilities, instrumentation and results, *Kerntechnik*, vol. 71, pp. 163-173.

Prasser, H.-M., Scholz, D., Zippe, C., 2001, Bubble size measurement using wire-mesh sensors, *Flow Measure. Instrument.*, 12, pp. 299–312,

Prasser, H.-M., Misawa, M., Tiseanu, I., 2005, Comparison between wire-mesh sensor and ultra-fast X-ray tomograph for an air–water flow in a vertical pipe. *Flow Measure. Instrument.* 16, 73–83.

Prince, M.J. and Blanch, H.W., 1990, Bubble coalescence and break-up in airsparged bubble columns, *AIChE J*., vol. 36, pp. 1485-1499.

Schaffrath, A., Krüssenberg, A.-K., Weiß, F.-P., Hicken, E.F., Beyer, M., Carl, H., Prasser, H.-M., Schuster, J., Schütz, P., Tamme, M., Zimmermann, W., 2001, TOPFLOW- a new multipurpose thermalhydraulic test facility for the investigation of steady state and transient two phase flow phenomena, *Kerntechnik*, Vol. 66, 209-212.

Schiller, L. and Naumann, A., 1933, *VDI Zeitschrift*, vol. 77, pp. 318.

Seidel, T., Vallée, C., Lucas, D., Beyer, M., Deendarlianto, 2010, Two-Phase Flow Experiments in a Model of the Hot Leg of a Pressurised Water Reactor, *Wissenschaftlich – Technische Berichte/Forschungszentrum Dresden Rossendorf*; FZD-531.

Sekoguchi, K., Sato, T. and Honda, T., 1974, Two phase bubble flow (first report), *Trans. Japan Soc. Mech Engng*., Vol. 40 (333), pp. 1395-1403

Serizawa, A., Kataoka, I., and Michiyoshi, I., 1975, Turbulence Structure of Air/Water Bubbly Flow, *International Journal of Multiphase Flow*, 2(3), pp. 221 -234.

Shemer, L., Barnea, D., 1987, Visualization of the instantaneous velocity profiles in gas–liquid slug flow, *Physic. Chem. Hydrodyn*., vol. 8, pp. 243–253.

Shemer, L., 2003, Hydrodynamic and statistical parameters of slug flow, *International Journal of Heat and Fluid Flow*, 24, pp. 334–344.

Shemer, L., Gulitski, A., Barnea, D., 2005, Experiments on the turbulent structure and void fraction distribution in the Taylor bubble wake, *Multiphase Sci. Technol.*, 17, pp. 103–122.

Shemer, L., Gulitski, A., Barnea, D., 2007, On the turbulent structure in the wake of Taylor bubbles rising in vertical pipes, *Phys. Fluids*, 19, 035108.

Strubelj, L., Ézsöl, G., Tiselj, I., Direct contact condensation induced transition from stratified to slug flow, *Nuclear Engineering and Design*, 240, pp. 266–27.

Sylvester, N.D., 1987, A Mechanistic Model for Two-Phase Vertical Slug Flow in Pipes, *Journal of Energy Resources Technology, Transactions of the ASME*, Vol. 109, pp. 206-213.

Taitel, Y., Barnea, D. dan Dukler, A.E., 1980, Modeling Flow Pattern Transition for Steady Upward Gas-Liquid Flow in Vertical Tubes, *American Institute of Chemical Engineering Journal*, 26, pp. 345-354.

Taitel, Y. and Barnea, D., 1983, Counter Current Gas-Liquid Vertical Flow, Model for Flow Pattern and Pressure Drop, *International Journal of Multiphase Flow*, 8, pp. 1-10.

Taylor G.I., Davies, R.M., 1950, The mechanics of large *bubble*s rising through extended liquids dan through liquids dan through liquids in tube, *Proc. R. Soc. London*, Ser. A, 200, 375.

Tomiyama, A., Sou, A., Zun, I., Kanami, N., Sakaguchi, T., 1995, Effect of Eötvos Number dan Dimensionless Liquid Volumetric Flux on Lateral Motion of a *Bubble* in a Laminar Duct Flow, *Advances in Multiphase Flow*, pp. 3-15.

Tomiyama, A., 1998, Struggle with computational bubble dynamics, *Proceedings of Third International Conference on Multiphase Flow, ICMF 98*, France: Lyon, June 8-12.

Tomiyama, A., Nakahara, Y., Adachi, Y., Hosokawa, S., 2003, Shapes and rising velocities of single bubbles rising through an inner subchannel, *J. Nucl. Sci. Technol.*, 40, 136.

Van Hout, R., Shemer, L., dan Barnea, D., 1992, Spatial Distribution of Void Fraction within a Liquid *Slug* dan Some Other Related *Slug*-Parameter, *Int. J. Multiphase Flow*, 18, pp. 831-845.

Van Hout, R., Barnea, D., Shemer, L., 2001, Evolution of statistical parameters of gas-liquid slug flow along vertical pipes, *International Journal of Multiphase Flow*, 27, pp. 1579-1602.

Van Hout, R., Barnea, D., Shemer, L., 2002, Translational velocities of elongated *bubble*s in continuous *slug* flow, *Int. J. Multiphase Flow*, 28, pp. 1333-1350, 2002.

Van Hout, R., Gulitski, A., Barnea, D., and Shemer, L., 2002, Experimental Investigation of the velocity field induced by a Taylor bubble rising in stagnant water, *Int. J. Multiphase Flow*, 28, pp. 579-596.

Wallis, G. B., 1969, One dimensional two-phase flow, *McGraw Hill Book Co.* , USA: New York.

Wang, S., Nesic, S., 2003. On coupling CO_2 corrosion and multiphase flow models. *CORROSION*.

Wellek, R.M., Agrawal. A.K., and Skelland, A.H.P., 1966, Shape of Liquid Drops Moving in Liquid Media, *American Institute of Chemical Engineering Journal*, 12, pp. 854-862.

White, E.T., Beardmore, R.H., 1962, The velocity of rise single cylindrical air bubbles through liquid contained in vertical tubes, *Chemical Engineering Sciences*, 17, pp. 351-361.

Yan, K., Che, D., 2011, Hydrodynamic and mass transfer characteristics of slug flow in a vertical pipe with and without dispersed small bubbles, *International Journal of Multiphase Flow*, 37, pp. 299–325.

Zheng, D., Che, D., 2006, Experimental study on hydrodynamic characteristics of upward gas–liquid *slug* flow, *International Journal of Multiphase Flow*, 32, pp. 1191–1218.

Zuber, N., Hench, J., 1962, Steady State and Transient Void Fraction of Bubbling Systems and Their Operating Limit. Part I: Steady State Operation, *General Electric Report*, 62GL100.

Zukoski, E.E., 1966, Influence of viscosity, surface tension, and inclination angle on motion of long bubbles in closed tubes, *J. Fluid Mech.*, 25, 821.

Zun, I., 1987, Transition from wall void peaking to core void peaking in turbulent bubbly flow, *Proceedings of the ICHMT Seminar on Transient Phenomena in Multiphase Flow*, Yugoslavia: Drubrovnik

APPENDIX

1. Visualization of Taylor bubbles

Image segmentation results of slug flow in different measurement station.

Matrix point 114 (J_G = 0.219 m/s and J_L = 0.0405 m/s)

A-STATION		D-STATION	
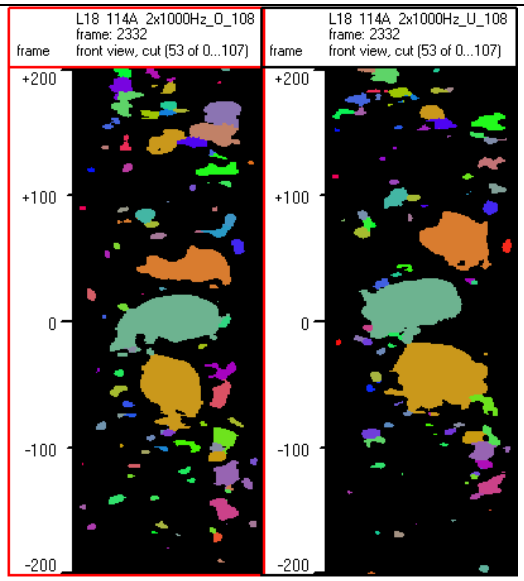		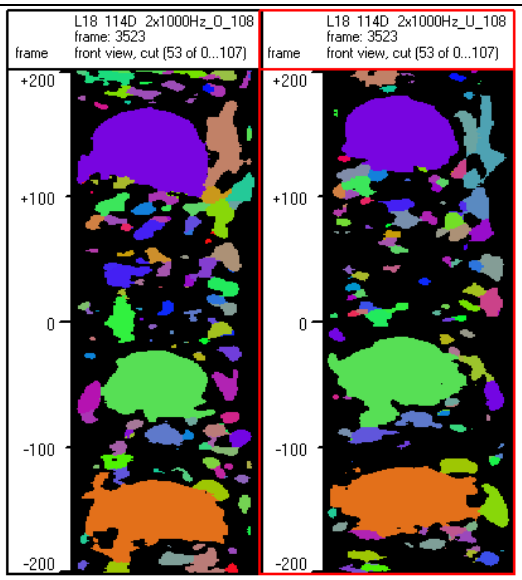	
Upper plane	Lower plane	Upper plane	Lower plane

G-STATION		J-STATION	
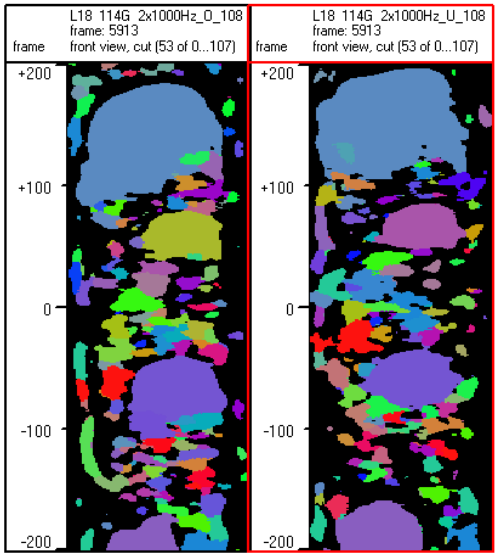		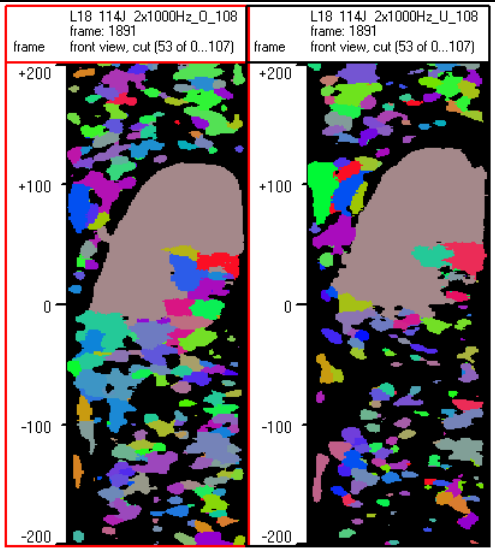	
Upper plane	Lower plane	Upper plane	Lower plane

M-STATION		P-STATION	
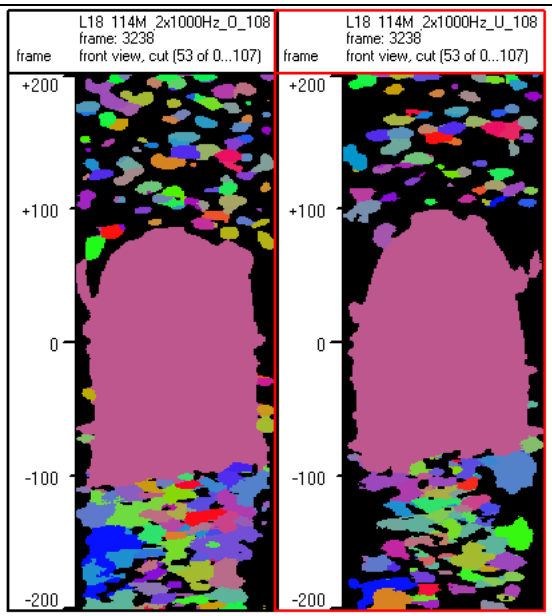		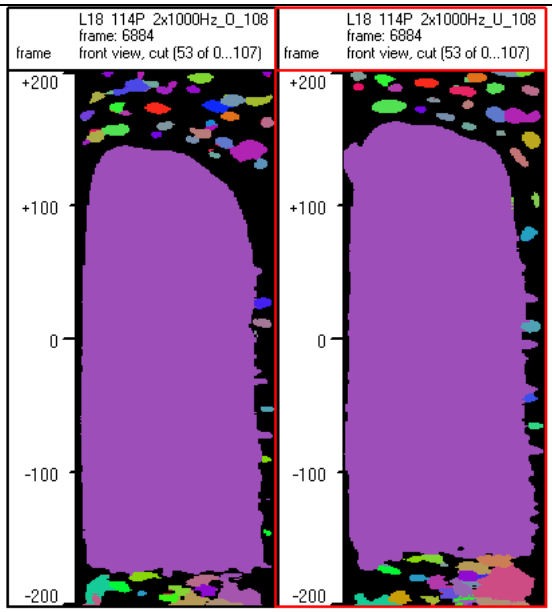	
Upper plane	Lower plane	Upper plane	Lower plane

Matrix point 140 (J_G = 0.534 m/s and J_L = 1.017 m/s)

A-STATION		D-STATION	
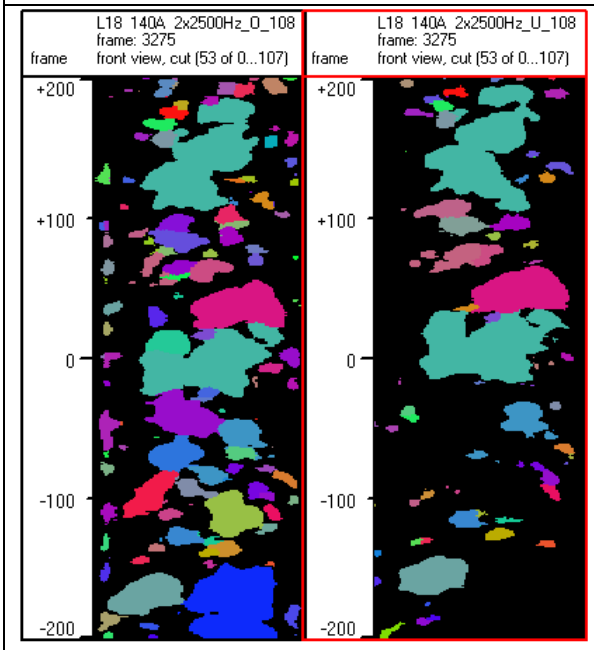		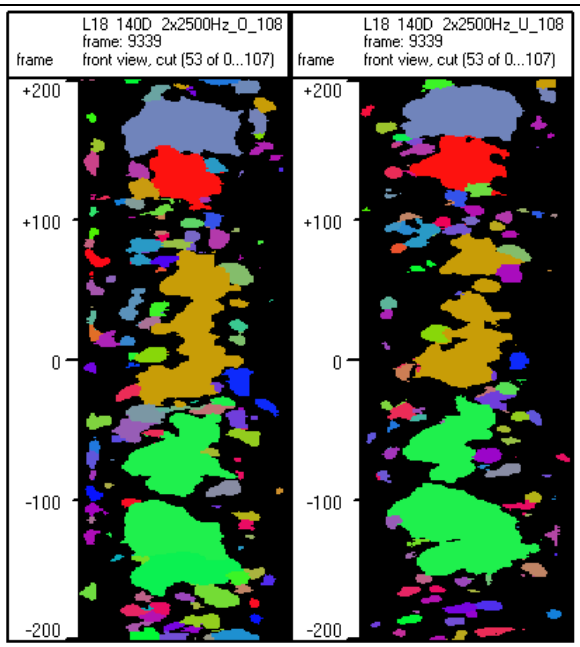	
Upper plane	Lower plane	Upper plane	Lower plane

G-STATION		J-STATION	
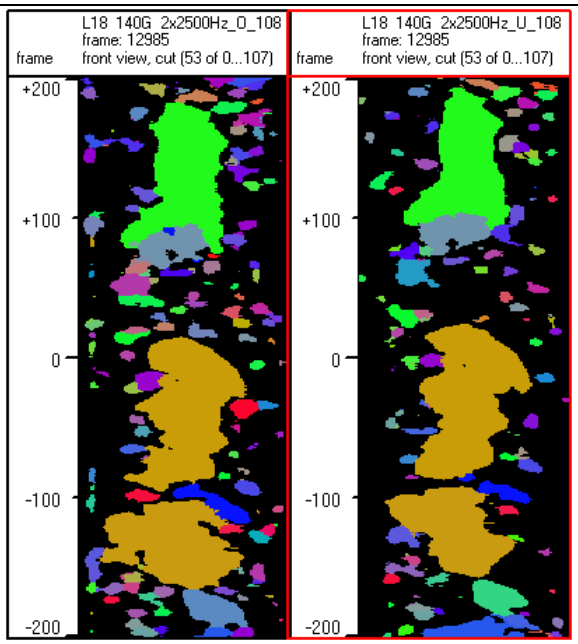		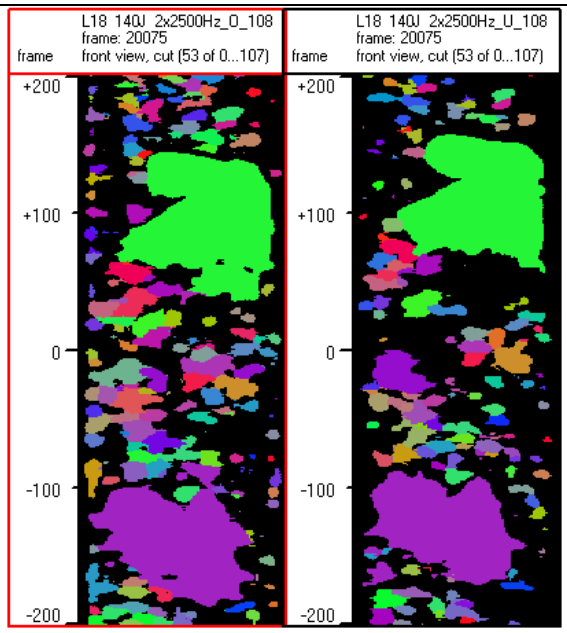	
Upper plane	Lower plane	Upper plane	Lower plane

M-STATION		P-STATION	
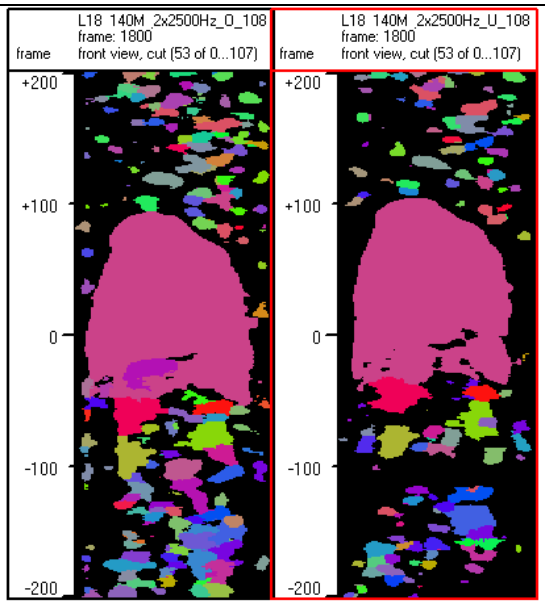		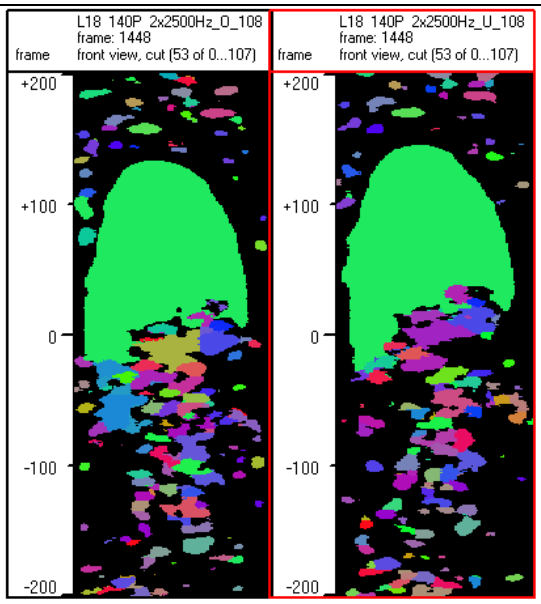	
Upper plane	Lower plane	Upper plane	Lower plane

Matrix point 118 (J_G= 0.219 m/s and J_L = 1.017 m/s)

A-STATION		D-STATION	
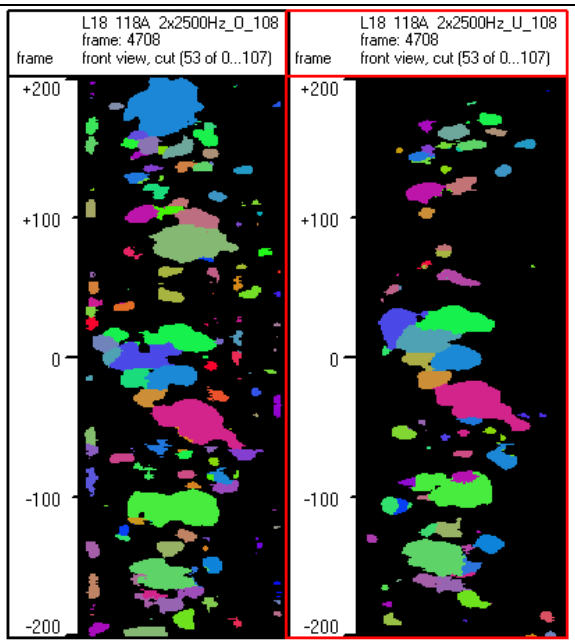		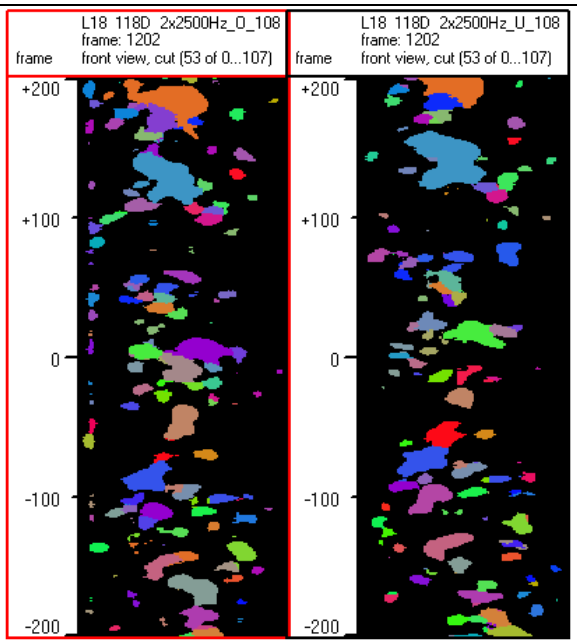	
Upper plane	Lower plane	Upper plane	Lower plane

G-STATION		J-STATION	
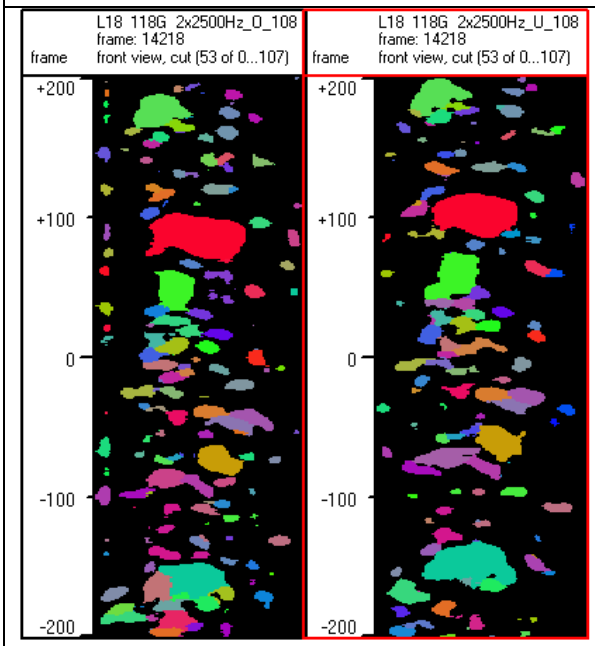		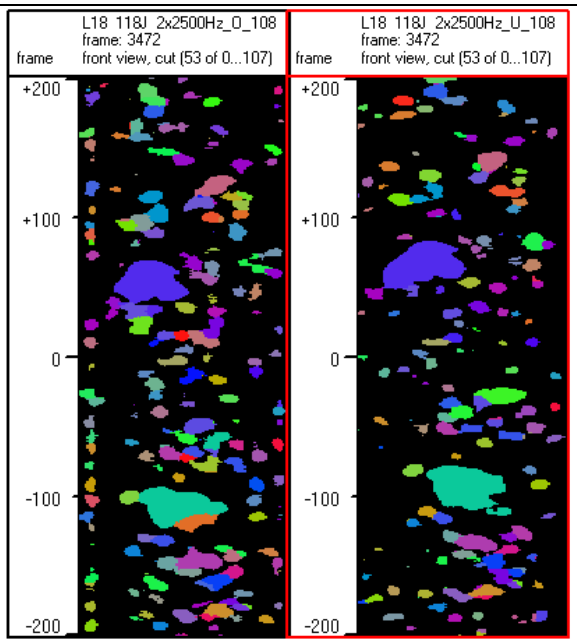	
Upper plane	Lower plane	Upper plane	Lower plane

M-STATION		**P-STATION**	
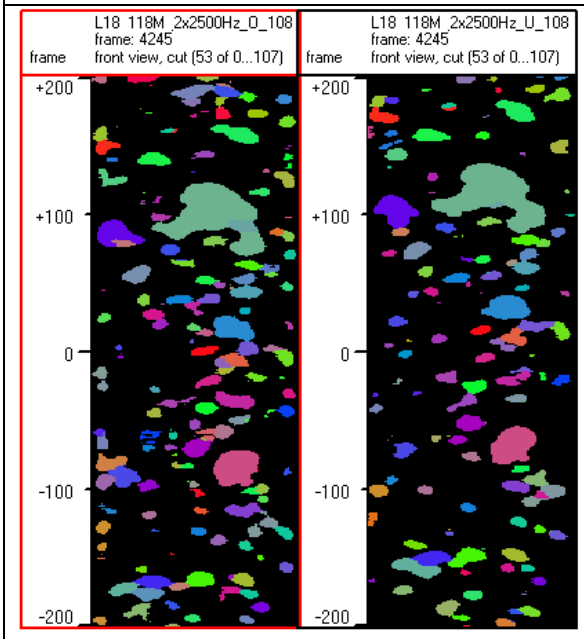		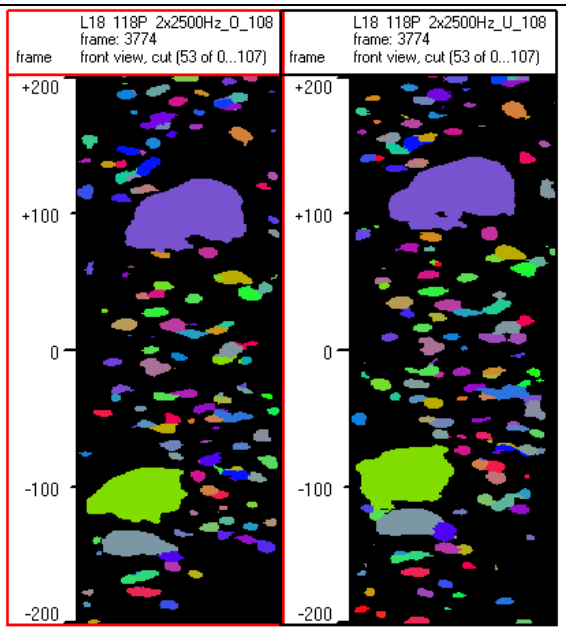	
Upper plane	Lower plane	Upper plane	Lower plane

2. Time-series data of void fraction

Cross-sectional averaged void fraction data during 10 seconds measurement time are presented. Sign of (---) indicates lower measurement plane and (—) indicates upper measurement plane.

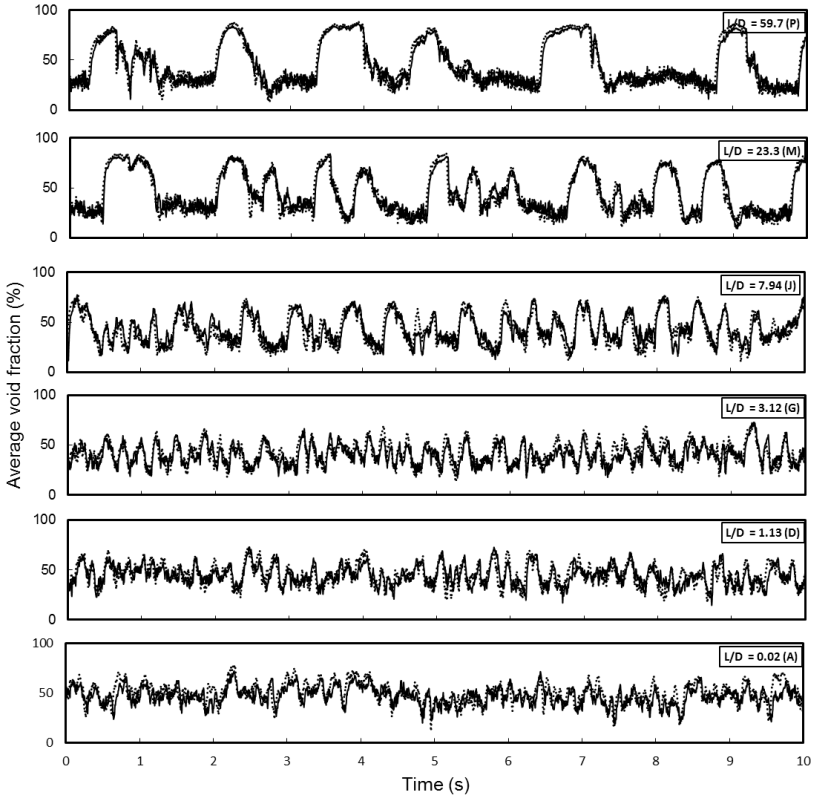

Data 111 (J_G= 0.219m/s and J_L = 0.0405 m/s)

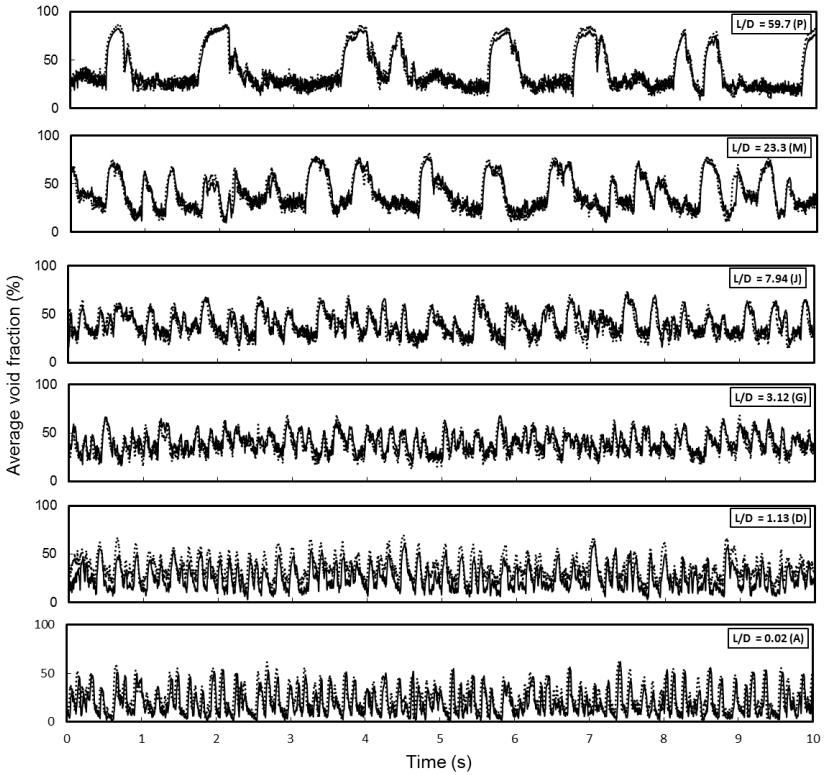

Data 114 (J_G= 0.219 m/s and J_L = 0.161 m/s)

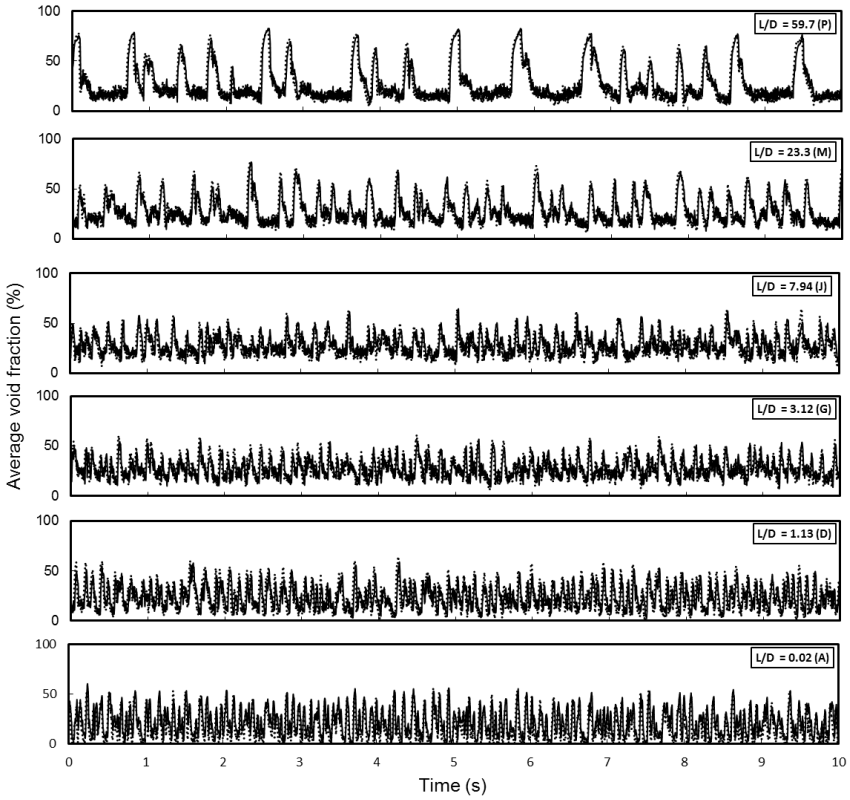

Data 116 (J_G= 0.219 m/s and J_L = 0.405 m/s)

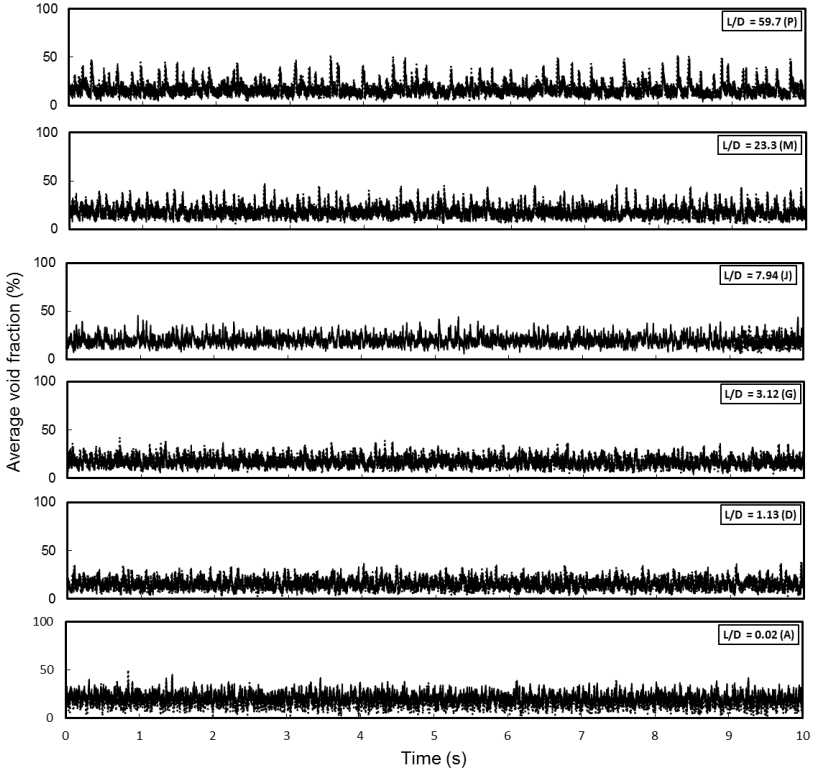

Data 118 (J_G= 0.219 m/s and J_L = 1.017 m/s)

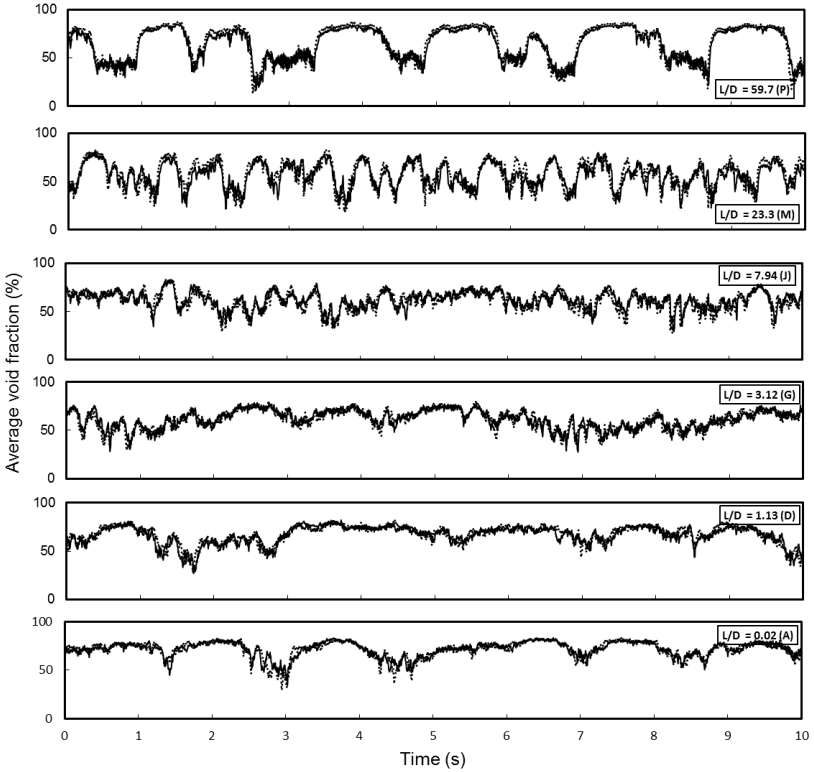

Data 133 (J_G= 0.534 m/s and J_L = 0.0405 m/s)

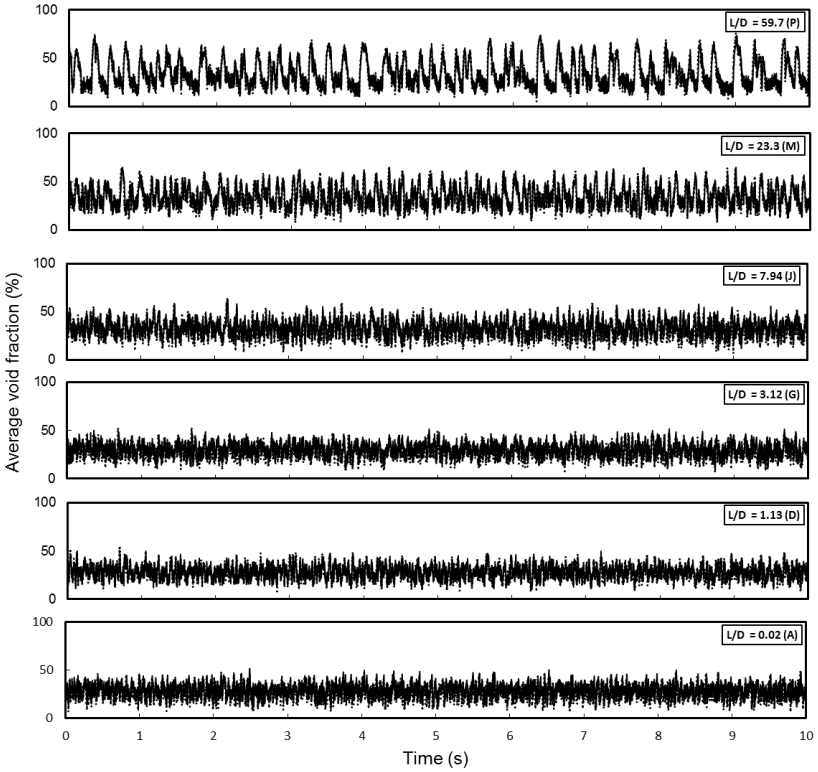

Data 140 (J_G = 0.534 m/s and J_L = 1.017 m/s)

3. Void fraction distribution

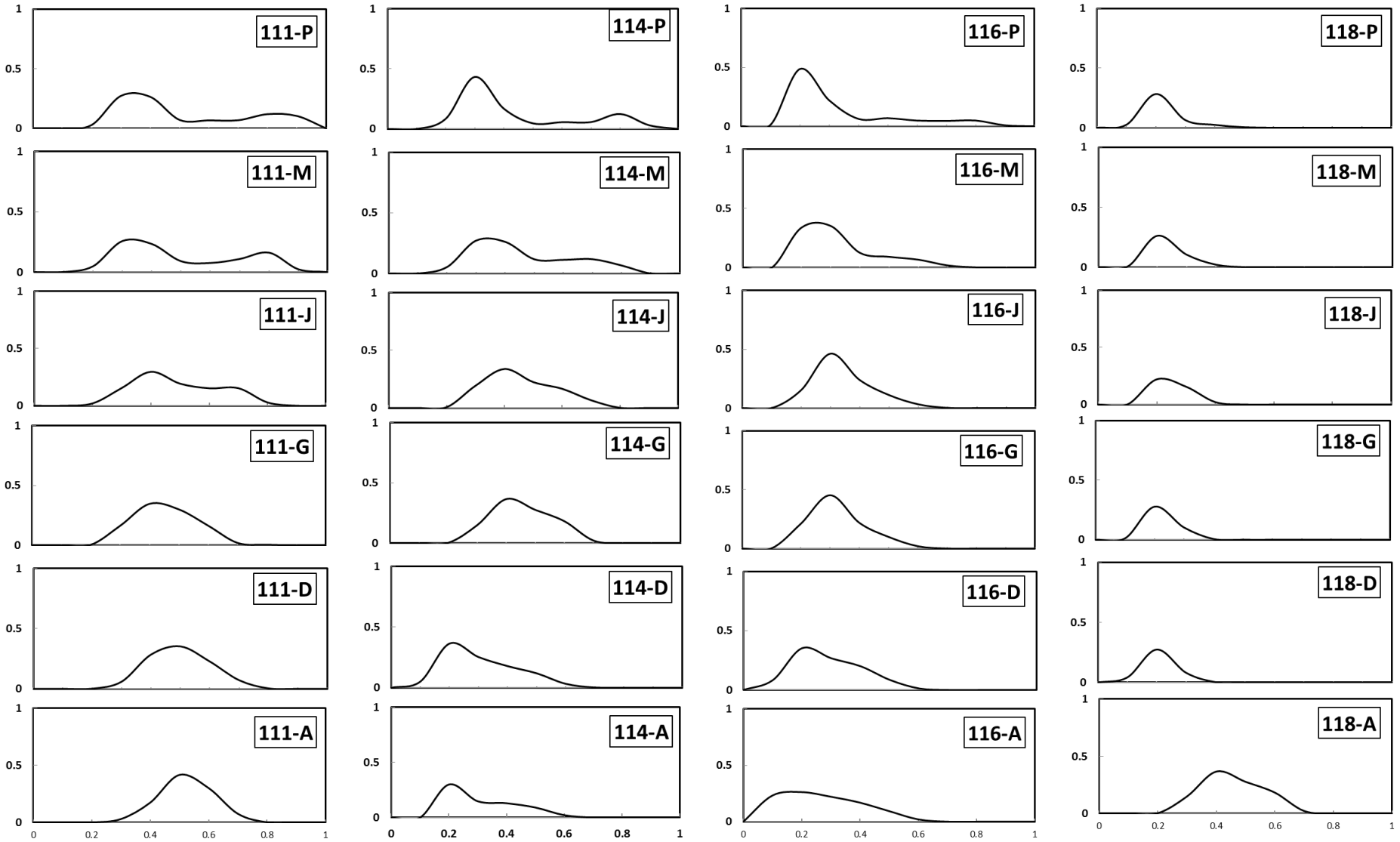

J_G= 0.219 m/s and J_L = 0.0405 m/s | J_G= 0.219 m/s and J_L = 0.161 m/s | J_G= 0.219 m/s and J_L = 0.405 m/s | J_G= 0.219 m/s and J_L = 1.017 m/s

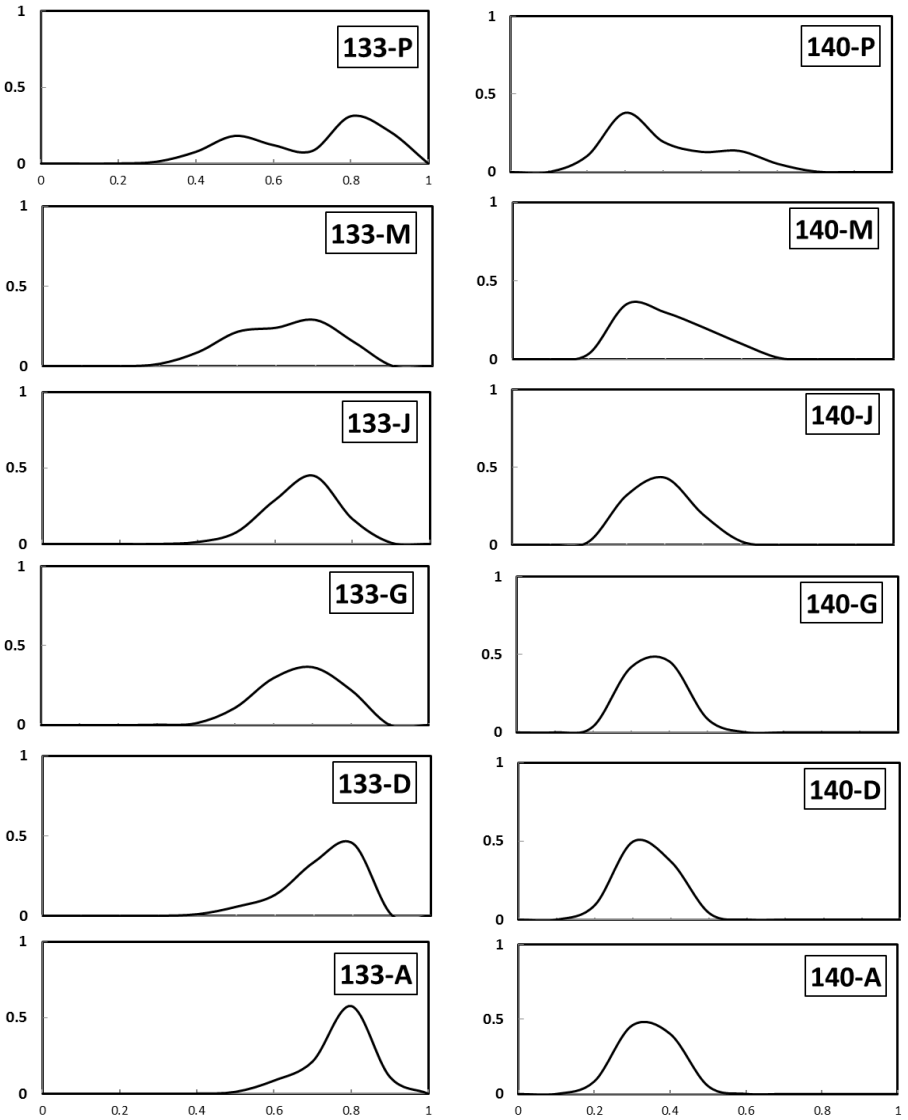

J_G= 0.534 m/s and J_L = 0.0405 m/s

J_G= 0.534 m/s and J_L = 1.017 m/s

4. Quantitative data of Taylor bubble and bubbles in other slug region properties at different stations

114		Taylor bubble		CAPS bubble			Falling Film		
Axial Stations (L/D)		Freq TB	mean Uaxial (m/s)	freq (bubbles/s)	mean Uaxial (m/s)	mean deqv (mm)	freq (bubbles/s)	mean Uaxial (m/s)	mean deqv (mm)
A	0.03	0	0	0.400	0.642	40.687	6.500	0.447	3.380
D	1.13	0	0	1.100	0.745	46.023	27.700	0.468	4.716
G	3.12	0	0	0.900	0.820	46.928	30.100	0.474	5.609
J	7.94	0.4	0.7681	0.800	0.779	47.531	48.400	0.477	5.542
M	23.3	0.9	0.8261	0.400	0.742	47.189	44.700	0.453	5.290
P	59.7	0.8	0.67907047	0.100	0.100	22.452	22.000	0.498	5.421

swelling			wake			dev bubble		
freq (bubbles/s)	mean Uaxial (m/s)	mean deqv (mm)	freq (bubbles/s)	mean Uaxial (m/s)	mean deqv (mm)	freq (bubbles/s)	mean Uaxial (m/s)	mean deqv (mm)
21.000	0.293	2.922	27.200	0.499	3.480	616.100	0.452	3.376
84.600	0.243	3.243	141.300	0.500	4.576	541.700	0.463	4.387
61.300	0.252	4.290	119.300	0.508	5.660	560.900	0.477	5.171
83.000	0.211	4.456	268.800	0.510	5.630	406.100	0.488	5.095
56.100	0.064	4.380	231.100	0.514	5.711	780.100	0.485	4.968
4.800	-0.468	4.753	108.800	0.525	5.938	1420.300	0.477	4.936

118		Taylor bubble		CAPS bubble			Falling Film		
Axial Stations (L/D)		Freq TB	mean Uaxial (m/s)	freq (bubbles/s)	mean Uaxial (m/s)	mean deqv (mm)	freq (bubbles/s)	mean Uaxial (m/s)	mean deqv (mm)
A	0.03	0	0	0	0	0	0	0	0
D	1.13	0	0	0	0	0	0	0	0
G	3.12	0	0	0	0	0	0	0	0
J	7.94	0	0	0	0	0	0	0	0
M	23.3	0	0	0	0	0	0	0	0
P	59.7	0	0	0.100	1.594	39.609	1.000	1.373	4.815

swelling			wake			dev bubble		
freq (bubbles/s)	mean Uaxial (m/s)	mean deqv (mm)	freq (bubbles/s)	mean Uaxial (m/s)	mean deqv (mm)	freq (bubbles/s)	mean Uaxial (m/s)	mean deqv (mm)
0	0	0	0	0	0	492.400	1.472	6.367
0	0	0	0	0	0	948.500	1.465	5.499
0	0	0	0	0	0	1169.100	1.423	5.428
0	0	0	0	0	0	1685.500	1.367	5.222
0	0	0	0	0	0	2352.900	1.345	5.184
5.100	1.099	4.677	11.200	1.404	5.441	2752.000	1.356	5.014

140		Taylor bubble		CAPS bubble			Falling Film		
Axial Stations (L/D)		Freq TB	mean Uaxial (m/s)	freq (bubbles/s)	mean Uaxial (m/s)	mean deqv (mm)	freq (bubbles/s)	mean Uaxial (m/s)	mean deqv (mm)
A	0.03	0	0	0	0	0	0	0	0
D	1.13	0	0	0	0	0	0	0	0
G	3.12	0	0	0	0	0	0	0	0
J	7.94	0	0	0.700	2.240	46.565	7.100	1.762	5.993
M	23.3	0.6	2.2395	3.500	2.055	48.425	42.800	1.696	5.853
P	59.7	2.4	2.0963	1.500	2.050	50.287	45.900	1.684	5.559

swelling			wake			dev bubble		
freq (bubbles/s)	mean Uaxial (m/s)	mean deqv (mm)	freq (bubbles/s)	mean Uaxial (m/s)	mean deqv (mm)	freq (bubbles/s)	mean Uaxial (m/s)	mean deqv (mm)
0	0	0	0	0	0	443.400	1.749	6.653
0	0	0	0	0	0	546.500	1.750	6.394
0	0	0	0	0	0	533.100	1.689	6.054
23.000	1.231	4.986	34.400	1.741	6.537	424.100	1.691	6.383
119.100	1.186	4.818	191.900	1.784	6.527	384.200	1.709	6.051
97.700	0.960	4.710	167.400	1.838	6.493	847.800	1.713	5.336

5. Graphics of Taylor bubble and bubbles in other slug region properties at different stations

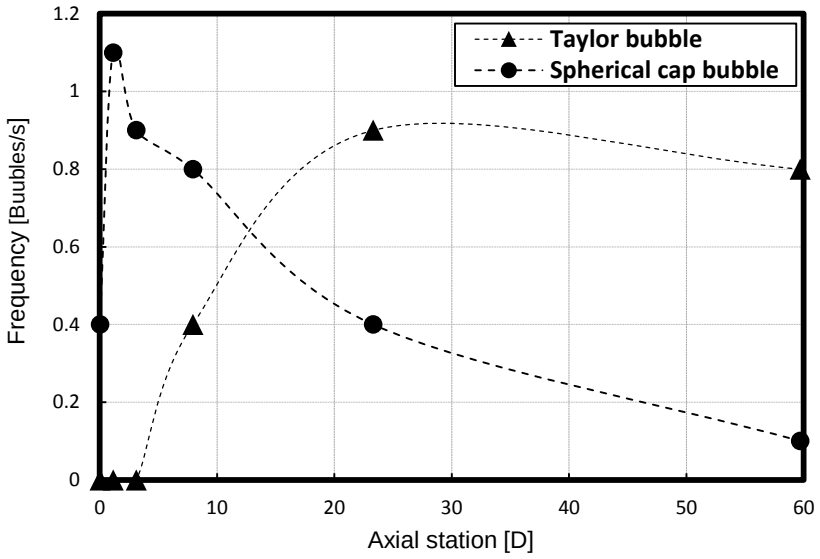

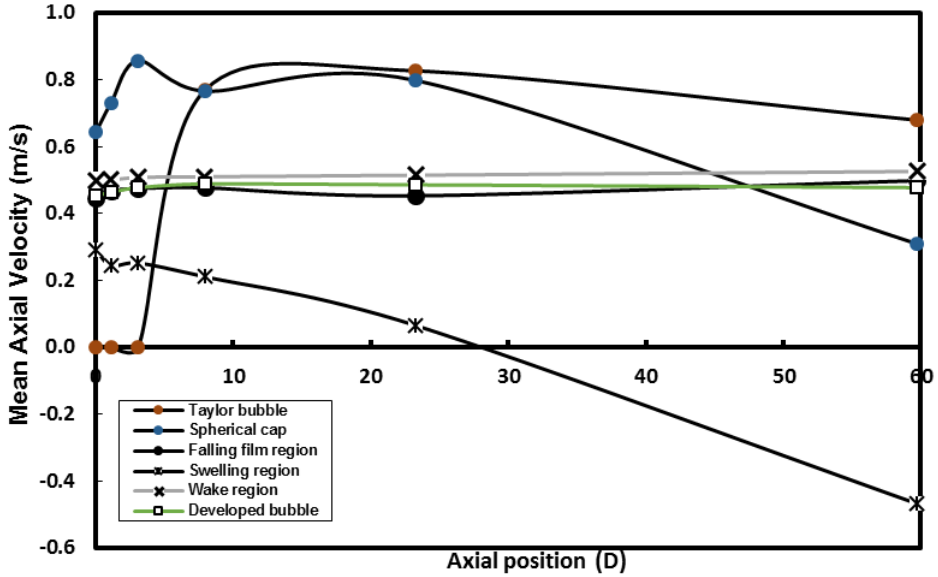

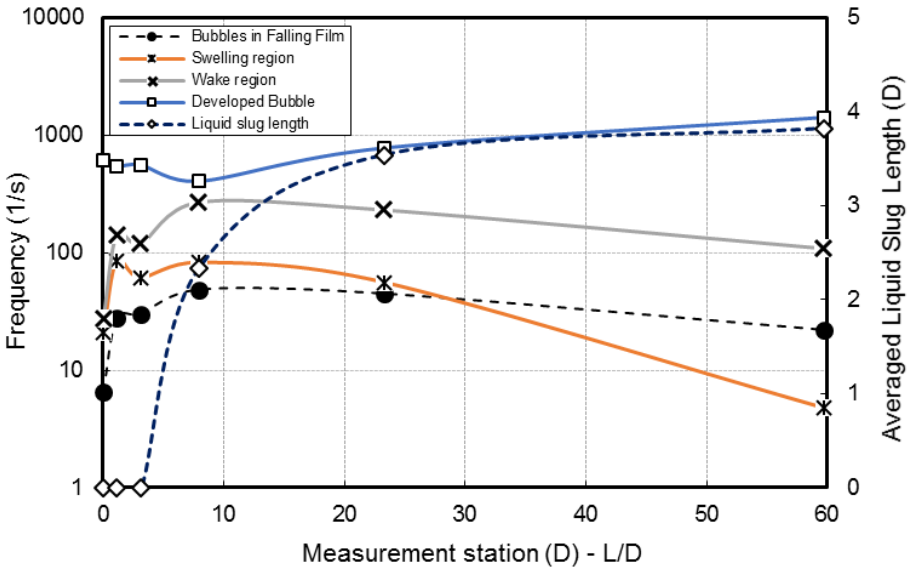

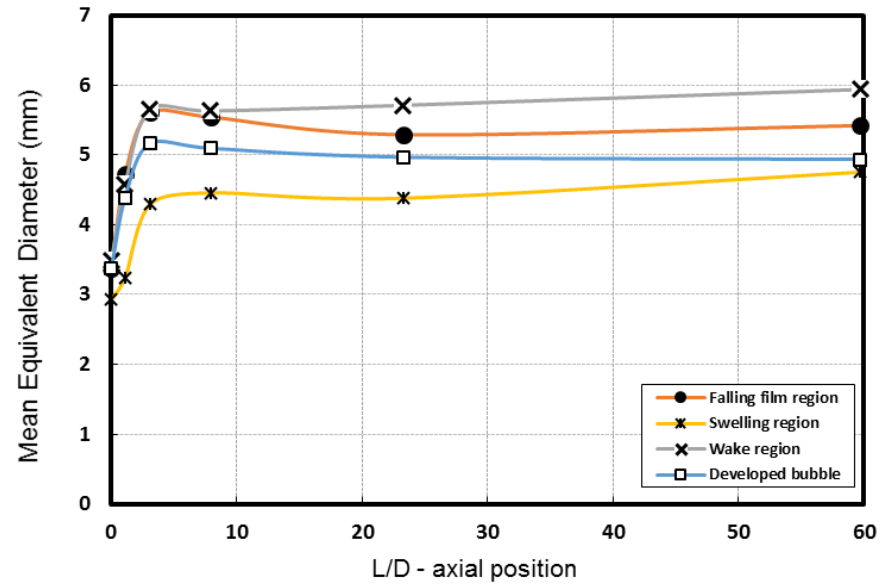

Data 114 (J_G= 0.219 m/s and J_L = 0.161 m/s) AP-14

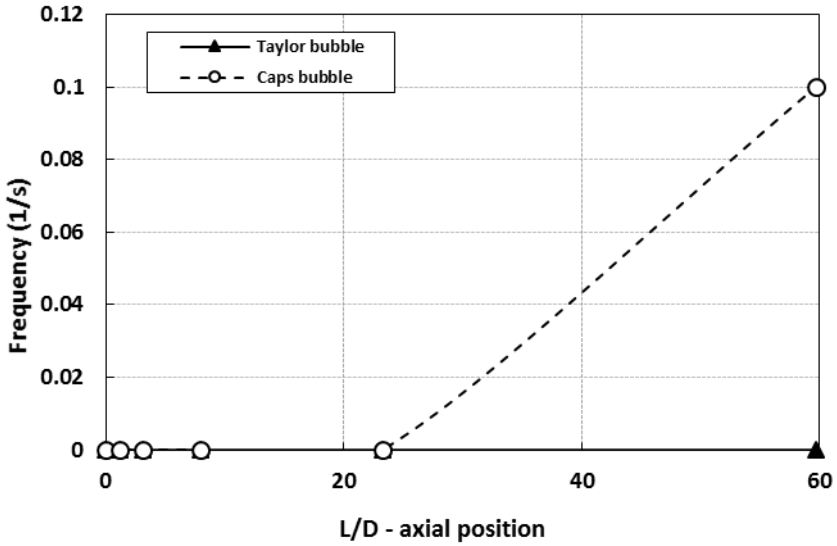

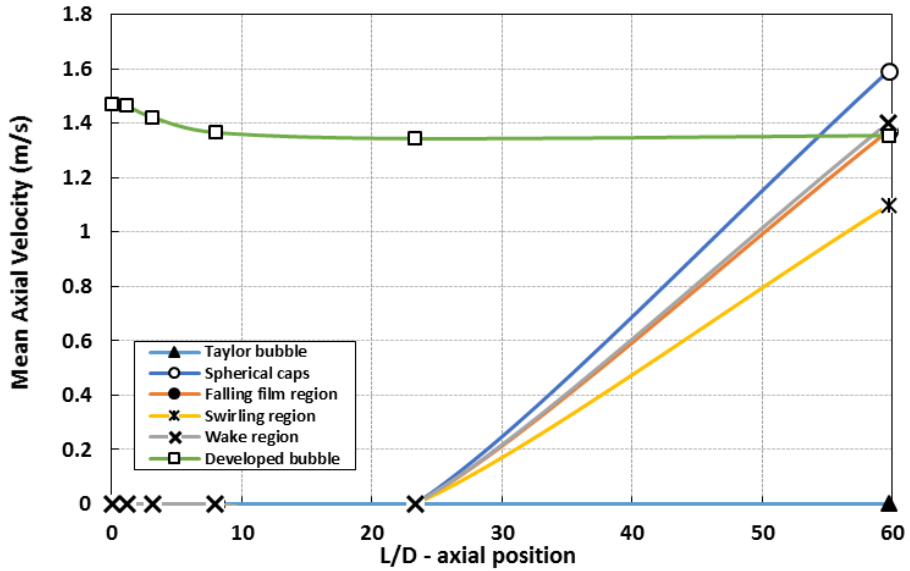

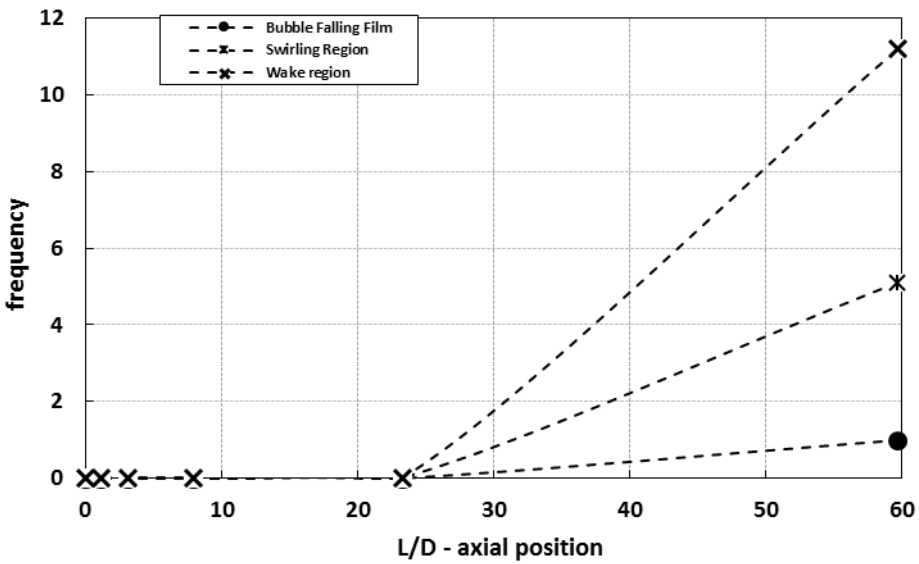

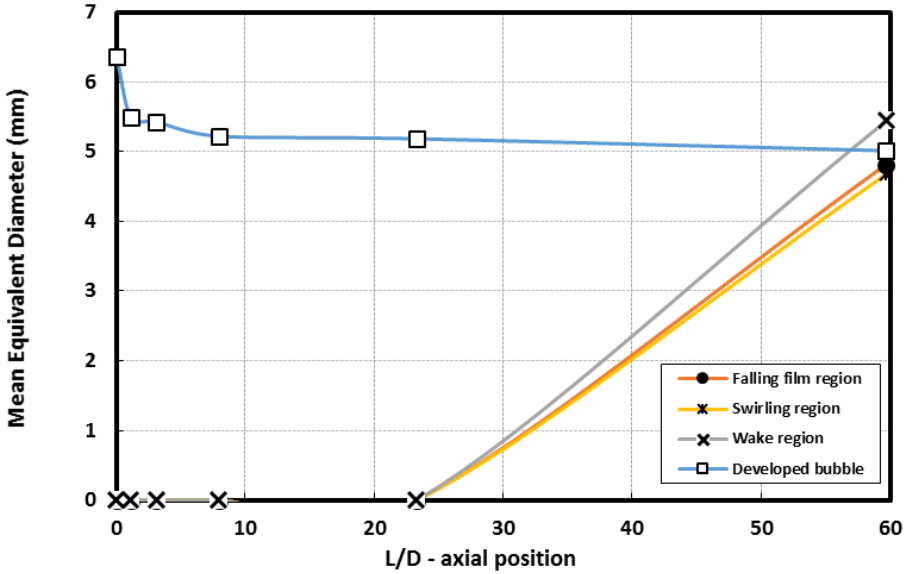

Data 118 (J_G= 0.219 m/s and J_L = 1.017 m/s)

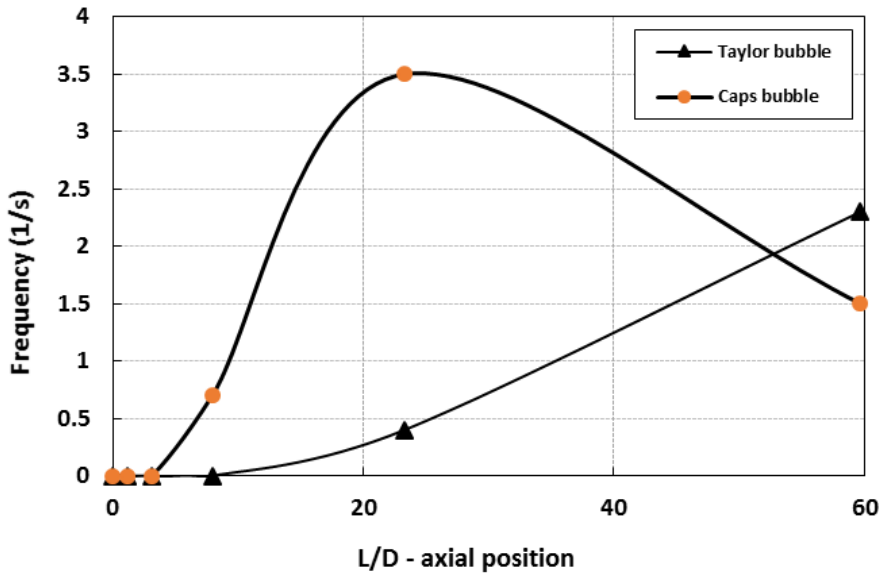

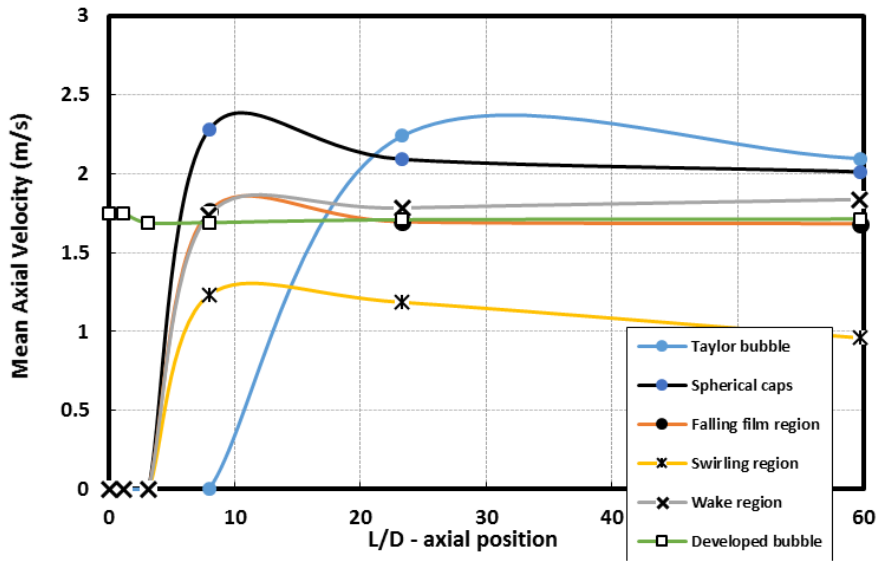

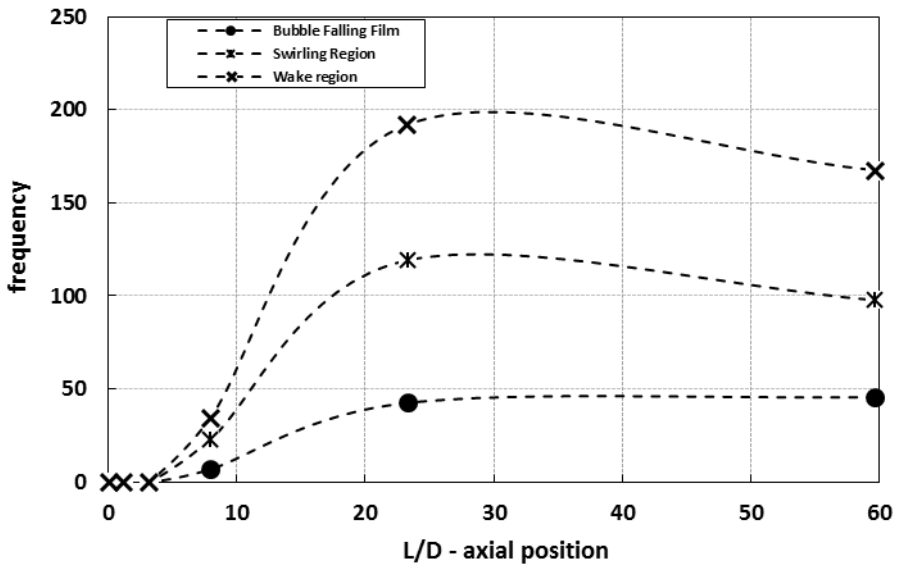

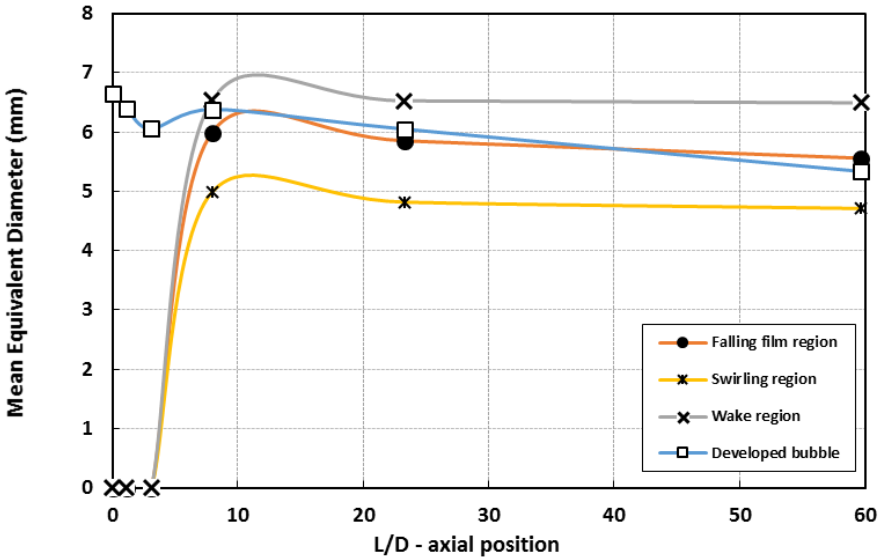

Data 140 (J_G= 0.534 m/s and J_L = 1.017 m/s)

6. Quantitative data of Taylor bubbles in matrix point 114-P

114 - P

Bubble pair row	UPPER layer		LOWER layer		order	TB length U		TB length O		delta (mm)	relative length to lower plane %
	number O	row at AO	number U	baris di AU		corr LU (mm)	D	corr LU (mm)	D		
681	16	1	4054	3	1	132.111	2.410785	139.482	2.545292	7.371	5.58
74	3101	15	4718	9	2	285.6	5.211679	289	5.273723	3.4	1.19
359	46	2	5082	50	3	293.448	5.354891	285.602	5.211715	-7.846	2.67
1281	62	3	4840	16	4	174	3.175182	169.2	3.087591	-4.8	2.76
1344	71	4	5149	67	5	189.6	3.459854	191.4	3.492701	1.8	0.95
174	77	5	5172	74	6	145.35	2.652372	142.8	2.605839	-2.55	1.75
3537	88	6	4660	7	7	147.019	2.682828	157.24	2.869343	10.221	6.95
5439	90	7	8194	1953	8	121.2667	2.212895	111.0667	2.026764	-10.2	8.41
					MEAN	186.0493	3.395061	185.7238	3.389121		3.783668

AXIAL VELOCITY		VELOCITY COMPONENT				NOSE OSCILLATION				Void fraction (%)	RADIAL POSITION	
nose velocity	tail velocity	RADIAL TB	HORIZONT TB	3D_Vel TB	TB alpha	RADIAL nose_vel	HORIZ nose_vel	3D_vel nose	ALPHA nose		TB radpos	NOSE radpos
0.567	3.400	-0.004	0.017	0.567	1.685	-0.467	1.126	1.260	63.278	1.861	0.039	0.697
0.680	1.275	-0.008	0.013	0.680	1.123	0.182	0.236	0.720	19.117	3.051	0.096	0.537
0.785	2.550	0.004	0.011	0.785	0.794	0.360	0.493	0.926	32.119	2.545	0.095	0.289
0.600	0.850	-0.020	0.034	0.601	3.272	-0.140	0.208	0.635	19.117	2.084	0.057	0.312
0.600	0.637	-0.017	0.024	0.600	2.315	0.235	0.251	0.650	22.725	2.323	0.110	0.555
0.850	-0.443	-0.008	0.008	0.850	0.562	-0.066	0.879	1.223	45.960	1.188	0.115	0.629
0.785	-0.785	-0.008	0.076	0.788	5.515	-0.054	0.122	0.794	8.811	1.314	0.059	0.543
0.567	Inf	-0.003	0.008	0.567	0.794	0.050	0.178	0.594	17.426	1.319	0.132	0.734
0.679	1.069	-0.008	0.024	0.680	2.008	0.013	0.436	0.850	28.569	1.961	0.088	0.537

Bubble pair row	UPPER layer		LOWER layer			TB length U		TB length O			
	number O	row at AO	number U	baris di AU	order	mm	(D)	mm	D	delta (mm)	relative le.U %
621	3267	171	3105	12	1	115.1143	2.100626	120.9429	2.206986	5.82858	5.063299
18090	1405	13	3131	15	2	208.5333	3.805353	224.4	4.09489	15.86666	7.608693
56	3426	229	3811	127	3	189.55	3.458942	184.45	3.365876	-5.09999	-2.69058
20623	4403	575	3252	28	4	193.8	3.536496	316.2	5.770073	122.4	63.1579
693	525	4	2700	2	5	153.68	2.80438	146.2	2.667883	-7.48001	-4.86726
16069	388	2	3317	35	6	167.6625	3.059534	112.2	2.047445	-55.4625	-33.0798
18798	2339	35	4889	509	7	117.3	2.140511	228.225	4.16469	110.925	94.56521
420	1269	9	3475	43	8	207.9231	3.794217	200.8615	3.665357	-7.06154	-3.39623
1042	533	5	3011	6	9	210.8	3.846715	212.5	3.877737	1.7	0.806452
					MEAN	173.8181	3.171864	193.9977	3.540104	20.17958	14.12974

AXIAL VELOCITY		VELOCITY COMPONENT			NOSE OSCILLATION				void fraction (%)	RADIAL POSITION	
nose velocity	tail velocity	RADIAL TB	HORIZONT TB	3D_Vel TB	RADIAL nose_vel	HORIZ nose_vel	3D_vel nose	ALPHA nose		TB radpos	NOSE radpos
0.728571	0.463636	-0.01211	0.07593	0.732517	-0.12527	0.571429	0.92593	38.10758	0.720992	0.055829	0.364964
	0.443478	0.173706	0.189867	1.149127	0.148181	0.372678	1.193035	18.2026	0.694448	0.121813	0.66324
0.85	1.7	0.002343	0.030046	0.850531	0.27487	0.428985	0.952118	26.77952	1.197822	0.070863	0.116845
	0.087179	0.235209	0.255797	1.161842	0.649573	0.795435	1.384616	35.06325	1.052293	0.011541	0.040804
0.68	2.55	0.044514	0.053333	0.682088	-0.13876	0.368179	0.773276	28.43285	1.238905	0.062151	0.77442
0.6375	-0.14366	-0.00914	0.013975	0.637653	0.6677	0.686078	0.936541	47.10193	1.033858	0.106279	0.465239
0.6375	0.053684	0.053664	0.115244	0.647833	-0.05305	0.25	0.684767	21.41297	1.216273	0.110999	0.359447
0.784615	2.55	-0.00663	0.034401	0.785369	-0.01582	0.086003	0.789315	6.255286	1.278018	0.043947	0.33648
0.85	0.728571	-0.09978	0.100692	0.855943	0.090286	0.125	0.859142	8.365885	0.90222	0.101405	0.245504
0.738312	0.936988	0.042421	0.096587	0.833656	0.166411	0.409309	0.944304	25.52465	1.037203	0.076092	0.374105

Bubble pair row	UPPER layer		LOWER layer		order	TB length U		TB length O		delta (mm)	relative le.U %
	number O	row at AO	number U	baris di AU		mm	(D)	mm	D		
1374	1242	42	2555	20	1	121.6714	2.220281	131.8714	2.406413	10.20001	8.383242
353	129	9	2199	5	2	108.8	1.985401	114.4667	2.088808	5.66667	5.208336
1568	3347	325	3273	102	3	127.0364	2.318182	135.3818	2.470471	8.34546	6.569348
3543	3577	431	3452	134	4	136	2.481752	131.75	2.404197	-4.25	-3.125
					MEAN	123.3769	2.251404	128.3675	2.342472	4.990535	4.258982

AXIAL VELOCITY		VELOCITY COMPONENT			NOSE OSCILLATION				Void fraction (%)	RADIAL POSITION	
nose velocity	tail velocity	RADIAL TB	HORIZONT TB	3D_Vel TB	RADIAL nose_vel	HORIZ nose_vel	3D_vel nose	ALPHA nose		TB radpos	NOSE radpos
0.728571	0.364286	0.085869	0.109031	0.736685	0.239374	0.319438	0.795523	23.67479	0.517228	0.040146	0.450697
0.566667	0.364286	0.020331	0.035136	0.567755	0.022482	0.078567	0.572087	7.893643	0.803364	0.093048	0.263179
0.927273	0.51	-0.06672	0.089996	0.93163	-0.14883	0.41907	1.017573	24.32004	0.491982	0.264013	0.712614
0.85	1.457143	-0.16568	0.198081	0.872775	0.029811	0.171796	0.867187	11.4263	0.442045	0.240682	0.261274
0.768128	0.673929	-0.03155	0.108061	0.777211	0.03571	0.247218	0.813093	16.82869	0.563655	0.159472	0.421941

140 - P

Bubble pair row	UPPER layer		LOWER layer			TB length U		TB length O			
	number O	row at AO	number U	baris di AU	order	mm	(D)	mm	D	delta (mm)	relative le.U %
310	3947	8	2392	2	1	151.1455	2.75813	157.6364	2.876577	6.49092	4.294484
38	13146	486	12381	310	2	116.9081	2.13336	117.6927	2.147677	0.78461	0.671134
1080	9668	55	8485	19	3	184.4482	3.365844	135.1486	2.466215	-49.2997	-26.7282
970	9535	46	11377	116	4	144.6538	2.639668	140.0175	2.555063	-4.63633	-3.20512
5387	1307	1	2119	1	5	126.6489	2.311112	121.5487	2.218041	-5.10027	-4.02709
598	12029	246	10441	66	6	131.029	2.391041	137.3055	2.505575	6.27649	4.790153
3878	9956	74	13114	504	7	146.1986	2.667858	137.6987	2.51275	-8.49991	-5.81395
1664	1709	3	12600	362	8	127.8934	2.333822	105.1396	1.918607	-22.7538	-17.7912
6783	4992	11	8990	28	9	136.9694	2.499441	155.1829	2.831805	18.21353	13.29752
3820	11345	177	12632	367	10	124.099	2.264581	111.3487	2.03191	-12.7504	-10.2744
947	3619	5	9089	31	11	147.0484	2.683365	152.9984	2.791942	5.95004	4.046314
22	11414	187	10697	85	12	164.8901	3.008944	164.8891	3.008925	-0.00104	-0.00063
435	18530	2476	16520	1706	13	130.7481	2.385915	120.5481	2.199783	-10.2	-7.80125
20517	10307	84	9400	36	14	115.6	2.109489	119	2.171533	3.39999	2.941168
28	12651	364	7255	7	15	134.1766	2.448478	144.3776	2.634627	10.20096	7.602638
334	11681	205	4211	3	16	114.743	2.09385	118.142	2.155875	3.39896	2.962237
1126	11708	208	11017	100	17	136.0055	2.481853	128.3561	2.342264	-7.64948	-5.62439
3752	6182	14	11040	101	18	150.2222	2.741281	161.3493	2.94433	11.12706	7.407068
199	6355	15	9759	39	19	130.8922	2.388544	133.4414	2.435063	2.54923	1.94758
11225	6568	16	11206	107	20	173.4226	3.164647	159.5117	2.910797	-13.911	-8.02142
1334	6750	17	13038	476	21	149.0993	2.720791	148.3157	2.706491	-0.78359	-0.52555
656	10916	119	11471	153	22	136.8564	2.49738	124.1059	2.264706	-12.7505	-9.31671
4633	14079	720	17310	2059	23	110.0209	2.00768	112.9365	2.060884	2.91556	2.650006
1962	12012	240	12246	267	24	153.9464	2.809241	158.5857	2.893899	4.63925	3.013549
					MEAN	139.0694	2.537763	136.0532	2.482722	-3.01622	-1.81275

AXIAL VELOCITY		VELOCITY COMPONENT				NOSE OSCILLATION				void fraction (%)	RADIAL POSITION	
nose velocity	tail velocity	RADIAL TB	HORIZONT TB	3D_Vel TB	TB alpha	RADIAL nose_vel	HORIZ nose_vel	3D_vel nose	ALPHA nose		TB radpos	NOSE radpos
2.318	1.417	0.072	0.082	2.320	2.024	-0.093	0.114	2.321	2.806	0.228	0.044	0.552
1.962	1.821	0.013	0.027	1.962	0.794	-0.011	0.192	1.971	5.599	0.279	0.020	0.330
2.125	-0.554	0.007	0.104	2.128	2.806	-0.248	0.312	2.148	8.366	0.230	0.135	0.263
2.318	4.250	0.029	0.114	2.321	2.806	0.300	0.341	2.343	8.366	0.225	0.048	0.132
2.125	4.250	0.229	0.233	2.138	6.255	-0.482	0.521	2.188	13.772	0.179	0.095	0.364
1.962	1.214	0.087	0.104	1.964	3.022	0.000	0.000	1.962	0.000	0.211	0.143	0.194
2.125	12.749	-0.209	0.214	2.136	5.764	-0.254	0.699	2.237	18.203	0.220	0.114	0.438
1.962	-1.594	0.069	0.096	1.964	2.806	-0.256	2.076	2.856	46.619	0.253	0.021	0.271
1.821	0.654	0.008	0.162	1.829	5.073	-0.124	0.644	1.932	19.468	0.309	0.146	0.380
2.125	-8.499	-0.085	0.208	2.135	5.599	0.468	0.521	2.188	13.772	0.192	0.175	0.197
2.125	1.342	-0.086	0.118	2.128	3.174	0.644	2.874	3.574	53.517	0.283	0.135	0.214
2.125	2.125	-0.023	0.029	2.125	0.794	-0.360	0.376	2.158	10.023	0.261	0.343	0.462
2.318	Inf	-0.064	0.082	2.320	2.024	1.553	2.416	3.348	46.183	0.189	0.181	0.220
1.700	1.275	-0.086	0.120	1.704	4.044	-0.401	0.449	1.758	14.788	0.313	0.055	0.475
1.962	0.981	0.000	0.000	1.962	0.000	0.286	0.751	2.101	20.950	0.356	0.047	0.129
2.125	1.594	0.017	0.066	2.126	1.776	2.329	3.801	4.355	60.797	0.225	0.096	0.129
2.125	8.499	-0.076	0.133	2.129	3.592	-0.208	0.295	2.145	7.894	0.234	0.112	0.420
2.318	1.109	-0.141	0.203	2.327	5.011	-0.841	3.390	4.107	55.635	0.244	0.195	0.511
2.125	1.700	-0.024	0.066	2.126	1.776	0.689	0.699	2.237	18.203	0.257	0.099	0.341
2.318	-6.373	-0.214	0.305	2.338	7.493	0.159	0.568	2.387	13.772	0.263	0.157	0.673
1.962	2.125	-0.126	0.136	1.967	3.966	0.112	0.347	1.992	10.023	0.340	0.052	0.232
2.125	-8.499	-0.086	0.106	2.128	2.862	0.009	0.208	2.135	5.599	0.193	0.219	0.420
1.822	1.417	0.043	0.089	1.824	2.806	-0.285	0.572	1.909	17.426	0.291	0.127	0.347
2.318	1.594	-0.139	0.164	2.324	4.044	-0.123	0.161	2.324	3.966	0.210	0.152	0.111
2.096	1.069	-0.033	0.123	2.101	3.346	0.119	0.930	2.445	19.823	0.249	0.121	0.325

140 - M

Bubble pair row	UPPER layer		LOWER layer			TB length U		TB length O			
	number O	row at AO	number U	baris di AU	order	mm	(D)	mm	D	delta (mm)	relative le.U %
2298	4419	30	4148	17	1	134.954	2.463	131.815	2.405	-3.139	-2.326
1727	1104	8	9120	60	2	157.250	2.870	160.650	2.932	3.400	2.162
187	11857	438	11374	304	3	120.705	2.203	119.855	2.187	-0.850	-0.704
434	6208	45	10216	144	4	119.855	2.187	123.255	2.249	3.400	2.837
18360	13572	837	13341	921	5	157.080	2.866	139.740	2.550	-17.341	-11.039
19011	10793	246	10334	149	6	123.420	2.252	130.559	2.382	7.140	5.785
					MEAN	135.544	2.473	134.312	2.451	-1.232	-0.548

AXIAL VELOCITY		VELOCITY COMPONENT				NOSE OSCILLATION				Void fraction (%)	RADIAL POSITION	
nose velocity	tail velocity	RADIAL TB	HORIZONT TB	3D_Vel TB	TB alpha	RADIAL nose_vel	HORIZ nose_vel	3D_vel nose	ALPHA nose		TB radpos	NOSE radpos
1.962	2.833	0.148	0.215	1.973	6.255	-0.149	0.192	1.971	5.599	0.244	0.075	0.132
2.125	1.594	-0.161	0.163	2.131	4.379	0.680	0.840	2.285	21.564	0.242	0.269	0.624
2.125	2.318	0.068	0.086	2.127	2.315	-0.166	0.295	2.145	7.894	0.177	0.089	0.312
2.125	1.594	-0.104	0.104	2.128	2.806	-0.219	0.233	2.138	6.255	0.190	0.197	0.423
2.550	-3.642	0.195	0.200	2.558	4.485	0.268	0.354	2.574	7.894	0.175	0.263	0.475
2.550	1.500	-0.049	0.237	2.561	5.314	-1.210	1.275	2.851	26.561	0.165	0.159	0.865
2.239	1.033	0.016	0.167	2.246	4.259	-0.133	0.531	2.327	12.628	0.199	0.175	0.472

HZDR

HELMHOLTZ ZENTRUM DRESDEN ROSSENDORF

Helmholtz-Zentrum Dresden Rossendorf | PF 51 01 19 | D-01314 Dresden

Zur Vorlage

Zentralabteilung Verwaltung
Abteilung Personal
Julia Zlotowitz
Leiterin
Tel +49 351 260-3030
Fax +49 351 260-3199
j.zlotowitz@hzdr.de
Unser Zeichen sche
25.11.2014

Helmholtz-Zentrum Dresden-Rossendorf e.V.

Besucheranschrift:
Bautzner Landstraße 400
D-01328 Dresden
http://www.hzdr.de

Vorstand:
Prof. Dr. Dr. h. c. Roland Sauerbrey
Prof. Dr. Dr. h. c. Peter Joehnk

Registergericht: Amtsgericht Dresden
Registernummer: VR 1693

Bankverbindung:
Commerzbank AG
Konto 0402 657 300
BLZ 850 800 00
SWIFT DRESDEFF850
IBAN DE42 8508 0000 0402 6573 00

Ust.-Nr. DE140213784

Bescheinigung

Herr Akmal Irfan Majid, geboren am 30.11.1990 in Yogyakarta (Indonesien), war vom 01.08.2014 bis 30.11.2014 als Stipendiat (Fachpraktikant) im Helmholtz-Zentrum Dresden - Rossendorf e. V. (HZDR) beschäftigt.

Certificate

Mr. Akmal Irfan Majid, born on 30.11.1990 in Yogyakarta (Indonesia), was employed as a Scholarship Holder (Research Internship) in the Helmholtz-Zentrum Dresden - Rossendorf e. V. (HZDR) from 01.08.2014 till 30.11.2014.

i.V. Schoore

Helmholtz-Zentrum
Dresden - Rossendorf e.V.
Abteilung Personal
Postfach 510119
01314 Dresden

Zertifikat seit 2008 audit berufundfamilie

DRESDEN concept

Bundesagentur für Arbeit
Zentrale Auslands- und Fachvermittlung (ZAV)

Arbeitsmarktzulassung – AMZ
Team 321
53107 Bonn

Praktikum im Rahmen des § 15 Nr. 5 BeschV für:

Majid	Akmal Irfan	Indonesien
Familienname	Vorname	Staatsangehörigkeit

Geboren am: 30.11.1990 Geschlecht: männlich

Arbeitgeber: Helmholtz Zentrum Dresden-Rossendorf e.V.

Universität: Gadjah Mada Universit

Straße: Bautzner Landstr. 400
PLZ / Ort 01328 Dresden
Ansprechpartner: Frau Gudrun Scheere
Tel.: 0351-2603021
Fax: 0351-2603199

Studienfach: Master, Mechanical Engineering

Für den Betrieb zuständige Ausländerbehörde: Kamenz

Branche: Forschung
Tätigkeit: Fachpraktikum

Vergütung: 670,00 €/ Monat (brutto) Unterkunft: ja Verpflegung: nein
Sonstiges: Für Unterkunft werden 221,00 € mtl. von der Vergütung abgezogen.

Genehmigter Beschäftigungszeitraum: von **01.08.2014** bis **30.11.2014**

Zentrale Auslands- und Fachvermittlung der Bundesagentur für Arbeit
Die beabsichtigte Tätigkeit gemäß Praktikumsplan ist ein Fachpraktikum im Sinne von § 15 Nr. 5 BeschV und erfolgt im Einvernehmen mit der Bundesagentur für Arbeit.
Diese Bestätigung dient zur Vorlage bei der Ausländerbehörde / Auslandsvertretung.
Das Einverständnis für eine mögliche Verschiebung des Beschäftigungszeitraumes ab Einreise wird unter dem Vorbehalt erklärt, dass die Immatrikulation weiterhin besteht.
(Studierender ist immatrikuliert bis 15.01.2015)

Dienststempel
Bonn, den 15.04.2014
Im Auftrag

Original für Praktikanten
Original für Ausländerbehörde
Original für Arbeitgeber

HELMHOLTZ ZENTRUM DRESDEN ROSSENDORF

Helmholtz-Zentrum Dresden-Rossendorf | POB 510119 | D-01314 Dresden

Mr. Akmal Irfan Majid
Gejayan Gg. Jambu 145 Condongcatur,
Kecamatan Depok, Sleman
D.I. Yogyakarta
INDONESIA

Institute of Fluid Dynamics
Experimental Thermal Fluid Dynamics Division
Manuel Banowski

Phone +49 351 260-3442
Fax +49 351 260-
m.banowski@hzdr.de@hzdr.de
Our Reference
31.03.2014

Helmholtz-Zentrum Dresden-Rossendorf e.V.

Visitors' Address:
Bautzner Landstr. 400
D-01328 Dresden
http://www.hzdr.de

Board of Directors:
Prof. Dr. Dr. h. c. Roland Sauerbrey
Prof. Dr. Dr. h. c. Peter Joehnk

Company Registration Number:
VR 1693, Amtsgericht Dresden

Bank Details:
Commerzbank AG
Account No. 0402 657 300
(Bank Code 850 800 00)
BIC DRESDEFF850
IBAN DE42 8508 0000 0402 6573 00

VAT-ID-No.: DE140213784

Invitation letter

Dear Mr. Akmal Irfan Majid,

I would like to invite you for four (4) months trainee (Praktikant) at Helmholtz-Zentrum Dresden-Rossendorf (HZDR), Institute of Fluid Dynamics. Your visit should start on August 1st, 2014 and last until November 30th, 2014.

HZDR will pay a grant (Stipendium) of 670 Euro per month and will also support the costs for your flight to Dresden (Germany) for the economy class. For the accommodation, we will prepare a single room at the HZDR residential accommodation (Bautzner Landstrasse 398, 01328 Dresden, Germany) just nearby the research centre. You have to contribute to the expense for the accommodation (about 640 € /month) a fixed amount of 221 € per month.

You are offered our scientific facilities and infrastructures for the "Investigation of Taylor bubble properties and their reaction on the two-phase flow".

I'm looking forward to meet you here at our Institute.

Yours sincerely

Manuel Banowski

Anlage 3

GADJAH MADA UNIVERSITY

(Bezeichnung der Universität/Hochschule. **Name of the university/college**)

ist staatlich oder staatlich anerkannt und akkreditiert von der zuständigen Stelle des Landes.
is a state or officially recognized and accredited by the competent authority of the country.

Immatrikulationsbescheinigung
Certificate of Enrolment

Nachname(n)
Surname(s) MAJID

Vorname(n)
Given name(s) AKMAL IRFAN

geboren am
Date of birth 30 (Tag/day) . 11 (Monat/month) . 1990 (Jahr/year)

Staatsangehörigkeit
Citizenship INDONESIA

Studiengang in einer anerkannten und akkreditierten Studienform
Programme of study in a recognized and accredited form of study

☐ Bachelorstudium **undergraduate** ☑ Masterstudium **graduate** ☐ Doktoratsstudium **postgraduate** ☐ andere Hochschulbildung mit Mindestlaufzeit von 3 Jahren **other higher education with minimum duration of 3 years**

Studienfach und akad. Grad
Subject of study and degree MECHANICAL ENGINEERING - MASTER PROGRAM

Eingeschriebene/r Student/in seit
Enrolled as a student since 01 (Tag/day) . 07 (Monat/month) . 2012 (Jahr/year)

Regeldauer des Studiums
Standard duration of study 2.5 Jahre **years**

Wenn alle formalen Voraussetzungen des Studiums erfüllt sind, wird das Studium am 15 (Tag/day) . 01 (Monat/month) . 2015 (Jahr/year) beendet.
If all formal requirements of the study are fulfilled, it is expected to graduate on

Anschrift und Telefonnummer der Universität/Fachochschule
Address and telephone number of the university/college

DEPT. OF MECHANICAL AND INDUSTRIAL ENGINEERING,
FACULTY OF ENGINEERING, GADJAH MADA UNIVERSITY,
JALAN GRAFIKA 2, YOGYAKARTA 55281 - INDONESIA
PHONE/FAX: (+62) 274 521673

Homepage der Universität/Fachhochschule
Homepage of the university/college

www.ugm.ac.id

Datum
Date 28 (Tag/day) . 03 (Monat/month) . 2014 (Jahr/year)

Prof. Ir. Panut Mulyono, M.Eng., D.Eng.

Stempel der Universität/Fachhochschule
und Unterschrift einer autorisierten Person
Stamp/seal of the university/college
and signature of an authorised person

Die Bundesagentur für Arbeit benötigt diese Angaben für die Genehmigung eines studienfachbezogenen Praktikums. Danke für Ihre Mitwirkung!
The Federal Employment Agency requires this information to approve an internship in Germany. Thank you for your cooperation!

Bundesagentur für Arbeit
Zentrale Auslands- und Fachvermittlung (ZAV)